ROMA TRE
UNIVERSITÀ DEGLI STUDI

DOCTORAL SCHOOL IN MECHANICAL ENGINEERING

XXVI CYCLE

Woody biomass combustion modeling in moving grate furnaces

June 2014

Advisor
Prof. Giancarlo Chiatti

PhD Student
dott. Nello Troccia

PhD School Coordinator
Prof. Edoardo Bemporad

Preface

It is well known that the interest in renewable energy is growing day by day due to different reasons. Some of these are closely related with the present legislation which imposes ever lower emission limits, others are more related with economic features, such as making countries less dependent on fossil fuels. Among the renewable energy sources, biomass plays an important role since it covers about two third of all renewables and it is the fastest growing sector in absolute terms [1]. On this background, in 2009 CRA-Ing (Consiglio per la Ricerca e la Sperimentazione in Agricoltura – Unità di Ricerca per l'Ingegneria Agraria) in cooperation with Roma Tre University launched a project named BTT Project (Bio Thermo Test Project) with the aim of advanced research on biomass utilization for heat and power generation. The project can be roughly divided in three areas: physical and chemical biomass characterization as fuel, biomass combustion characterization in an experimental test bench and biomass combustion simulations. In this thesis the model developed to simulate the biomass combustion process in moving grate furnaces, together with the studies aimed at the elaboration of the model and the obtained results are presented.

The combustion model represents an important tool both for researchers, to better understand how the physical and chemical combustion phenomena depend on the combustion parameters (physical and chemical characteristic of biomass and control parameters of the furnaces), and for the construction companies of furnaces to achieve better design of the combustion system with the aim to meet the emission regulations and to optimize the thermal conversion process inside furnaces.

Working as a unique group together with the CRA-Ing, a large amount of scientific results have been produced, presented and published. The results strictly related with the thesis have been presented at the 20th and 21st European Biomass Conference and Exhibition (Milan 2012 and Copenhagen 2013, respectively) [2] and [3]. Furthermore, in this thesis a literary review on biomass combustion in moving grate furnaces and a work on the study of the sensitivity of thermal conversion processes of biomass on combustion parameters are presented and discussed. In addition to these, there are results that cover other areas of the BTT Project in which I did not participate as a main character and which have been presented, or are going to be presented, in international conferences as well [4] - [8].

The topic of biomass utilization for heat and power generation and in particular the simulation of the thermal conversion of biomass in moving grate furnaces is a multidisciplinary theme that involves different scientific disciplines. Some of these disciplines are not the main components of the knowledge of a newly graduate MSc in mechanical engineering. For this reason I took part in two intensive courses on combustion.

The first course took place in September 2012 in Siena (Italy), organised by UIT (Unione Italiana Termofluidodinamica) under the supervision of Prof. G. Croce of the University of Udine. The main object was Computational Thermo-Fluid Dynamics and during the course the thermal heat exchange in compressible and incompressible flows, turbulence and simulation of multiphase flows were presented and discussed.

The second has been organised by CECOST (Centre for Combustion Science and Technology) at Lund University (Sweden) in August 2013. The course (CISS 2013 – Combustion Institute Summer School) had as main objects: Chemical Kinetics by Prof. H. Curran, Turbulent Combustion by Prof. N. Peters and Laser Diagnostic by Prof. M. Aldén.

Moreover, since combustion simulation also deals with numerical problems, a remarkable effort has been made for the discretization and the numerical solution of the partial differential equations system which describes the combustion process. For this reason, I undertook an internship of seven months at Eindhoven University of Technology, working with the Combustion Technology Group headed by Prof. L. P. H. de Goey. During this period, I worked under the supervision of Prof. R. J. M. Bastiaans and Prof J. van Oijen improving the performance of the simulation program and making it more reliable and efficient.

Acknowledgments

During this scientific trip I have been supported by a large number of people. Here I would like to thank some of them. First of all, I would like to thank my advisor Prof. G. Chiatti. Three years ago he gave me the opportunity to cooperate with his group in this project. During this period, he supported and advised me, reviewing my work continuously. Nowadays I can say that this chance changed my life completely giving to me the opportunity to grow as a man and under a professional point of view. I would like to thank Ing. F. Gallucci and Dott. L. Pari of the CRA research centre. They managed and they are still managing at best one of the most advanced projects on renewable energy conducted in Italy. Thank you to PhD. F. Palmieri for the support given during the initial phase of my PhD studies, when I started to deal with biomass combustion. Thank you to Ing. M. Amalfi, we worked together for three years sharing difficulties and nice moments. It will be difficult to forget this scientific and, first of all, life experience with him.

I would like to thank you Prof. L. P. H. de Goey, Prof. R. J. M. Bastiaans and Prof J. van Oijen that gave me the opportunity to work with The Combustion Technology Group at the Technology University of Eindhoven, improving the performance of my model. Thank you to all the PhD

students and postdocs of Combustion Technology Group, in a particular way to MSc U. M. Goktolga, and PhD A. Donini.

Finally, I would like to think of the people which are part of my life. My parents, Alessandro and Vilma and my sisters Francesca and Marta together with my grandmother Teresa and my uncle Maurizio. You are my family and you always supported me in my decision, thanks a lot for this. All my friends of the *"Saturday Night Group"*, we grew together and together with you I spent the most beautiful moments of my life. Thank you friends!. Thank you to PhD C. De Luca. Once I met you in Siena, you became my close friend and technical confidant. Thanks to your support I overcame the most difficult moments of my PhD studies. The last thank you to Stéphanie. You became part of my life while I was in Eindhoven, making my period abroad one of the most adventurous experiences in my life.

Rome, April 2014.

Nello Troccia

Contents

Index of the figures

Index of the tables

1. Introduction

1.1.Background

The control of greenhouse gas emissions, responsible for climate changes, is a problem that needs global solutions. Indeed, emissions have no boundaries and cause global effects irrespective of the geographical location of the emitting source. For this reason, the European Union (EU) has introduced a new strategy concerning the renewable sources, energy efficiency and the greenhouse gas emissions, eliminating, at least on a political level, the boundaries among the policies on climate changes and the energetic policies.

The new European strategy is named *"20 20 20"* [9] and establishes three ambitious targets to achieve by 2020:

- A 20% reduction in EU greenhouse gas emissions from 1990 levels;
- Raising the share of EU energy consumption produced from renewable resources to 20%;
- A 20% improvement in the EU's energy efficiency.

The operative implementation of this strategy is the *Climate–Energy Package*. This package contains all the main instruments through which EU intends to achieve its targets on greenhouse emissions reduction, energy efficiency and renewable energy sources.

In addition to this, it is of non-minor importance that the production of oil is concentrated in a limited number of countries. This scenario drives the interest of countries with small fossil fuel reserves on the valorisation of renewable energy sources.

In this context biomass energy sources represent an important opportunity. Indeed, they are a complex form of solar energy accumulation and if they are produced, processed and used with efficient and sustainable methods, they represent a key renewable energy source.

The term biomass includes a wide collection of substances (e.g. energy crops, residues of agricultural and forestry activities, municipal waste, etc.). Furthermore, energy use of biomass can be obtained by direct combustion or through its conversion in solid, liquid or gaseous fuel. This study considers only woody biomass from energy crops or as residues of agricultural and forestry activities and its direct thermal conversion as fuel in moving grate furnaces. Indeed,

this technology is the most utilized, from small scale for civil applications to large scale for industrial applications. The advantages of the latter, in respect to fluidized bed furnaces or pulverized fuel furnaces, are: the minor pre-treatment of fuel, lower installation and management costs and better knowledge of technology.

As always, there are advantages and disadvantages in the utilization of biomass as renewable energy source. Differently from wind and solar energy, biomass can be stored in a less expensive way [4] - [5] and it is less sensitive to the temporary change in the meteorological conditions. Moreover, it can be used in existing plants originally developed for fossil fuels with minimal or no modifications. This is the case, for instance, of the grate furnaces deigned for coal combustion.

The main technical disadvantage is related with sustainable production and supply. A huge amount of effort is done to improve the recovery and the harvesting techniques [10] - [12] and to solve the problems related with biomass logistics [13] - [14]. The other disadvantage has more social implications and is related with the increase of the cost of food due to the competition for land and water between biomass energy crops and crops for food supply.

This global scenario attracts the interest of numerous research institutions and universities committed in scientific projects on different aspects of the same problem: make the energy biomass utilization more sustainable, affordable and accessible.

1.2.Aim of the project

During the combustion process in grate furnaces not only the thermal conversion of biomass into energy, but also the formation of pollutants occurs. Thus, it is readily apparent that a detailed understanding of the occurring phenomena is central to define the right strategies for controlling and optimizing the combustion process.

With these intentions, it is possible and interesting to investigate biomass combustion via experiments. Observation on full-scale furnaces operation can show temperature distribution over the solid bed and flue gas composition via probing and or laser techniques. Unfortunately, in most cases full scale experiments are prohibitively expensive and the alternatives are laboratory-scale experiments. The resulting information must be extrapolated to full scale and this is not always a simple and reliable task. The problem can be solved with the use of numerical calculations which guarantee features such as low cost and high speed also in case of parametrical investigation.

Since biomass combustion in moving grate can be roughly divided in two stages, the heterogeneous in-bed combustion stage and the over chamber gaseous phase combustion, to achieve the goal of flexible controlling strategies, the development of a packed bed combustion simulation model is of primary importance. The aim of the thesis is the formulation of a model able to simulate the combustion process in a fuel packed bed. The outputs of the model are organised in terms of temperature, gaseous species concentration and gas flow rate profiles at the boundary layer between the solid fuel and the over bed combustion chamber. These results

can be used as input in a CFD model of the grate furnace to simulate the gaseous combustion outside the fuel bed layer and to obtain comprehensive results on biomass combustion.

1.3.Outline

Chapter 2 consists of a brief overview on biomass combustion systems. The three main technologies available are presented with focus on grate furnaces. The combustion process of biomass is described in detail and advantages of modeling are explained.

In Chapter 3 the mathematical relations chosen to model the physical and chemical phenomena that occur during biomass combustion are presented and critically discussed.

In Chapter 4 the continuity equations, that describe the system's behaviour, and the discretization and solution method applied to solve the PDE's are introduced.

In Chapter 5 the validation of the developed simulation code is performed against experimental results reported in literature by other authors.

In Chapter 6 the results of the six simulations performed with the aim of understanding the influence of the biomass characteristic and operational conditions on the thermal conversion of biomass are presented and discussed.

Finally, Chapter 7 reports general conclusions on the numerical study reported in this thesis.

2. Biomass utilization for power generation

The energy use of biomass can be obtained by direct combustion or through its conversion in solid, liquid or gaseous fuel. In this chapter the current technologies available for direct conversion of biomass will be introduced with particular regards to the thermal conversion in grate furnaces.

2.1.Biomass combustion systems

Biomass energy conversion via combustion has the advantage to rely on well-developed technologies of heterogeneous burners like coal furnaces, which are the foundation of energy power generation around the world. Biomass combustion technologies show also, especially for large-scale applications, similarities to waste combustion systems, but since biomass fuels are utilized, the necessary flue gas cleaning technologies are less complex and therefore cheaper. Generally speaking coal plants could be inexpensively retrofitted to burn biomass, MSW or a blend of these products in a process called co-firing.

However traditional technologies have shown difficulties on burning inhomogeneous fuels, like poor power regulation and problems concerning emissions. It is necessary to develop new furnace systems to burn biomass in an efficient, cheap and clean way. Biomass burning systems are still affected by those penalties which require further investigation and developing to solve these problems .

Industrial furnaces usually utilize electronic air supply regulation and oleo-dynamic fuel feeding systems. The combustion technologies may be distinguished in three categories: fixed bed, fluidized bed and pulverized bed. In fixed bed systems, which concern grate furnaces and underfeed or cigarette stokers, primary air flows through a porous fixed bed where drying, devolatilization and solid combustion take place. Secondary air is fed upside the bed to complete reactions and limit emissions with staging air techniques.

Fluidized bed furnaces utilize a mixture of fuel and an inert material like sand which flows through nozzles in the combustion chamber. Fuel feeding may be operated at different velocities, making it possible to distinguish between bubbling fluidized beds (BFB) and circulating fluidized beds (CFB).

Pulverized fuel systems use fuel reduced in small particles as it can be fed to the furnace with the primary air supply. Char combustion and gas burnout are achieved without secondary air injection.

2.1.1. Grate furnaces

Grate furnaces can be divided into fixed grates, moving grates, travelling grates, rotating grates and vibrating grates. These systems have different performances in relation to the fuel burnt. Grate furnaces are well suited to biomass with a high moisture ratio, different particle sizes and high ash content, so they can be fed with blends. To cope with non woody biomass such as straw or grass it is necessary to utilize special grate constructions like rotating or vibrating grates. This is needed due to differences in combustion behavior and ash melting point between woody and non woody biomass. A good system should work with homogenous fuel and air distribution along the grate. This is the best condition to limit fly ashes and high excess air ratios. As can be seen in experimental work done by Amalfi [15], fuel feeding and grate movement has to be smooth to avoid CO and organic compounds release in flue gases.

Grate systems usually employ air staging also along the grate, this with the purpose of supplying the specific amount of air to the different zones where drying, pyrolysis and char combustion occur. Air staging along the grate also allows partial load operation and correct combustion with different fuels. The reliability of the grate mechanism can be improved with water cooling to limit slagging on surfaces. In grate furnaces, it is of crucial importance how secondary air mixes with bed gases. This because primary chambers lack the turbulence necessary for a proper mixing and thus a good homogenous combustion. A better mixing means less air excess ratio, thus higher thermal efficiency of the burner. The geometry of these systems may be counter, co-current or cross flow operations in relation to how fuel and flue gas flow in respect to each other.

Counter flow systems are well suited to fuels with high moisture content and low heating value. The flame passing above fresh fuels permits fast drying and good water vapor evacuation from the chamber. Co-current flow chambers increase residence time of both fuel and gases in the furnace which may lead to a better combustion at low air ratio which directly reflects on NOx and unburned emission reductions. This geometry is usually used with straw based fuels and preheated air supply. Cross-flow systems are a combination of the first two geometries.

2.1.2. Fluidized bed furnaces

FBC systems have been operating since 1960 for the burning of industrial waste. They consist of vertical vessels where air injection is performed on the bottom trough a perforated plate and bed material is mixed with silica or dolomite while being suspended by air flow. They perform intense heat transfer and good mixing which allow a good combustion even with low excess air ratio. They suffer from ash sintering in the bed so it is necessary to limit the temperature of the chamber to 650-900 °C by internal heat exchangers, EGR or water injection. Due to good mixing abilities, FBC systems can also burn various fuel mixtures, however these systems are

limited by fuel particle size and impurity content. Particle sizes below 40mm and fuel pretreatment are recommended. Regarding emissions they perform well on NOx CO flue gas fractions due to good mixing and effective air staging with low excess ratio, it is also possible to use additives like limestone to trap S, but they suffer from inert dust entrained on flue gas which require massive and efficient dust separators before the chimney. FBC furnaces are expensive and therefore interesting only for large scale applications of above 20 MWth.

2.1.3. Pulverized bed furnaces

In these furnaces fuel, in the form of sawdust, is pneumatically injected in the chamber, using primary air as fuel vector. This kind of burners require carefully controlled operation of the fuel injector and fuel preparation to ensure stable working conditions. Indeed small fuel particles exhibit concurrent devolatilization and char combustion in an explosion-like reaction. Usually injectors fire the chamber tangentially to assure rotational flows and flue gas recirculation as turbine burner scheme .This mechanism permits rapid load changes and low excess air ratio but cause high energy density levels on the chamber which requires water cooling. Muffle dust furnaces are commercially available in the size 2-8 MWth. They offer good emission control due to good mixing and air staging but high flue gas velocities determine issues like walls erosion and bottom ash carriage in flue gas.

2.2.Biomass combustion in grate furnaces

The process of biomass combustion involves a series of physical and chemical phenomena strictly coupled with each other. Under a technological point of view, there are different solutions for biomass combustion: from simple fixed bed applications to the high complexity pulverized bed power plants. Anyway, irrespective of the complexity of the combustion technology and fuel characteristics, the combustion process can be divided into several general phenomena: initial heating, moisture evaporation, devolatilization of volatile matter and char formation, heterogeneous and homogeneous reactions and particles shrinkage [1]. While these phenomena proceed, the gases flowing through the packed bed and the biomass particles exchange heat and mass between each other. With regard to the grate furnaces, the overall combustion process can either be a continuous or a batch process, and air addition can be carried out either by forced or natural draught. Batch combustion is used in some small-scale combustion units, some of which also use natural draught. This is typical for traditional wood-stoves. Medium to large-scale combustion units are always continuous combustion applications, with forced draught [16].

Physical and chemical phenomena previously introduced are strictly connected to the temperature of the fuel and, as shown in Figure 1, it is possible to identify a reaction front which moves downwards through the fuel bed.

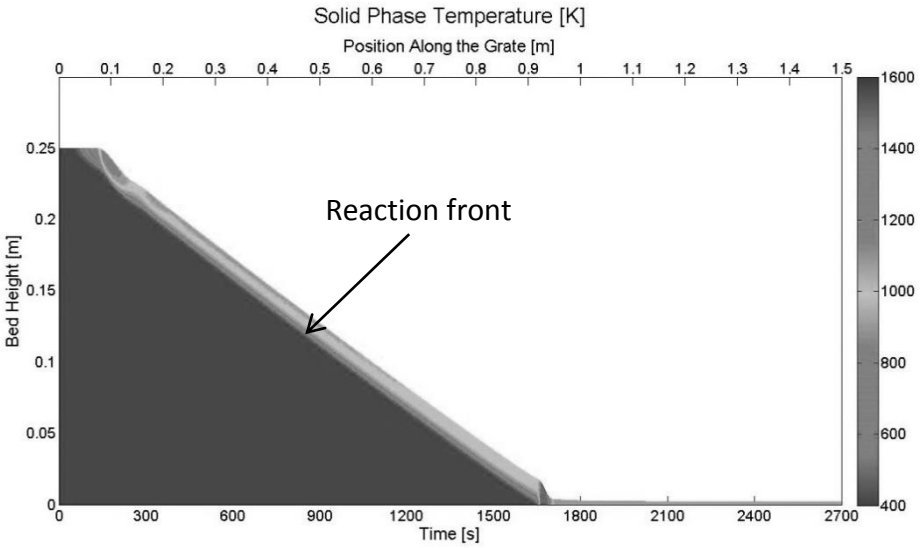

Figure 1 A typical outline of a burning biomass bed.

When the fuel enters the combustion chamber, the radiative heat power coming from the flames and the walls of the furnaces heats up the bed of biomass and the evaporation process can start. Since drying uses the energy released from fuel combustion for water evaporation, during this process the temperature of the biomass remains around 100 °C. This means that evaporation of moisture lowers the temperature in the combustion chamber and slows down the combustion process. In wood-fired boilers, for instance, it has been found that the combustion process cannot be maintained if the wood moisture content exceeds 60 % on a wet basis. The wet wood requires so much energy to evaporate contained moisture, and subsequently to heat the water vapour, that temperatures are reduced below the minimum temperature required to sustain combustion. Consequently, moisture content is a very important fuel variable that influences the combustion process [16]. Once the evaporation is ended the temperature of the solid bed can increase again and the devolatilization process can take place. The devolatilization of volatile matter can be defined as thermal degradation of the virgin biomass and during this process the fuel is decomposed, due to the rise of temperature, into three main products: gas, tar and char. The numerous studies concerning this process, that can be found in literature, show that the devolatilization of volatile matter is a combination of successive endothermic and exothermic reactions. However, the explanations of the biomass' behavior during the degradation differ significantly through the different authors. Park et al [17] justify the temperature behavior of biomass particles considering the formation of a new solid phase named *"intermediate solid"* from virgin biomass through an endothermic reaction, which degrades into char with an exothermic reaction. Bilbao et al [18] presumed that the first endothermic reaction is due to the cellulose and hemicellulose decomposition, whereas lignin decomposition accounts for the second exothermic reaction. Also Di Blasi et al [19] explain the exothermal process with lignin decomposition while the endothermic process is attributed to

the holocellulose and extractives decomposition. Instead, Gronli et al [20] attributed the exothermic behavior of wood pyrolysis to the tar cracking reaction. The gases released by the biomass are mainly composed of H_2O, CO, CO_2, CH_4 and H_2, whose mass fractions depend on the heating condition (heating rate and temperature value) and the chemical composition of the virgin biomass. For engineering applications, a constant composition of the released gases is usually assumed [34], [39] and [50]. As well as gases also tar (condensable fraction of volatile matter) is released during devolatilization. The gases released during the thermal conversion of the biomass can react among each other resulting in new species or they can oxidize with oxygen present in the air supplied from under the grate. The oxidation of the gases starts inside the solid bed and is completed in the combustion chamber above the solid layer by supplying secondary air. When the devolatilization of volatile matter is completed the bed is mainly composed of char. The reaction of the char with oxygen (heterogeneous reactions) gives as product CO (gasification) and CO_2 (complete combustion). The fraction of CO and CO_2 produced during char combustion depends mostly on the combustion temperature but also on the air excess. The gasification of char can occur also with water vapour resulting in H_2 and CO. During this phase the bed temperature reaches the maximum value (approximately 1200 °C) and once the char combustion has taken place only ash is left on the grate. In the last part of the grate the ash formed by the char combustion is cooled by the air supplied from under the grate.

As said at the beginning of the paragraph, the phenomena described are typical of the biomass combustion process and their occurrence does not depend on the combustion system technology and the fuel characteristics. Anyway, the physical and chemical properties of the fuel such as biomass particles dimension, moisture content, low heating value and chemical composition; and the operational variables of the combustion system such as primary and secondary air flow rate and the grate movement have a relevant influence on the duration of each phenomenon and the temperature values reached during the global combustion process. Thus, these parameters have a significant impact on the overall efficiency of the thermal conversion system.

2.3.Modelling biomass combustion

Due to the considerable variations in the quality of the biomass fuel that can be used in biomass power plants, one of the main aims of the studies in biomass combustion is to gain wider knowledge on what happens when biomass is burned and, in particular, what changes occur when the fuel characteristics and the operational variables of the conversion system vary. Modelling, together with experiments, enables a cost-effective approach for future biomass combustion application design, and can improve the competitiveness of biomass combustion for heat and electricity generation. Modelling improves our understanding of the fundamental processes involved in biomass combustion, and may significantly reduce the *"trial and error"* development time needed if experiments only are used for design optimization. Parametric studies can be carried out that reveal the relative influence of different combustion process variables on emission levels and energy efficiency. This enables us to make the correct

decisions with respect to the optimal design and operational principles of the biomass combustion applications.

Combustion in grate furnaces occurs in two distinct regions: the solid bed region, where the combustion process takes place within the fuel bed that is travelling on the grate and the freeboard region, where the volatiles emitted from the bed surface undergo combustion reactions. Thus, as shown in Figure 2, a complete biomass combustion model is always composed of two parts: the model which simulates the combustion of the solid phase on the grate, coupled with a Computational Fluid Dynamics (CFD) model of the gaseous phase combustion in the chamber above the solid bed. The outcome of the first one, in terms of gas temperature, composition and flow rate, represent the inlet data for the CFD model. At the same time, the results by the CFD in terms of gas temperature represent an input for the biomass bed model.

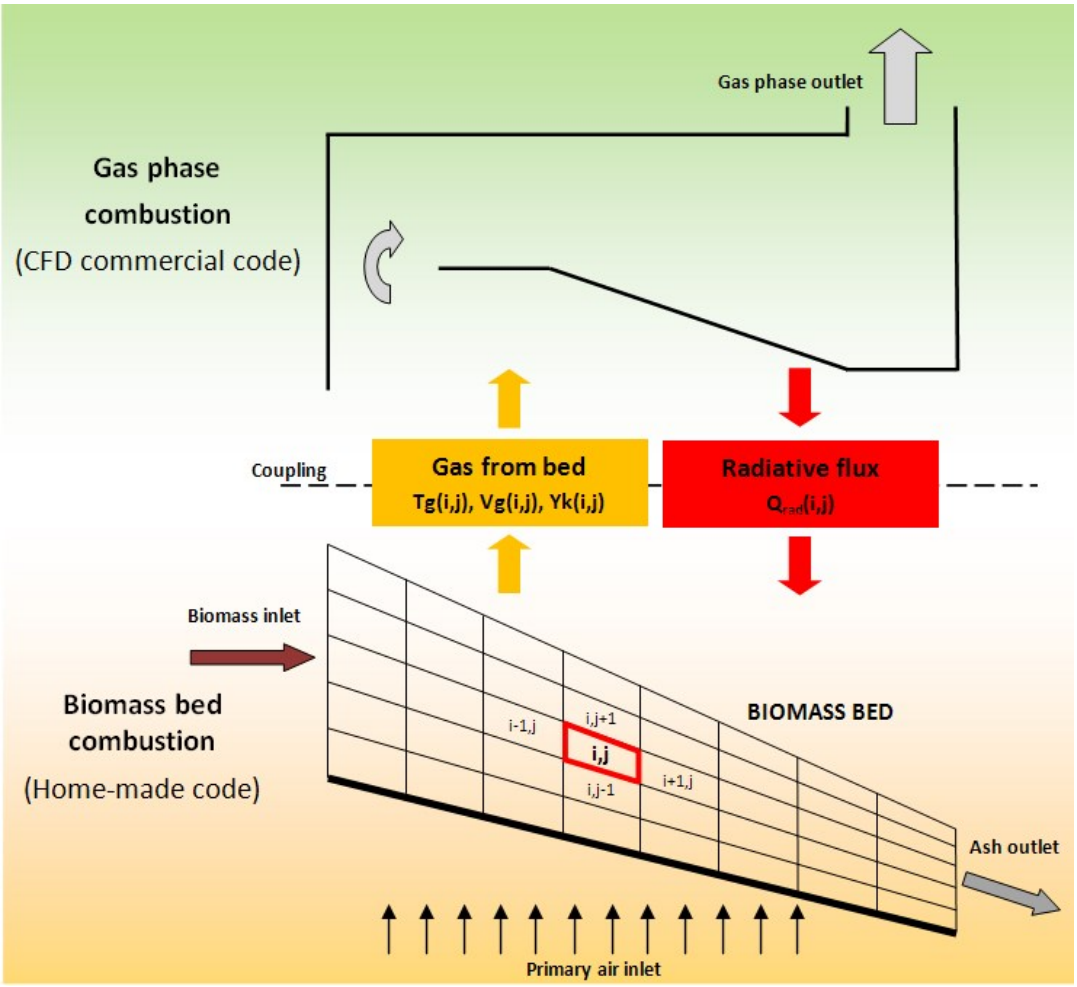

Figure 2 Schematic representation of a biomass combustion model.

3. Biomass combustion phenomena

3.1.Introduction

During the last two decades, mathematical models of biomass combustion have been developed by many authors: Shin and Choi [23] have developed a one dimensional transient model of waste incineration in moving grate furnace, van der Lans et al [24] have presented a two dimensional model of straw combustion in a cross current moving bed, Goh et al [25] have developed a mathematical model for combustion of solid waste in a travelling grate incineration based on an unsteady-state static bed model. Yang et al [26] - [33] have conducted different studies regarding combustion of biomass material, from the influence of the fuel properties to the influence of the physical and chemical phenomena occurring during biomass combustion, considering municipal solid waste as well as straw and other kind of biomass fuels. Zhou et al [34] have developed a one dimensional transient model of straw combustion, Johansson et al [35] have conducted an analysis of the uncertainty of model parameters related to heat transport, reaction rates and composition of volatiles, Albrecht et al [36] have introduced a new modelling approach for biomass furnaces using a flamelet model for the prediction of combustion and NO_x emission in a pilot-scale low-NO_x biomass grate furnace, van Kuijk et al [37] and [38] have developed a sub-model to simulate reverse combustion, Asthana et al [39] have proposed a steady-state two dimensional model to simulate on-grate municipal solid waste incineration, Boriouchkine et al [40] have developed a one dimensional transient model to study the effect of operation parameters on biomass firing, Miljkovic et al [41] have proposed a two dimensional approach for straw combustion modelling in moving grate furnaces and Martinez and Nussbaumer[42] have developed a one dimensional transient model of biomass combustion with combustion optimization purposes.

3.2.Physical and chemical models

During the biomass combustion process a series of physical, chemical and thermal phenomena occur. As previously reported in paragraph 0, these phenomena are: initial heating, moisture evaporation, devolatilization of volatile matter and char formation, heterogeneous and homogeneous reactions and bed shrinkage. Thus, the development of a model that simulates the biomass thermal conversion requires the description, through mathematical relations, of

each mentioned phenomena. In this chapter, the mathematical models used by different authors are introduced and discussed in order to show the various possibilities of the phenomena modelling and define which are suitable for an implementation in our model.

3.2.1. Moisture evaporation

Woody biomass used in industrial furnaces presents an amount of moisture which can vary between 5 % and 50 % on dry basis [31]; depending on the biomass type, pre-treatment (e.g. drying) as well as storage time and mode. The drying of porous media, such as a wood chips bed, is a complex process involving heat and mass transfer phenomena and it was studied in detail by several authors e.g. Kowalski [43], Younsi et al [44] and Di Blasi [45]. In a saturated wood particle, water is bounded in the porous structure in three ways: chemical bounded water, physical-chemical bounded water and physical-mechanical bounded water. The first one does not participate to the drying process because too much energy is required to break the chemical bounds; the second one is enclosed in the organic material of plants and is also referred to as adsorptive water and the last one is the free water that fills the pores of the wood. The free water leaves the biomass first because its evaporation process is less energy demanding than adsorptive water. Moisture evaporation from biomass particles can be modelled using three main different models:

- Diffusion limited model;
- Radiative model;
- Arrhenius law model.

The third method is applied by Di Blasi et al [46] to describe moisture evaporation kinetics in updraft gasifiers to reduce the complication in numerical calculation, and this is done as well by Boriouchkine et al [40] and Johansson et al [35] in their biomass combustion models. The second method is used in coupling with the first as in the work of Goh et al [25] and Yang et al [29] - [33]. In these works when the biomass temperature is under 273 K the evaporation mechanism is diffusion limited and when the temperature is over 273 K the mechanism is radiative. In this situation all the heat is used to dry the biomass fuel. Other authors, such as Shin and Choi [23], Zhou et al [34] and Asthana et al [39] prefer to use a diffusion limited model only. The relations used to describe each model are listed in Table 1.

Table 1 Moisture evaporation rate [kg/m^{3}s].

Diffusion limited model	$h_m S\left(C_{ws} - C_{wg}\right)$	(3.1)
Radiative model	$\frac{S\left[h_t\left(T_g - T_s\right) + \varepsilon\sigma\left(T_w^4 - T_s^4\right)\right]}{H_{evap}}$	(3.2)
Arrhenius law model	$A_{evap} e^{\left(-E_{evap}/RT_s\right)} \rho_s X_{H_2O}$	(3.3)

Where S is the specific surface area per volume of solid matter, ε the emissivity of the grey body, T_g and T_s the gaseous and solid phase temperature, respectively. T_w the temperature of the walls of the combustion chamber, σ the Stefan-Boltzmann constant, H_{evap} the latent heat of water evaporation, A_{evap} and E_{evap} the frequency factor and the activation energy of the Arrhenius law, R the universal gas constant, ρ_s the mass density of the solid phase, X_{H2O} the mass fraction of moisture in the solid phase, C_{ws} and C_{wg} the water vapour mass concentrations on the particle surface and in the gaseous phase, respectively. The value of C_{ws} is assumed to be equal to the water vapour concentration in the saturation conditions at the temperature of the solid particle. The mass transfer coefficient h_m and the convective heat transfer coefficient h_t are determined using the relations reported for a packed bed of spherical particles by Wakao and Kaguei [47] (see Table 2).

Table 2 Dimensionless number for convective mass and heat transfer.

Sherwood Number	$Sh = 2 + 1.1Re^{0.6}Sc^{1/3}$	(3.4)
Nusselt Number	$Nu = 2 + 1.1Re^{0.6}Pr^{1/3}$	(3.5)

Where *Re, Sc* and *Pr* are the dimensionless number of Reynolds, Schmidt and Prandtl, respectively.

Since we are at an early development of our code, the less computational demanding Arrhenius model by Di Blasi et al [46] has been implemented. This decision does not preclude any further development of the code with the implementation of more detailed and computational demanding models such as the diffusion-radiative model.

3.2.2. Devolatilization of volatile matter

When subjected to external heating, solid fuels start to decompose, giving a mixture of volatile species and solid carbonaceous residual products. The products of this thermal degradation process are usually grouped into a few main components. Each component represents a sum of numerous species which are lumped together to simplify the schematization. Generally, the product groups considered are: gas, tar and char [21]. Char is the carbon-rich non-volatile residue. Tars are any several high molecular weight products that are volatile at the devolatilization temperature but condense near room temperature. Gases include all lower molecular weight products (e.g. CO, CO_2 and CH_4).

As reported by Di Blasi [21], kinetic models of biomass devolatilization can be classified into three main groups:

- One-step global models;
- One-stage, multi-reaction models;
- Two-stage, semi-global models.

A simple way to represent the reactions of these three main groups is reported in Table 3.

In the one-step global models a one-step reaction is used to describe degradation of the solid fuel. An Arrhenius law is used to describe the temperature dependence of the weight loss of the fuel. The one-stage multi reaction models use one-stage kinetics models but describe the degradation of the solid to char and several gaseous species. The two-stage models include both primary reactions of virgin solid degradation and secondary reactions of evolved degradation products. In addition to these, in literature it is possible to find more complicated models, such as those proposed by Park et al [17] and Grieco and Baldi [48], used to explain the thermal behavior of the fuel particle during the thermal degradation or the competing parallel reaction model originally proposed by Shafizadeh and Chin [49]. In conclusion it is relevant to note, as reported by Di Blasi [21], that kinetic data about devolatilization of biomass varies considerably due to the different set up and techniques of experiments (e.g. heating rate, direction of heat flux, temperature and pressure) as well as physical and chemical properties of biomass (e.g. particle size, moisture content, chemical composition). This means that values of kinetic parameters are not representative of the true physic-chemical process governing the degradation of solid fuels but are valid only for correlating experimental data.

Table 3 Devolatilization reaction models.

Reaction Model	Reaction Scheme		
One-step global model	$WOOD \xrightarrow{k} VOLATILES + CHAR$		(3.6)
One-stage, multi-reaction model	$WOOD \xrightarrow{k_i} PRODUCTi$		(3.7)
	Primary reactions	Secondary reactions	
Two-stage, semi-global model	$WOOD \xrightarrow{k_{tar}} TAR$	$TAR \xrightarrow{k_{tar-char}} CHAR$	(3.8)
	$WOOD \xrightarrow{k_{gas}} GAS$	$TAR \xrightarrow{k_{tar-gas}} GAS$	
	$WOOD \xrightarrow{k_{char}} CHAR$		

In the works related with the biomass combustion modeling, since the main aim is not only the description of the thermal degradation of the biomass due to the devolatilization but the overall combustion process, the models used to describe the devolatilization are simple one-step global models [24], [29] - [31], [33] - [35], [39] - [42].

This means that the devolatilization rate is proportional to the remaining mass of the volatile in the solid phase through the rate constant defined by an Arrhenius law (see Table 4).

Table 4 Devolatilization model.

Devolatilization rate	$S_{devol} = k_{devol} X_{vol} \rho_s$	(3.9)
Devolatilization rate constant	$k_{devol} = A_{devol} e^{(-E_{devol}/RT_s)}$	(3.10)

Where X_{vol} is the mass fraction of volatile in the solid phase, A_{devol} and E_{devol} the frequency factor and the activation energy for the devolatilization process. In our model, the parameters reported by Yang et al [29] for slow case were used.

Regarding the composition of the volatiles released due to the biomass decomposition, different approaches can be found in literature. Yang et al [33], Zhou et al [34], Asthana et al [39] and Di Blasi [50] apply a decomposition of the volatiles in different species using constant values; Shin and Choi [23] and Yang et al [29] consider the volatile as a unique species $C_nH_mO_l$.

In this work we follow the approach of Asthana et al [39] considering a decomposition of the volatile in different species using constant values which meet the elemental composition, the proximate analysis and the calorific value of the woody biomass fuel considered.

3.2.3. Homogeneous reactions

Volatile species, released during biomass devolatilization, react inside the packed bed with each other, with the oxygen supplied from the bottom and with the carbonaceous solid residue of the solid fuel. In literature, different approaches are developed to simulate the gaseous phase combustion inside the packed bed. Van der Lans et al [24] assume that only char reacts with O_2 inside the bed, instead Shin and Choi [23] consider the generic hydrocarbon C_xH_y to be the only product of the devolatilization and assume that it is first partially oxidized to CO and then further converted to CO_2. Yang et al [29] - [31] uses the same scheme of Shin and Choi but they also take into account the production of the species H_2 from the C_xH_y reaction with O_2. Moreover, they consider that gaseous species first have to mix with surrounding air before their combustion can take place. For this reason they introduce a mixing rate proportional to the energy loss through the bed and define the actual reaction rates of volatile species as the minimum of the kinetic rates and the mixing rates with the oxygen. Also Zhou et al [34] take into account that the volatile combustion is not only controlled by kinetic rates but also by the mixing rates of the gases with the primary air flow, but they differentiate the volatiles species in CO, CO_2, CH_4, C_nH_m, H_2 and tar. The tar is modeled as the hydrocarbon $CH_{1.84}O_{0.96}$ with a molecular weight equal to 95 and gives as combustion products CO and H_2O.

In our model we follow the scheme of Asthana et al [39] considering as gaseous species CO, CO_2, CH_4, H_2O. In addition, we consider that the gases released during devolatilization first

have to mix with the air stream provided from under the grate. For this reason, we introduce a mixing rate as defined by Johansson et al [35].The complete scheme of the reactions is reported in Table 5.

Table 5 Gaseous phase combustion model.

Reaction	Reaction rate	
$CH_4 + \frac{3}{2}O_2 \rightarrow CO + 2H_2O$	$r_{CH_4} = 1.5 \cdot 10^8 e^{(24163/T_g)} C_{CH_4}^{0.7} C_{O_2}^{0.8}$	(3.11)
$CO + \frac{1}{2}O_2 \rightarrow CO_2$	$r_{CO} = 1.3 \cdot 10^8 e^{(-15102/T_g)} C_{CO} C_{O_2}^{0.5} C_{H_2O}^{0.5}$	(3.12)
Mixing rate		
$r_{mix} = C_{mix}\left(150\frac{D_g(1-\epsilon)^{2/3}}{d_p^2\epsilon} + 1.75\frac{v_g(1-\epsilon)^{1/3}}{d_p\epsilon}\right) \cdot min\left\{\frac{C_{fuel}}{\Omega_{fuel}}, \frac{C_{O_2}}{\Omega_{O_2}}\right\}$		(3.13)

Where C_i are the molar concentrations of gaseous species expressed in [mol/m^3], C_{mix} is an empirical constant (usually equal to 0.65) and Ω the stoichiometric coefficient in the chemical reaction.

3.2.4. Heterogeneous reactions

Heterogeneous reactions involve the combustion/gasification of the char remaining after devolatilization with the oxygen and the other gaseous species present in the gaseous phase flowing through the bed. The overall rates that control these reactions are given by the combination of the chemical reaction rates and the mass diffusion rates of the gaseous species toward the surface of the solid fuel, where the reactions take place. The primary products of char combustion are CO and CO_2. Final burnout of CO takes place in the gaseous phase.The appropriate stoichiometric coefficient for oxidation of char is not readily apparent and it is necessary to define the term Θ, that depends on the ratio r_{CO/CO_2} of CO/CO_2 formation rate. In Table 6 the relations implemented in our model are reported.

Table 6 Char oxidation reaction.

Reaction	$C + \frac{1}{\theta} O_2 \rightarrow 2\left(1 - \frac{1}{\theta}\right) CO + \left(\frac{2}{\theta} - 1\right) CO_2$	(3.14)
Stoichiometric ratio	$\Theta = (1 + 1/r_c)/(1/2 + 1/r_c)$	(3.15)
CO/CO₂ ratio	$r_{CO/CO_2} = A_{CO/CO_2} e^{(-T_{co/co2}/T_s)}$	(3.16)
Reaction rate	$S\chi k_0 p_{O_2}$	(3.17)
Specific bed surface	$S = \frac{6(1-\epsilon)}{d_p}$	(3.18)
Surface reduction coefficient	$\chi = \frac{\rho_{char}}{\rho_{char} + \rho_{ash}}$	(3.19)
Overall rate constant	$k_0 = \left(\frac{1}{k_c} + \frac{1}{h_m}\right)^{-1}$	(3.20)
Chemical rate constant	$k_c = A_c e^{(-E_c/RT_s)}$	(3.21)
Mass transfer coefficient	$h_m = \frac{D_{O_2-N_2}^{2/3} v_g}{\upsilon^{2/3}\epsilon}\left(\frac{0.765}{Re^{0.82}} + \frac{0.365}{Re^{0.386}}\right)$	(3.22)

Where χ is the active surface reduction coefficient, k_0 the overall rate constant of char combustion/gasification, k_c and h_m the chemical rate constant of char combustion/gasification and the mass transfer coefficient of oxygen toward the reaction surface.

The scheme model implemented is common to different authors [24], [29], [31], [33], [34], [41] and [42] and it has been chosen since it takes into account both chemical and diffusional rate constants for char combustion. The active surface reduction coefficient χ is taken from the work of Asthana et al [39] and the mass transfer coefficient h_m is defined as reported by van der Lans et al [24].

In this work, no char reaction with gaseous species different from oxygen is considered. This decision does not preclude a further development of the code with the implementation of more detailed models such as implemented by Johansson et al [35], Asthana et al [39] and Boriouchkine [40], which consider also the gasification of char with water steam, H_2 and CO_2.

3.3.Volume change of bed during combustion

The reduction of the bed volume during the combustion process is related with the mass loss due to drying, devolatilization and char combustion. The volume shrinkage does not have the same magnitude during the different phases of the combustion process. For this reason, as a first approximation it can be considered that the mass released during drying and

devolatilization is replaced by internal porosity and no bed volume reduction occurs during these phases [39] and [42]. The change in bed height is then associated only with the char consumption.

The relation proposed to model this phenomena is reported below.

$$f_s = \frac{\left(1 - \frac{\rho_{char,burn}}{\rho_{char,0}}\right) + f_{ash,0}}{\left(1 + f_{ash,0}\right)} \tag{3.23}$$

Where $\rho_{char,burn}$ is the mass of char burned per unit volume of bed, $\rho_{char,0}$ the mass of char per unit volume of bed and $f_{ash,0}$ is the volume occupied by the ash. The subscripts *0* refers to the initial conditions.

4. Governing equations of the biomass combustion model

In this chapter, the governing equations of a 1-D transient model for biomass combustion in moving grate furnaces are introduced. To describe physical, chemical and thermal behaviour of biomass beds the following assumption are made:

- biomass particles are schematized as spherical particles[23], [29] - [31], [35] - [40] and [42];
- thermal gradients inside the particle are neglected [31] (packed bed is described as formed of two homogeneous phase: gaseous and solid phase);
- the gaseous phase is described as an ideal gas[34] and [40];
- the pressure of the gaseous phase through the bed is constant and equal to the atmospheric pressure [23] and [29] - [40];
- the gaseous species considered in the simulation are CO, CO_2, H_2O, O_2, H_2, CH_4, and inert gas N_2 [23], [29] and [31];
- heat produced in char combustion is accounted in the solid phase [40];
- temperature of the gas released from the solid is the same of the solid phase [40].

The bed behavior can be modeled as a 1-D transient phenomenon since the gradients, such as temperature and chemical species concentration gradients, in the direction of the movement of the grate are negligible compared to those in the direction of the gas flow. Then, heat and mass transfer in the direction of the bed movement can be ignored [23], [34], [37], [38], [40] and [42].

4.1.Solid phase equations

For a fixed bed mass continuity equations for solid phase can be written as follow:

$$Solidcontinuity: \frac{\partial\big((1-\epsilon)\rho_s\big)}{\partial t} = -S_g \tag{4.1}$$

$$Solidspeciescontinuity: \frac{\partial\big((1-\epsilon)\rho_s X_i\big)}{\partial t} = -S_i \tag{4.2}$$

Where t is the time, ρ_s the particle density, ϵ the void fraction of the fuel bed and S_g the conversion rate from solid to gaseous phase due to moisture evaporation, devolatilization and char combustion/gasification. X_i and S_i represent the mass fractions and the source terms of each solid components (moisture, volatile, char and ash), respectively.

The solid energy continuity equation is:

$$Solid\ enrgy: \frac{\partial\left((1-\epsilon)\rho_s c_s T_s\right)}{\partial t} = \frac{\partial}{\partial x}\left(\lambda_{s,eff}\frac{\partial T_s}{\partial x}\right) + \sum_i S_{gi}\Delta h_i - \sum_i S_{gi}c_{gi}T_s + \dot{Q}_{conv} + \dot{Q}_{rad} \quad (4.3)$$

Where x is the direction in the bed height, c_s and T_s the specific heat and the temperature of the solid fuel, respectively. The coefficient $\lambda_{s,eff}$ is the effective thermal conductivity of the solid phase and takes into account the conductive and radiant heat transfer among the solid particles. The term $S_{gi}\Delta h_i$ represents the heat source due to the heterogeneous reactions (evaporation, devolatilization and char reactions). The third term on the right hand side accounts for the enthalpy of the mass that passes from solid to gaseous phase. The term $\dot{Q}_{conv}$ represents the convective heat transfer between gaseous and solid phase and can be defined as follow:

$$\dot{Q}_{conv} = h_t S\left(T_g - T_s\right) \quad (4.4)$$

$$h_t = Nu\lambda_g/d_p \quad (4.5)$$

where h_t represents the convective heat transfer coefficient [47], T_g the gas temperature, S the bed surface area per unit of volume, λ_g the thermal diffusion coefficient of the gaseous phase, d_p the particle diameter, Nu the Nusselt number (see Table 2) and the last term $\dot{Q}_{rad}$denotes the radiative heat source.

Actually, there are two ways to model the radiant heat source: the two-flux radiation model [23] ,[29] - [31] and [33] and the conductivity radiation model [39], [40] and [42]. Johansson et al [35] have demonstrated that the less-demanding conductivity radiation model can be used instead of the two-flux radiation model, without relevant differences in the calculated variables. In case of conductivity radiation model the heat radiation source $\dot{Q}_{rad}$ can be defined as follows [39]:

$$\dot{Q}_{rad} = (J_0 - \sigma T_s^4)\beta e^{-\beta x'} \quad (4.6)$$

$$\beta = 3(1-\epsilon)/2d_p \quad (4.7)$$

Where σ is the Stefan-Boltzmann constant, β the absorption coefficient of the fuel bed, x' the distance from the bed surface and J_0 the incident radiation. The latter depends on the temperature of the walls of the combustion chamber and the temperature of the gases flowing out from the bed. Astana et al [39] have defined the incident radiation as the radiation of a grey body at 1273 K. In the experiments of Johansson et al [35], the bed is ignited by a radiating flame whose temperature is 1400 K. Once the reaction front has reached a few centimetres down into the bed, they remove the flame and assume, in the model, that the surroundings radiate back with a temperature equal to that one of the gasses flowing out from the bed. A similar way was used by Zhou et al [34].

In this radiation model, the thermal conductivity of the solid $\lambda_{s,eff}$ takes into account also the radiant heat transfer among the particles and depends on the third power of the temperature. It is defined as follows [39]:

$$\lambda_{s,eff} = (1-\epsilon)\lambda_{biomass} + \lambda_{rad} \quad (4.8)$$

$$\lambda_{rad} = \frac{16}{3}\sigma d_{e,rad} T_s^3 \quad (4.9)$$

$$d_{e,rad} = \frac{2\epsilon}{3(1-\epsilon)} d_p = \frac{\epsilon}{\beta} \quad (4.10)$$

Where $\lambda_{biomass}$ is the thermal conductivity of the wood, λ_{rad} is the radiant conductivity and $d_{e,rad}$ is the equivalent particle diameter for radiation heat.

4.2.Gaseous phase equations

The governing equations of the gas phase that enter from under the grate and pass through the bed can be written as follows:

$$Gascontinuity: \frac{\partial \epsilon \rho_g}{\partial t} + \frac{\partial (\epsilon \rho_g v_g)}{\partial x} = S_g \quad (4.11)$$

$$Gasspeciescontinuity: \frac{\partial (\epsilon \rho_g Y_i)}{\partial t} + \frac{\partial (\epsilon \rho_g v_g Y_i)}{\partial x} = \frac{\partial}{\partial x}\left(D_{a,eff} \frac{\partial \epsilon \rho_g Y_i}{\partial x} \right) + S_{gi} \quad (4.12)$$

Where ρ_g is the gas density and v_g the gas velocity. Y_i and S_{gi} represent the mass fractions and the source terms of each gaseous component (CO, CO_2, H_2O, O_2, H_2, CH_4), respectively. The term $D_{a,eff}$ represents the effective axial dispersion coefficient and takes into account both diffusion and turbulent contributions [29]. It can be defined as follows:

$$D_{a,eff} = D_i + 0.5 v_g d_p \tag{4.13}$$

Where D_i is the molecular diffusion coefficient of the gaseous species considered.

The gas energy continuity equation is:

$$Gas\ energy: \frac{\partial \epsilon \rho_g c_g T_g}{\partial t} + \frac{\partial \epsilon v_g \rho_g c_g T_g}{\partial x} = \frac{\partial}{\partial x}\left(\lambda_{g,eff} \frac{\partial T_g}{\partial x}\right) + \sum_i S_{gi} \Delta h_i + \sum_i S_{gi} c_{gi} T_s - \dot{Q}_{conv} \tag{4.14}$$

Where c_g is the specific heat of the gaseous phase, $S_{gi}\Delta h_i$ the heat source due to the homogeneous reactions and the third term on the right hand side considers the enthalpy of the mass that passes from the solid to the gaseous phase. The term $\lambda_{g,eff}$ represents the effective thermal dispersion coefficient and consist of diffusion and turbulent contributions, in a similar way as species dispersion [29]. It can be expressed as follows:

$$\lambda_{g,eff} = \lambda_g + 0.5 v_g d_p \rho_g c_g \tag{4.15}$$

4.1.Gaseous phase pressure inside the packed bed

The variables of the gaseous phase are: gas density ρ_g, gas velocity v_g, gas temperature T_g and the mass fractions of gaseous species Y_i. As a first approximation, the pressure inside the bed can be considered to be the atmospheric value [23], [24], [34], [36] - [38] and [40] - [42], and the ideal gas law can be considered to fully define the problem.

$$Ideal gas law: \rho_g = \frac{p_g M_g}{R T_g} \tag{4.16}$$

Where p_g is the gaseous phase pressure, R the ideal gas constant and M_g the molecular weight of the gaseous phase.

The assumption of a constant pressure for the gaseous phase can be justified since both the pressure drop due to the presence of the particles and the back pressure due to the increase of the mass flow rate and temperature can be considered negligible.

4.2.Solution method

The partial differential equations (PDE's) introduced in the previous paragraph present the same structure and, introducing a generic independent variable φ, can be written using the following general relation (referred to the 1-D case):

$$\frac{\partial}{\partial t}(\rho\varphi) + \frac{\partial}{\partial x}(\rho v\varphi) = \frac{\partial}{\partial x}\Gamma\frac{\partial}{\partial x}\varphi + S_\varphi \tag{4.17}$$

The first two terms on the left hand side of the equation are the unsteady and the convective term. On the other hand side there are the diffusion and the source term, respectively. The diffusion coefficient Γ and the source term S_φ assume a specific significance depending on the meaning assumed by the variable φ. For instance, if φ represents the mass fraction of a chemical species, then Γ is the molecular diffusion coefficient and S_φ is the net source term of the species considered.

In the case of construction of a computer program, the identification of a general form of the PDE's is relevant. Indeed, it is possible to write general instructions to solve the generic PDE and then repeat the instructions for the different PDE's, using the appropriate meaning of the diffusion and source term for each variable.

The next step for the definition of the solution method of the PDE's system, is the discretization of the continuum calculation domain. Indeed, once the calculation domain and the dependent variables are discretized, it is possible to replace the PDE's system with a system of algebraic equations, which is easier to solve.

In this work, the control-volume formulation proposed by Patankar [51] is used. The calculation domain is divided into a number of non-overlapping control volumes which surround each grid point. This enables one to obtain a meshed geometry in which all the variables are defined at the grid points. A generic representation of the discretized calculation domain is given in Figure 3.

Using the three-grid point representation (Figure 3), assuming that the interface n is located midway between P and N and w midway between S and P ($\delta x_n=\delta x_s=\delta x$) and considering a constant value for ρ within the control volume surrounding each grid point, it is possible to integrate the generic partial differential equation introduced at the beginning of the paragraph.

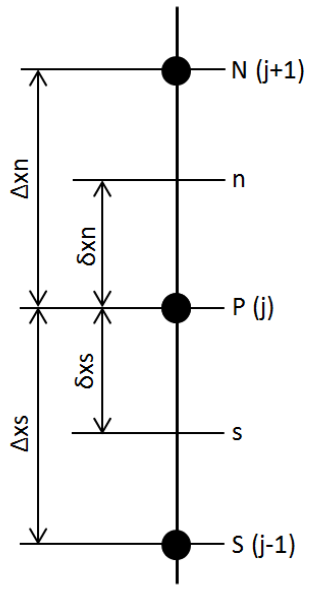

Figure 3 Calculation domain discretization.

The equation which is obtained from the integration is:

$$\int_s^n \int_t^{t+\Delta t} \frac{\partial}{\partial t}(\rho\varphi)dtdx + \int_t^{t+\Delta t} \int_s^n \frac{\partial}{\partial x}(\rho v\varphi)\, dxdt = \int_t^{t+\Delta t} \int_s^n \frac{\partial}{\partial x}\Gamma\frac{\partial}{\partial x}\varphi\, dxdt \frac{\partial}{\partial x}\Gamma\frac{\partial}{\partial x}\varphi + \int_t^{t+\Delta t} \int_s^n S_\varphi\, dxdt \tag{4.18}$$

To discretize the diffusion term of the equation a piecewise linear profile for φ is assumed, instead for the convective term the upwind scheme is adopted. In this scheme, the internal conditions of the cell in term of concentration, temperature, velocity and density define the output of the calculation node. The scheme is also called “tank-and-tube” model. As shown in Figure 4, the control volumes can be thought to be stirred tanks that are connected in series by short tubes. The flow through the tubes represents convection, while the conduction through the tank walls represents diffusion. Since the tanks are stirred, each contains a fluid with uniform characteristics (in terms of physical and chemical properties). Then, it is appropriate to suppose that the fluid flowing in each connecting tube has the temperature, density and concentration that prevails in the tank on the upstream side [51].

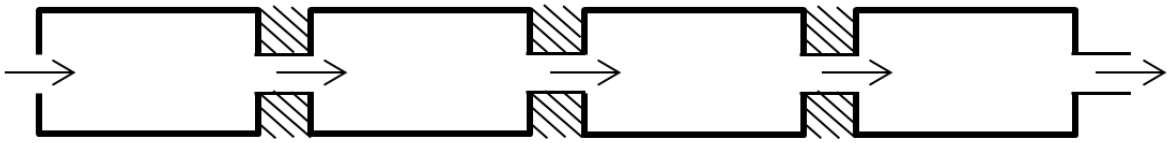

Figure 4 Tank-and-tube scheme.

Furthermore, since the PDE's system is stiff, the application of standard methods such as explicit methods may exhibit instability in the solution. For this reason, a fully implicit scheme is used.

On the basis of the assumptions made and considering that the only dependent variable that is changing in space and time is φ, the discretized equation that arises is the following:

$$\rho(\varphi_P - \varphi_P^0)\Delta x + \rho v(\varphi_P - \varphi_s)\Delta t = \left(\frac{\Gamma_n}{\delta x}(\varphi_N - \varphi_P) - \frac{\Gamma_s}{\delta x}(\varphi_P - \varphi_S)\right)\Delta t + (S_C + S_P\varphi_P)\Delta t\Delta x \quad (4.19)$$

Where we have considered that the fluid is flowing from the *s-face* to the *n-face*. The source term S_φ is considered as given by a constant term S_c and a term that depends on the value of the dependent variable φ_P. The superscript *0* denotes the value of the independent variable at the time *t*, the values of the other variables are considered at the actual time *t+Δt*.

Grouping the parameters of the equation (4.19), it is possible to rewrite the equation in the following form:

$$a_P\varphi_N - b_P\varphi_P + c_P\varphi_S + d_P = 0 \quad (4.20)$$

Where:

$$a_P = \frac{\Gamma_n}{\delta x} \quad (4.21)$$

$$c_P = \frac{\Gamma_s}{\delta x} + \rho v \quad (4.22)$$

$$b_{P0} = \frac{\rho\Delta x}{\Delta t} \quad (4.23)$$

$$b_P = a_P + b_{P0} + c_P - S_P \Delta x \tag{4.24}$$

$$d_P = b_{P0}\varphi_P^0 + S_C \Delta x \tag{4.25}$$

A reformulation of the convection-diffusion equation using the grid index *j* notation leads to the following discretized equation:

$$a_j \varphi_{j+1} - b_j \varphi_j + c_j \varphi_{j-1} + d_j = 0 \tag{4.26}$$

Where the coefficients becomes:

$$a_j = \frac{\Gamma_{j+1}}{\delta x} \tag{4.27}$$

$$c_j = \frac{\Gamma_{j-1}}{\delta x} + \rho v \tag{4.28}$$

$$b_{j0} = \frac{\rho \Delta x}{\Delta t} \tag{4.29}$$

$$b_j = a_j + b_{j0} + c_j - S_j \Delta x \tag{4.30}$$

$$d_j = b_{j0}\varphi_j^0 + S_{Cj} \Delta x \tag{4.31}$$

Once the system of PDE's has been discretized a system of algebraic non-linear equations coupled with each other is obtained. To solve this system a modified Newton method, similar to that one proposed by Somers [52], is implemented. To arrive at the formulation of the method implemented, first the residual for each dependent variable at each grid point has to be defined. Stating with $j \in [1, G]$ the index of the grid points and with $i \in [1, V]$ the index of the variables, the vector of the residuals is defined as:

$$r_{i,j} = a_{i,j}\varphi_{i,j+1} - b_{i,j}\varphi_{i,j} + c_{j,i}\varphi_{i,j-1} + d_{i,j} \tag{4.32}$$

Where *G* and *V* are the number of the grid points and the number of the variables, respectively.

Using the one-side difference scheme and imposing an artificial disturbance on the variables, the Jacobian matrix can be evaluated numerically as:

$$J_{i,j} = \frac{\tilde{r}_{i,j} - r_{i,j}}{\delta\varphi_i} \tag{4.33}$$

$$\tilde{r}_{i,j} = a_{i,j}\varphi_{i,j+1} - b_{i,j}\left(\varphi_{i,j} + \delta\varphi_i\right) + c_{j,i}\varphi_{i,j-1} + d_{i,j} \tag{4.34}$$

Where $\delta\varphi_i$ is the disturbance of the *i-th* variables and $\tilde{r}$ is the disturbed vector of the residuals.

Once the Jacobian matrix has been calculated, the algebraic system can be written using a matrix representation. For the *n-th* iteration it is expressed by the following relation:

$$\boldsymbol{J}^n \Delta\bar{\varphi}^{n+1} = -\bar{r}^n \tag{4.35}$$

The term $\Delta\bar{\varphi}^{n+1}$ is the correction term for the solution vector of the PDE's system. The method is iteratively applied until a sufficiently accurate value of φ is determined. This means that the method is applied till the values of the residuals are less than a convergence parameter (convergence parameter is usually of the order of 10^{-6}).

The solution technique implemented is named modified Newton method (MNM) since, in our implementation, the solution vector $\bar{\varphi}$ is not corrected for the entire correction term but the vector $\Delta\bar{\varphi}^{n+1}$ is relaxed using the parameter ω^n. Thus, the correction term is computed as:

$$\Delta\bar{\varphi}^{n+1} = -\omega^n \boldsymbol{J}^{-1}\bar{r}^n \tag{4.36}$$

where ω^n is the integration *steplenght*.

If only this variation is applied, the common Newton method (CNM) is called relaxed Newton method (RNM). The modification aims to increase the reliability of the solution method, but not necessary the cost per iteration. There are three possibilities as regards ω^n:

- If $\omega^n < 1$, the iteration step is said to be *underrelaxed* and ω^n is an *underrelaxation parameter.*
- $\omega^n > 1$, the iteration step is said to be *overrelaxed* and ω^n is an *overrelaxation parameter.*
- $\omega^n = 1$, for all *n*, RNM reduces to CNM.

The magnitude of the relaxing parameter is defined as that value that satisfies the following relations:

$$\|\bar{r}(\bar{\varphi}^n + \Delta\bar{\varphi}^{n+1})\|_2 \leq \|\bar{r}(\bar{\varphi}^n)\|_2 \quad (4.37)$$

Where

$$\|\bar{r}(\bar{\varphi}^{n+1})\|_2 = Max(|r_k^{n+1}|) \quad \forall \ k \in (1, G \cdot V) \quad (4.38)$$

In practise, the value of the parameter ω^n is calculated starting from $\omega^n = 1$ and multiplying this value by ½ till the equation (4.37) is satisfied. Thus, in our case, the integration *steplenght*ω^n is an *underrelaxation parameter.*

Another modification applied to the CNM regards the calculation of the Jacobian matrix. Indeed, since this computation is a high time-consuming task, the same matrix is maintained for several iteration steps. **Errore. L'origine riferimento non è stata trovata.** in Appendix C shows a flow chart which explains the criteria applied in the program for the evaluation of the relaxing parameter ω^n and the updating of the Jacobian matrix *J.*

4.2.1. Boundary and initial conditions

To solve the system of algebraic equations consistent boundary and initial conditions have to be defined. For the general time step *t+Δt*, the initial conditions are defined as the output from previous time step *t*. Regarding the boundary conditions, they are defined as follow:

- Top of the bed: the gradients of energy, density, flow rate and species concentration of both gaseous and solid phase are assumed to be zero (Neumann boundary conditions).
- Bottom of the bed: temperature, flow rate and species concentration of the gaseous phase are defined by the operating conditions. The gradients of solid variables are considered as zero.

5. Model validation

The intention of this chapter is the validation of the developed model against experimental results presented in literature. This task is not simple since it is difficult to determine all the parameters which should be set in a simulation, from the experimental work proposed.

5.1.Experimental rig

The experimental results chosen from literature to validate the model are those reported by Asthana et al [39]. The motivation of this choice lies in the fact that Asthana and his colleague Menard [57] give a better description of the experimental set up than the other researchers which have also conducted experiments on biomass combustion. For this reason, it was simpler to assign the right value to the many operational parameters that have to be set to perform a calculation.

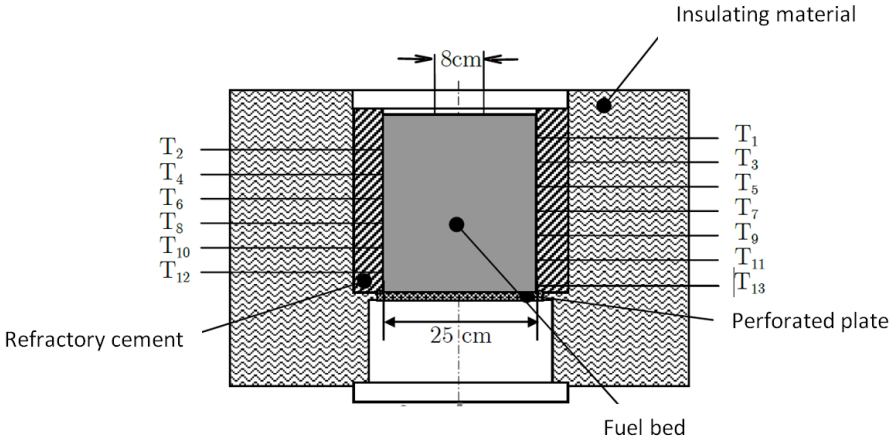

Figure 5 Schematic representation of the test rig of KLEAA [57].

The presented results were obtained in the experimental rig called KLEAA (Karlsruher Laboranlage zur Ermittlung des Abbrandverhaltens von Abfällen) located in Germany. The apparatus is composed of a cylindrical reactor with a diameter and a height of 25 and 30 cm, respectively. The reactor is equipped with thirteen thermocouples located along the axial direction at intervals of 1.5 cm. On the top of the bed an electrical device can heat the refractory material to a temperature of around 1130 K. The ignition of the charge is due to the

radiation from the hot hood. The system is installed on a scale to measure the weight variations of the fuel bed during the combustion process. Here only a schematic representation of the experimental test rig is shown in Figure 5, for a comprehensive description one refers to the work of Menard [57].

The charge utilized in the experiments was a mix of wood chips and inert material. The ultimate analysis of the wood in terms of mass fraction on dry basis and the experimental condition of the test are reported in Table 7 and Table 8.

Table 7 Ultimate analysis of the wood (mass fraction on dry basis).

C	O	H	N	S	Ash
47.3	45.3	5.7	0.33	0.17	1.2

Table 8 Experimental conditions.

m_g [kg/m^{2}s]	T_g [K]	LHV [MJ/kg]	ρ_b [kg/m^3]	Moisture %	Ash %
0.11	298	9.2	250	23.8	20.5

Where m_g is the inlet air flow rate, ρ_b the specific mass of the biomass bed. Moisture and ash content are expressed in mass fraction on wet basis and the last one takes into account also the inert matter added to the charge.

5.2.Comparison of experimental and numerical results

A comparison between the experimental results reported by Menard [57] and the results of the simulation performed is reported in Figure 6, which shows the bed temperature trends at different bed heights. The values reported in the legend stand for the distances from the grate. Focusing the attention on the experimental outcomes, it can be noted that during the first moments the heating up of the upper layers of the bed is taking place. The measured temperatures remain at the room value as a result of the low conductivity of the wood and the continuous cooling of the supplied air. The steep increase of the temperature is due to the propagation of the flame front towards the fuel bed. When the flame front reaches the plane where a thermocouple is located, the measured temperature rises quickly from the initial value (room temperature) to a value around 1000 K. Once the flame front has passed, the temperature remains almost constant till char burnout. When the char burnout occurs the measured temperature rises again to a value around 1300 - 1400 K, with peaks at almost 1600 K.

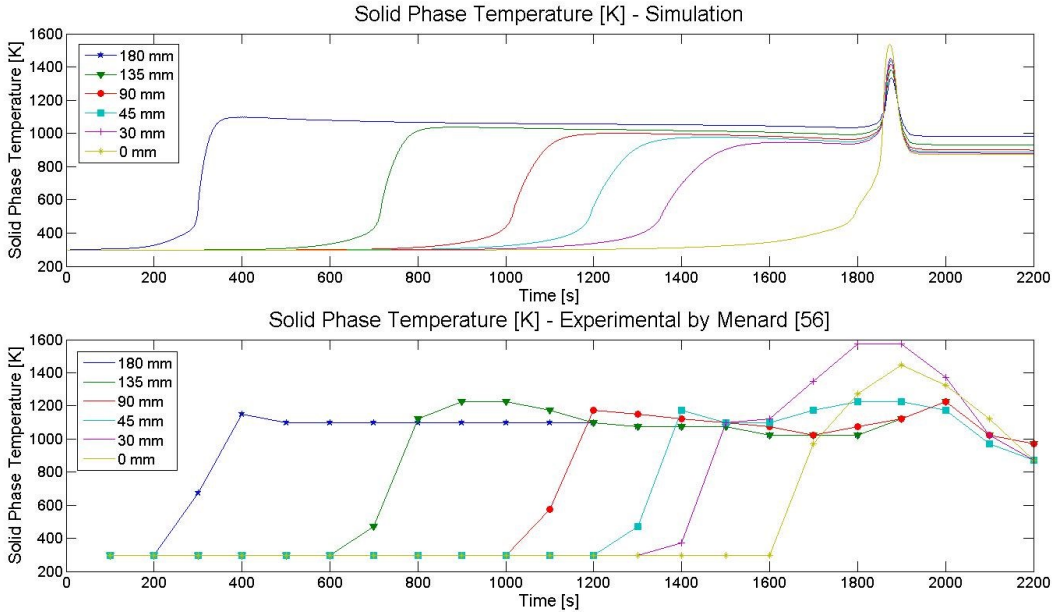

Figure 6 Comparison between experimental and calculated bed temperatures profiles. The values in the legend stand for distances from the grate.

As can be seen in Figure 6, the temperature profiles predicted by numerical simulation catch the qualitative trend of the temperatures measured during the experiment well. The predicted values are also in agreement with the measured ones. The differences between the calculated and the measured temperature can be attributed to the covering shells of the thermocouples which increase their thermal inertia. A part from that, a good estimation of the propagation rate of the reaction front can be observed. Indeed, the sudden increase of the temperature at different bed heights, as well as the char burnout, are predicted at the right time.

5.3.The equivalence with the grate combustion

This thesis proposes the study of biomass combustion in moving grate furnaces through the use of a 1-D transient model. This is clearly an approximation, but as noticed by different authors [23], [34], [37], [38], [40] and [42], since the physical variables gradients in the direction of the bed height are much higher than those in the direction of the bed length, thermal and mass exchanges in the grate direction can be neglected.

Considering these observations, the study of the combustion process in moving grate furnaces can be reduced to the observation of a vertical column of fuel that is moving along the grate inside the furnace. Thus, a 1-D transient system can be used to model the thermal conversion of the biomass fuel inside the combustion chamber. Figure 7 graphically shows the conversion from spatial to time coordinate.

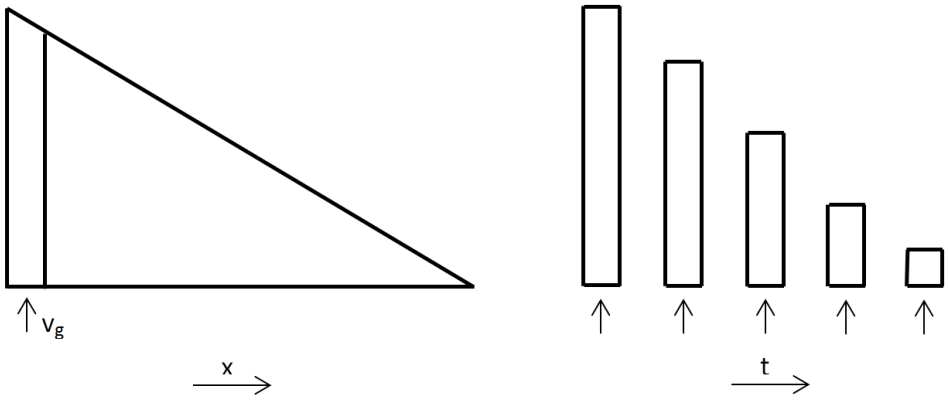

Figure 7 Biomass bed: from spatial to time coordinate.

If the forward movement of fuel on the grate takes place with a constant velocity, the spatial position inside the furnaces is directly proportional to the time and the following simple relation can be used to link time and position.

$$x = v_{grate} \cdot t \tag{5.1}$$

6. Simulation results

In this chapter the results of the simulations performed are reported. The calculations were done varying the operational conditions in terms of inlet air flow rate and temperature. As fuel, a typical woody biomass was chosen and, for the same type of biomass, the moisture content was varied. In the first part of the chapter the simulation settings are introduced, in the second part the simulation results are presented and discussed.

6.1. Simulation settings

The simulations have been performed with the aim of understanding the influence of the principal operational conditions on biomass combustion. A typical configuration, hereinafter referred to as *Simulation 1*, was chosen as a reference case (see Table 9). Referring to this configuration, the air flow rate and the inlet air temperature were changed. The same simulations have been performed also with a different value of moisture content of the woody biomass fuel.

Table 9 and Table 10 resumes the simulation settings. The values of the ultimate analysis are expressed in mass fractions on dry basis, whereas the values of the proximate analysis are mass fractions on wet basis. The dry bed density states for the density of the biomass bed considering its porosity, the low heating value (LHV) refers to the wet biomass and the pyrolysis yield are expressed in mass factions of volatile matter.

Table 10 shows how the operational parameters were varied through the different simulations. The values that are not reported were kept equal to *Simulation 1.*

6.2. Comparison of the simulation results

The results of the simulations are presented in the following figures. The figures are organised to compare the outcomes of two simulations with the same operational parameters but different amount of moisture in the biomass fuel (30 and 40 %). This means that *Simulation 1* is compared with *Simulation 4*, *Simulation 2* with *Simulation 5* and *Simulation 3* with *Simulation 6*.

The variables are presented with the following order: temperature and species mass fractions of the solid phase and, below, flow rate and species mass fractions of the gaseous phase. The

figures present a double abscissa axes: the lower one reports the time of the process and the upper one the position along the grate defined using a constant grate velocity of $5.5*10^{-4}$ m/s.

Table 9 Simulation settings for the reference case.

Simulation 1			
Biomass			
Ultimate Analysis %		Proximate Analysis %	
C	48	Moisture	30
H	6	Volatile	57.4
O	44	Fixed Carbon	11.2
Ash	2	Ash	1.4
Process Parameters			
Initial Solid Temp.	298 K	Flow Rate	0.11 kg/m^{2}s
Initial Gas Temp.	298 K	Wall Temperature	1123 K
Dry bed density	205 kg/m^3	LHV	MJ/kg
Pyrolysis Yield			
α_{CO}	0.259	α_{CO2}	0.284
α_{H2O}	0.175	α_{CH4}	0.282

Table 10 Simulation settings.

Simulations 2		**Simulation 5**	
Flow Rate	0.08 kg/m^{2}s	Moisture	40 %
Simulation 3		Flow Rate	0.08 kg/m^{2}s
Initial Gas Temp.	373 K	**Simulation 6**	
Simulation 4		Moisture	40 %
Moisture	40 %	Initial Gas Temp.	373 K

6.2.1. Simulation 1 Vs. Simulation 4

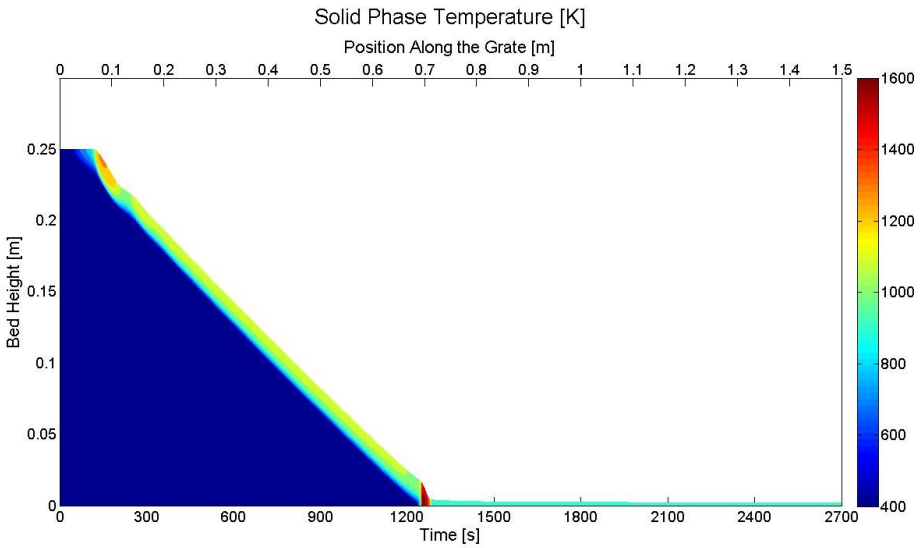

Figure 8 Solid phase temperature contour in *Simulation 1.*

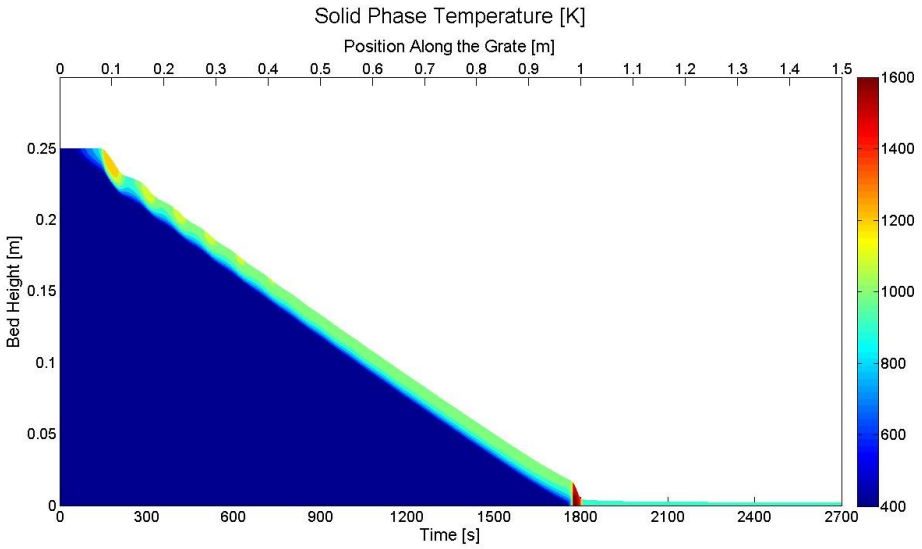

Figure 9 Solid phase temperature contour in *Simulation 4.*

Figure 8 and Figure 9 represent the contour of the biomass bed temperature against the process time and the position along the grate. The reduction in the bed height shown in these figures, as well as in the following ones, is related to the char consumption in accordance with the relation (3.23). Looking at these figures the first thing that stands out is the difference in the burnout time (or position along the grate) of the bed. Indeed, in Figure 8 the burnout time is approximately 1250 s, instead in Figure 9 it is around 1770 s. This delay in the completion of the combustion process is obviously due to the higher moisture content in *Simulation 2*, since the other operational parameters, such as inlet gas flow rate and temperature, were kept constant. The higher moisture content of the biomass fuel causes a longer drying time and lower bed temperature. The longer drying time is due to the higher quantity of moisture that has to be driven out of the biomass, but also to the lower bed temperature itself. Indeed, the evaporation rate is directly connected to the bed temperature through an Arrhenius law, thus, a lower evaporation rate corresponds to a lower temperature .

The lower value of the temperature can be explained with the lower concentration of CO and CH_4 in the gaseous phase (see Figure 20 and Figure 21) and the slower devolatilization rate that determines a lower amount of char available for combustion. As a consequence, a lower amount of combustibles (both gaseous and solid) causes a reduced amount of generated heat. Generally speaking, it is clear that a lower fuel bed temperature results in a reduction of the rate of the different phenomena that occur during the combustion process and determine, consequently, a longer burnout time.

The region with the highest temperature (around 1600 K) is the region where the char burns at a higher rate. The rise in the char combustion rate is due to the higher oxygen quantity available for char oxidation. This happens because drying and devolatilization are ended and the supplied oxygen is not diluted by other species coming from previous phenomena. Moreover oxygen is not consumed by CO and CH_4 combustion anymore.

Figure 10 and Figure 11 show the moisture mass fraction, whereas Figure 12 and Figure 13 show the volatile mass fraction in the fuel bed. The initial moisture content in *Simulation 4* is higher than in *Simulation 1*, as a consequence the initial volatile mass fraction in *Simulation 4* is lower when compared to *Simulation 1*. Apart from this aspect, that simply depends on the biomass characteristics, it is possible to notice the presence of a drying and a devolatilization front which move downwards through the fuel bed.

During drying the temperature of the biomass fuel remains around 373 K (see Figure 8 and Figure 9) since all the heat supplied to the fuel is utilized to expel the moisture. In this phase the volatile mass fraction increases as shown in Figure 14 and Figure 15. The increase in the volatile mass fraction is due to the fact that devolatilization has not occurred yet because of the low fuel temperature. Once the drying front has passed, the biomass temperature can rise and the release of the volatile matter can take place. The moisture and volatile content above the drying and devolatilization front are zero and only char and ash are still present in the solid phase.

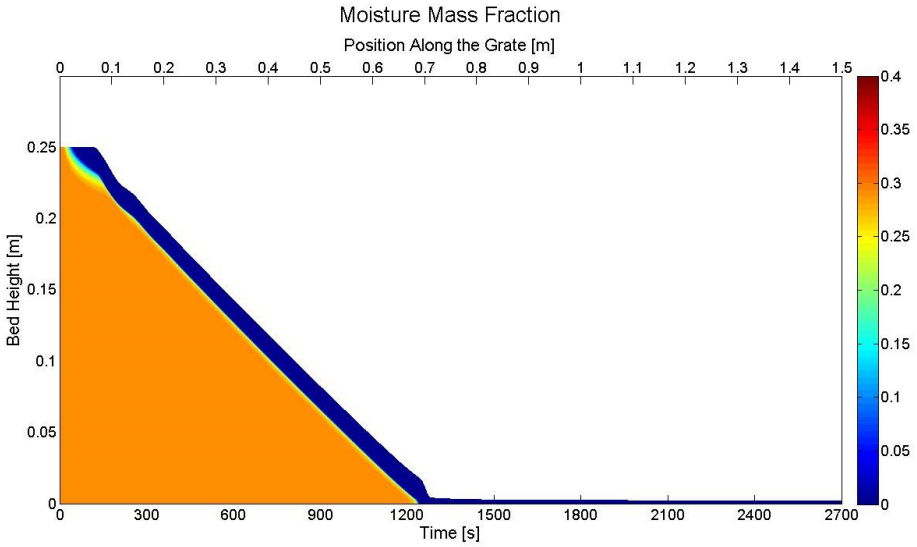

Figure 10 Solid phase moisture mass fraction contour in *Simulation 1.*

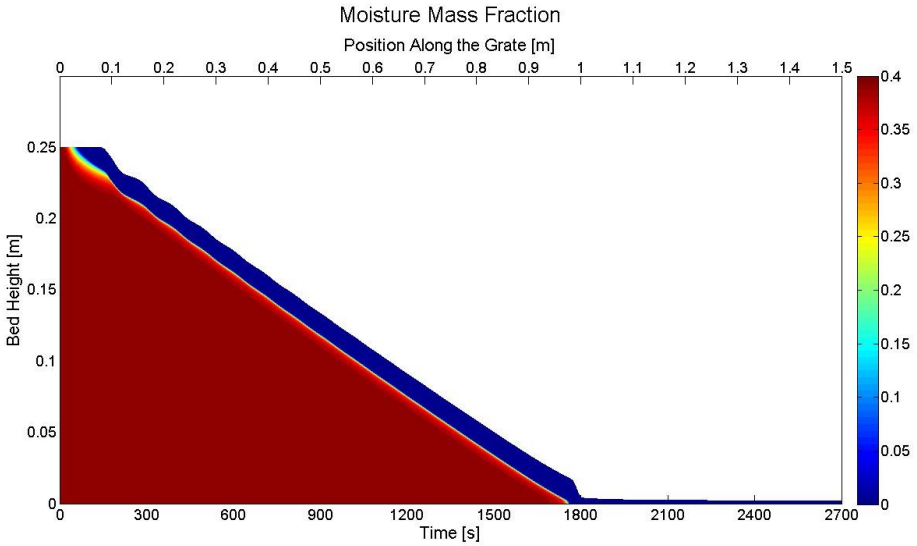

Figure 11 Solid phase moisture mass fraction contour in *Simulation 4.*

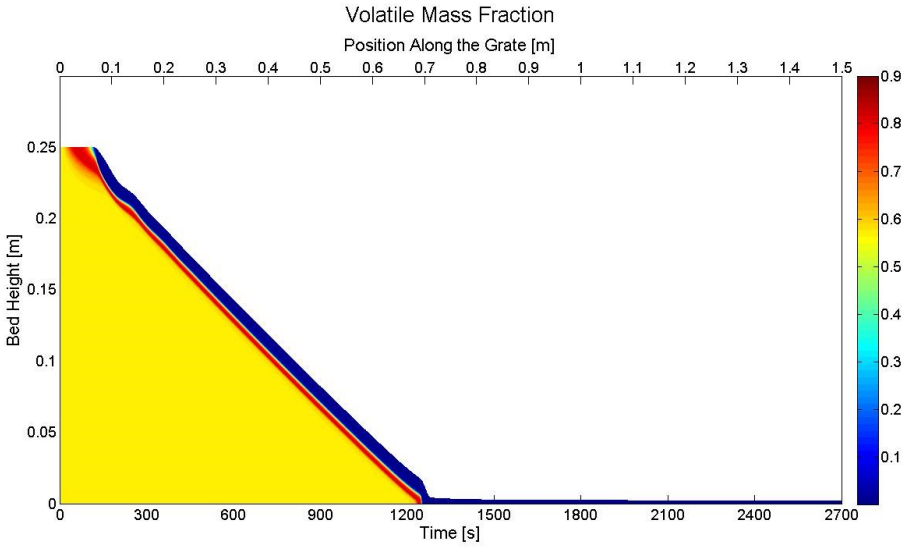

Figure 12 Solid phase volatile mass fraction contour in *Simulation 1.*

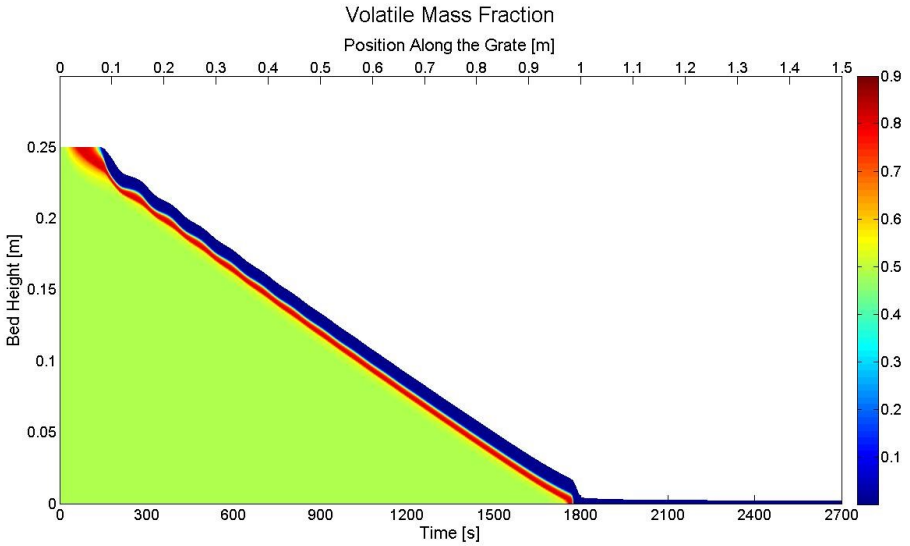

Figure 13 Solid phase volatile mass fraction contour in *Simulation 4.*

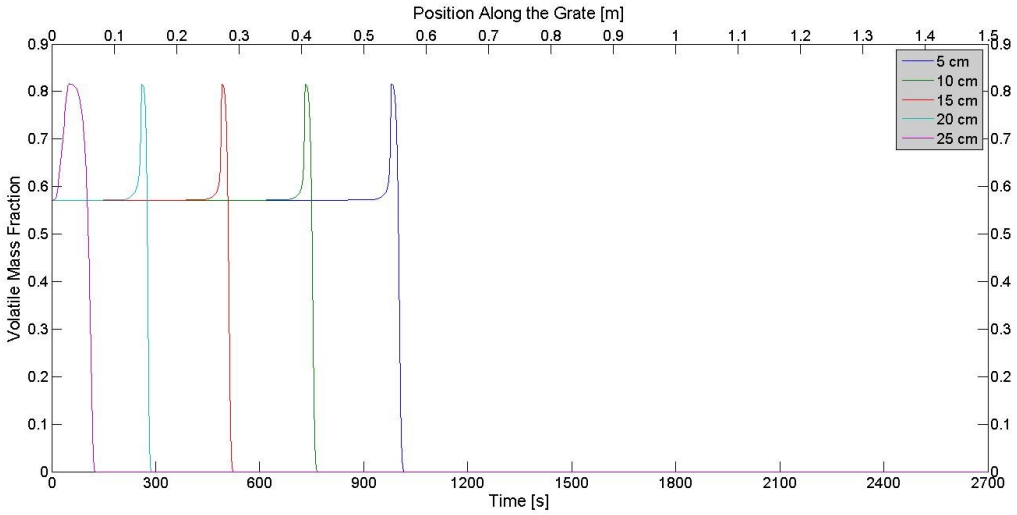

Figure 14 Solid phase volatile mass fraction at different heights from the grate in *Simulation 1.*

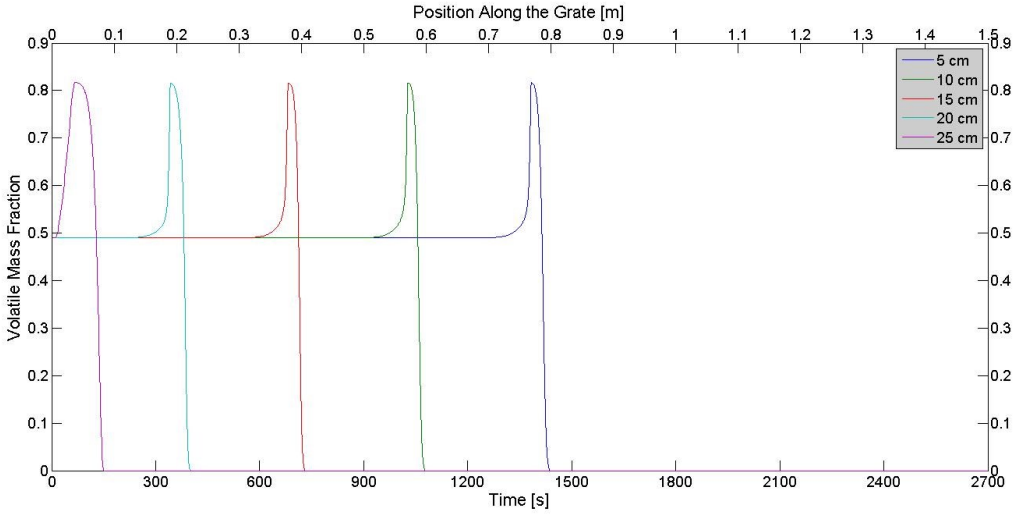

Figure 15 Solid phase volatile mass fraction at different heights from the grate in *Simulation 4.*

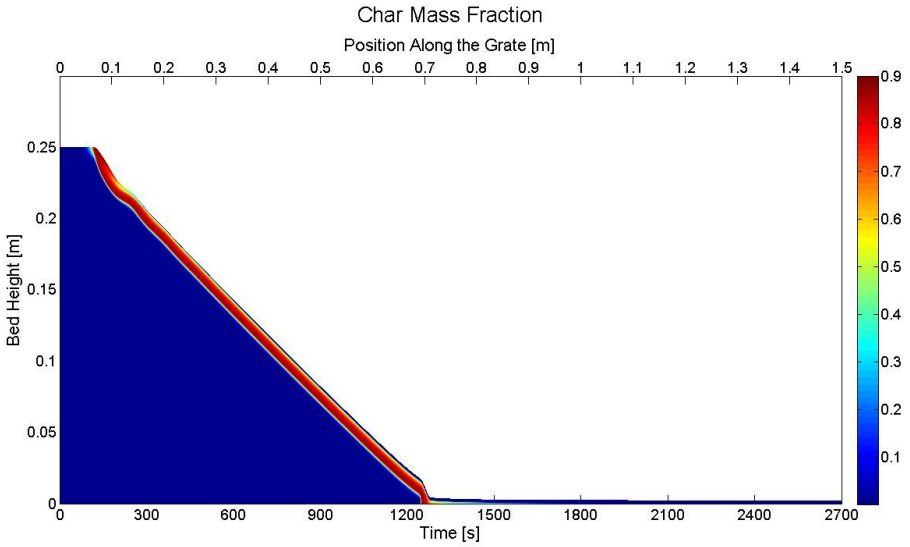

Figure 16 Solid phase char mass fraction contour in *Simulation 1.*

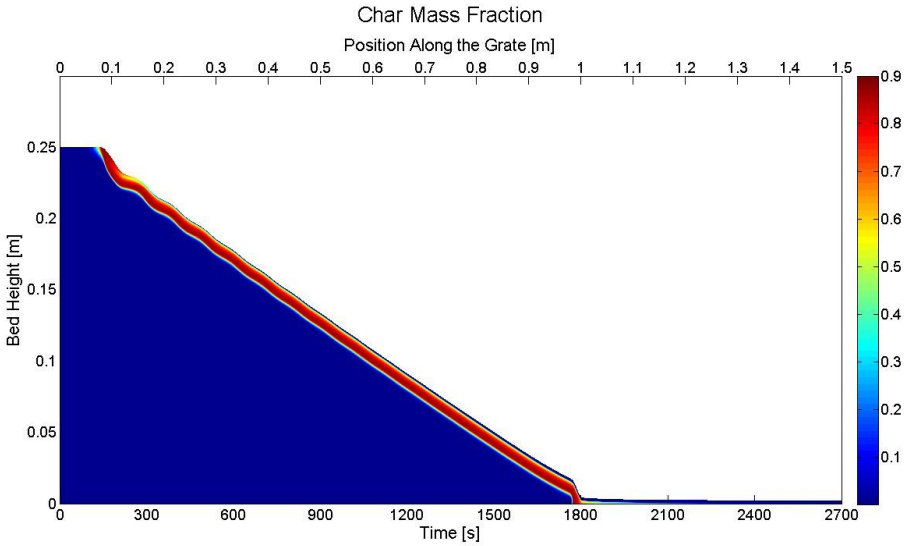

Figure 17 Solid phase char mass fraction contour in *Simulation 4.*

Figure 16 and Figure 17 show the char mass fraction in the two simulations taken into account. Char is the carbonaceous residue which remains in the solid phase after drying and devolatilization, for this reason its initial mass fraction is considered to be zero. Once formed char can react with the oxygen supplied from under the grate and can release heat allowing the increase of the biomass temperature. When drying and devolatilization are still taking place, the amount of oxygen available for char combustion is reduced due to the dilution by the released gases and the consumption by CO and CH_4 reactions. When these phenomena have ended, the availability of the oxygen for char combustion increases and char burns at a higher rate. This is evident in Figure 16 and Figure 17 by the steep reduction in the bed height and in Figure 8 and Figure 9 where a significant increase of the bed temperature is detected.

With the aim of interpreting the coming figures a brief description of the combustion environment, in which biomass is fed, is necessary. When biomass fuel enters the combustion chamber it is exposed to the radiative heat source by the flames and furnace walls. This causes a rapid increase of the temperature of the first layers of the fuel and, as a consequence, a rapid release of moisture and volatile matter with a sudden growth of the gases flowing out of the bed.

Figure 18 and Figure 19 depict the gas flow rate along the biomass bed surface and show how the flow rate increases sharply due to the high drying and devolatilization rates that characterize the first centimeters of the grate. Once the first layers of the fuel are dried and the volatile matter is driven out, the gas flow rate decreases and assumes, approximately, a constant value. In this second phase, drying and devolatilization rates are lower when compared to the initial phase since the effect of the radiative heat source is reduced due to the heat absorption of the upper solid layers. The temperature of the deeper solid layers, as well as the drying and devolatilization rates, mainly depends on the heat released by char and gases combustion in the nearby zones. When all the combustion phenomena have ended the gas flow rate returns to the initial value.

The main difference between Figure 18 and Figure 19 is the value of the flow rate after the initial peak. In Figure 18 this value is higher than in Figure 19, since, as explained at the beginning of the paragraph, the value of the solid temperature is higher in *Simulation 1* than in *Simulation 4.* This contributes to a higher rate of the drying and devolatilization and thus to a higher gas flow rate.

The species mass fractions on the top of the bed are shown in Figure 20 Figure 21. Also in this case the figures show a first stage where a rapid increase of CO CO_2 CH_4 and H_2O mass fraction is detected. The reasons of these trends are the same given to explain the gas flow rate behaviour. At the same time, the O_2 mass fraction undergoes a sharp decrease, due to dilution with the other gaseous species and consumption operated by combustion reactions. When drying, devolatilization and char combustion are ended the gaseous species concentration assume again the ambient value.

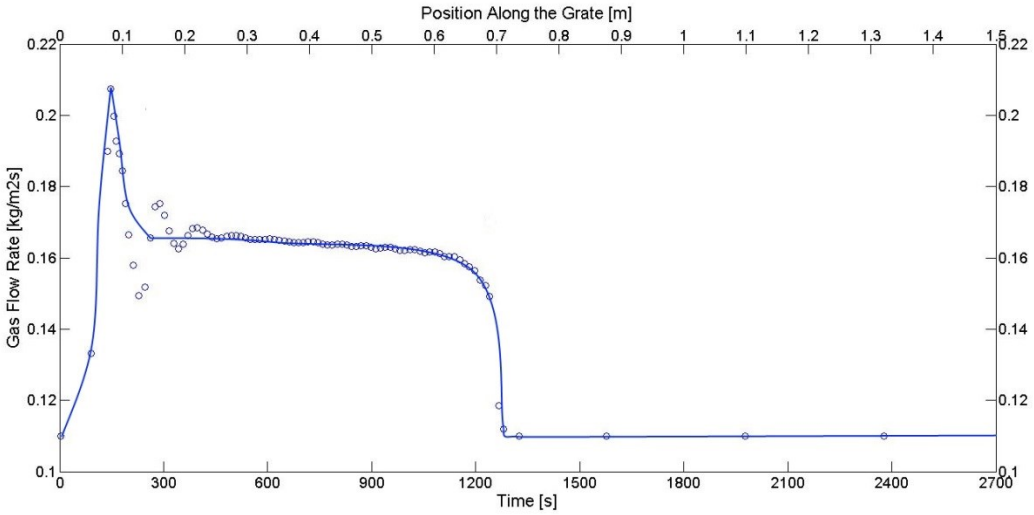

Figure 18 Gas flow rate above the bed surface in *Simulation 1.*

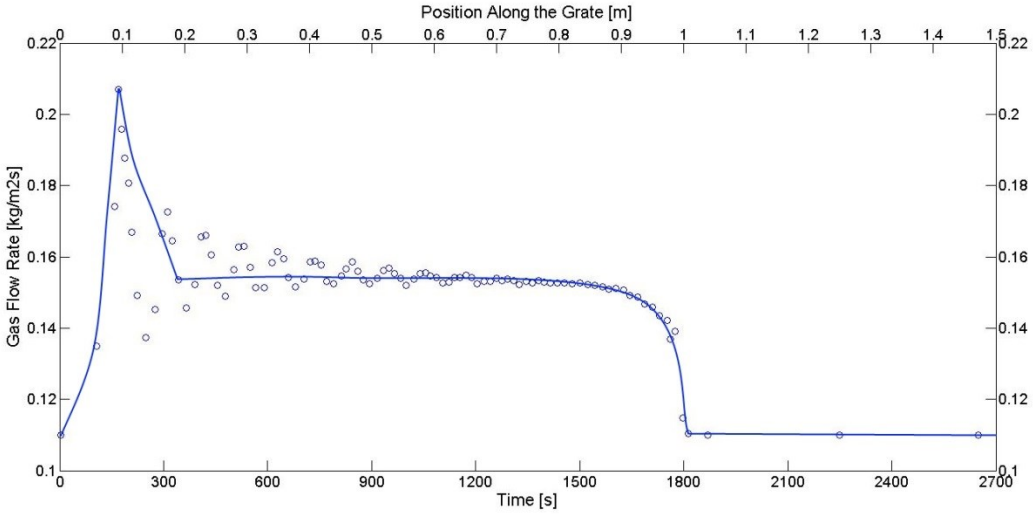

Figure 19 Gas flow rate above the bed surface in *Simulation 4.*

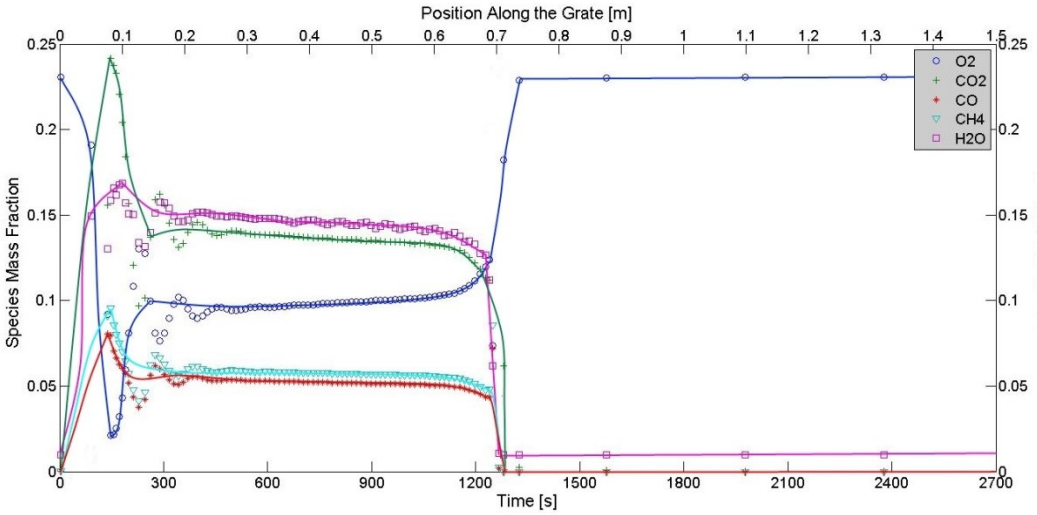

Figure 20 Gaseous species mass fraction above the bed in *Simulation 1.*

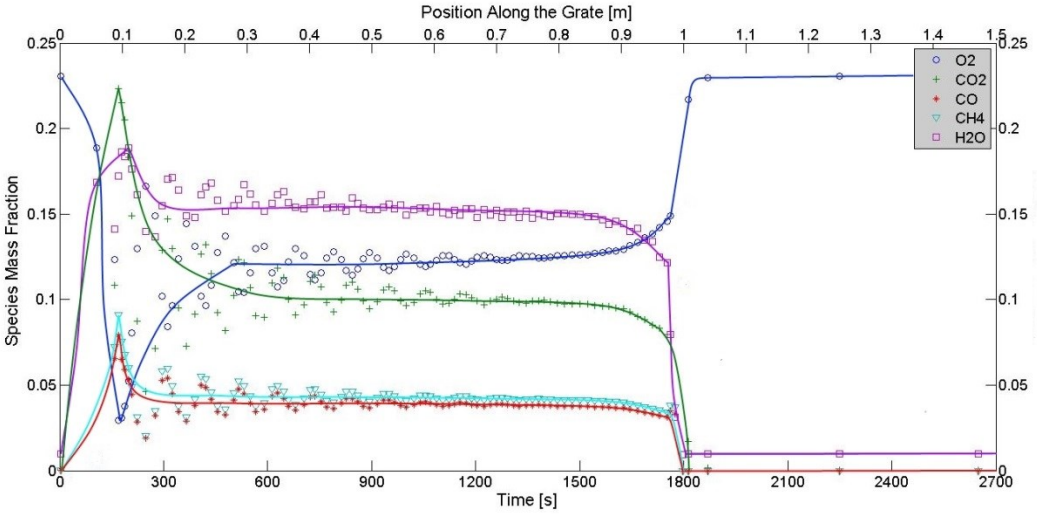

Figure 21 Gaseous species mass fraction above the bed in *Simulation 4.*

6.2.2. Simulation 2 Vs. Simulation 5

As reported at the beginning of this chapter, *Simulation 2* and *Simulation 5* have been performed with the same type of biomass as of *Simulation 1* and *Simulation 4*, respectively. The unique difference with the previous cases is related to inlet air flow rate, which has been reduced with 20 %, from 0.11 to 0.088 kg/m^{2}s. The sequence of phenomena is exactly the same as *Simulation 2* and *Simulation 5*, as well as the explanations of the differences between the outcomes obtained using the two different types of biomass.

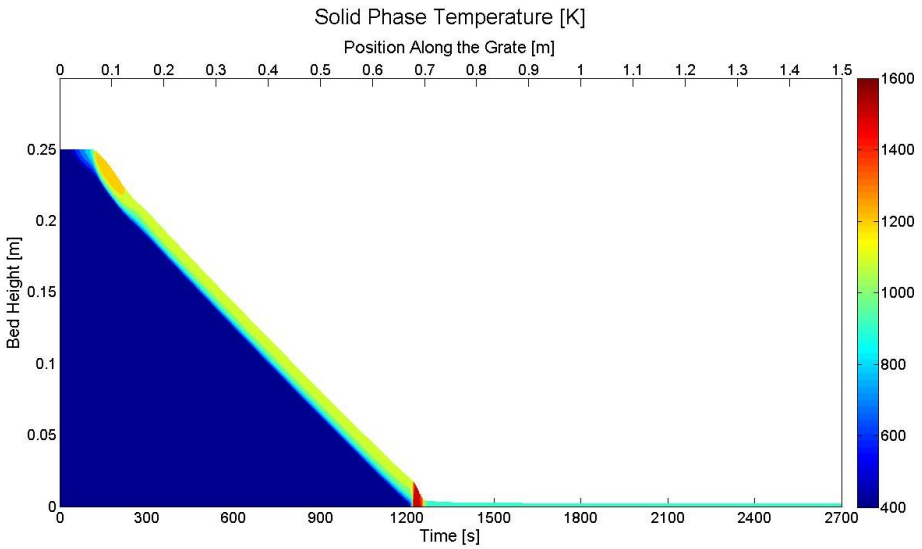

Figure 22 Solid phase temperature contour in *Simulation 2.*

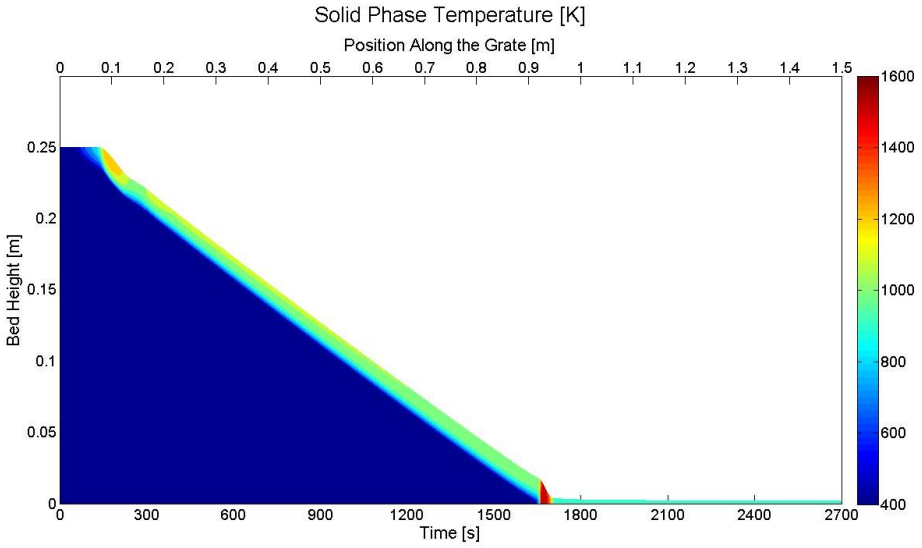

Figure 23 Solid phase temperature contour in *Simulation 5.*

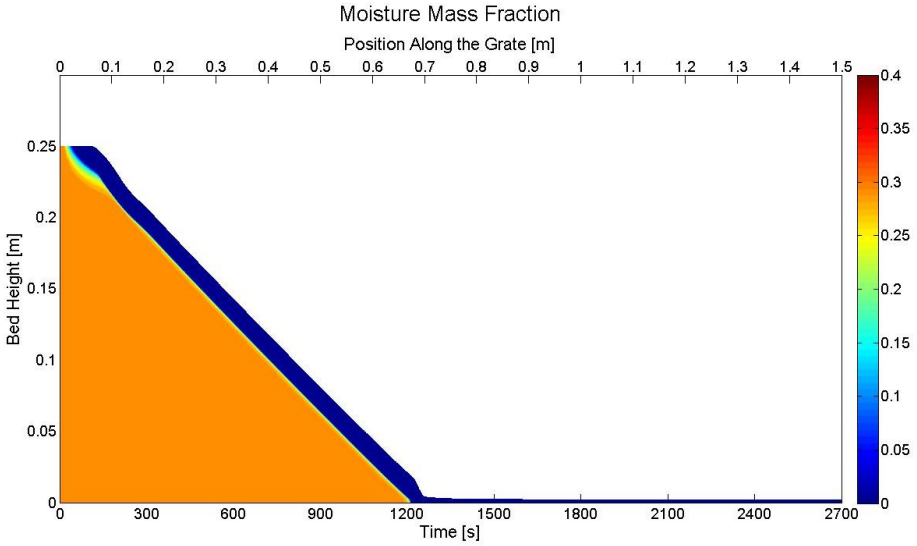

Figure 24 Solid phase temperature contour in *Simulation 2.*

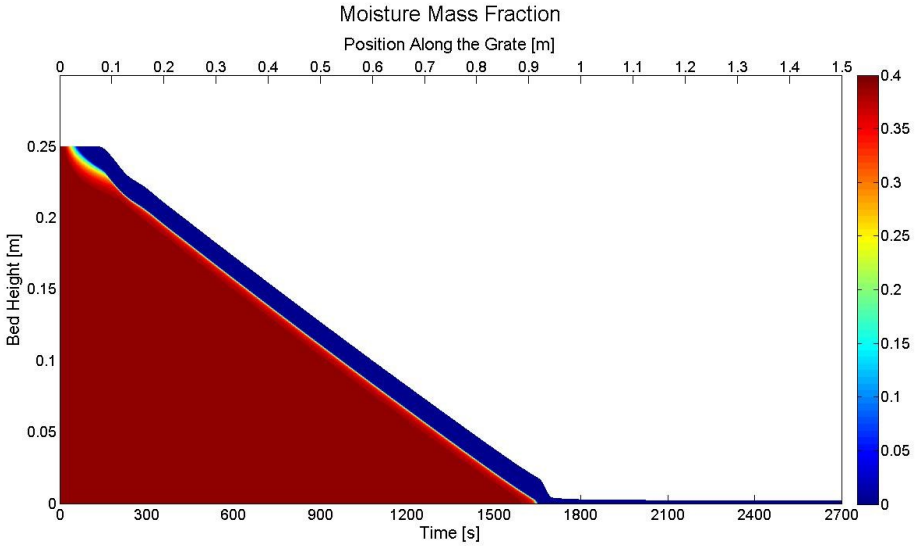

Figure 25 Solid phase moisture mass fraction contour in *Simulation 5.*

For this reason, no more clarifications on these aspects will be given, but only the differences depending on the diverse operational conditions will be discussed.

Comparing Figure 8 with Figure 22 and Figure 9 with Figure 23 the main difference that stands out is the reduction of the combustion time for the cases with a reduced inlet air flow rate (0.088 instead 0.11 kg/m^{2}s of the reference case). This reduction is less evident in the comparison of Figure 8 with Figure 22, where the combustion time passes approximately from 1250 to 1220 s, but it is clearly recognisable in the comparison of Figure 9 with Figure 23,

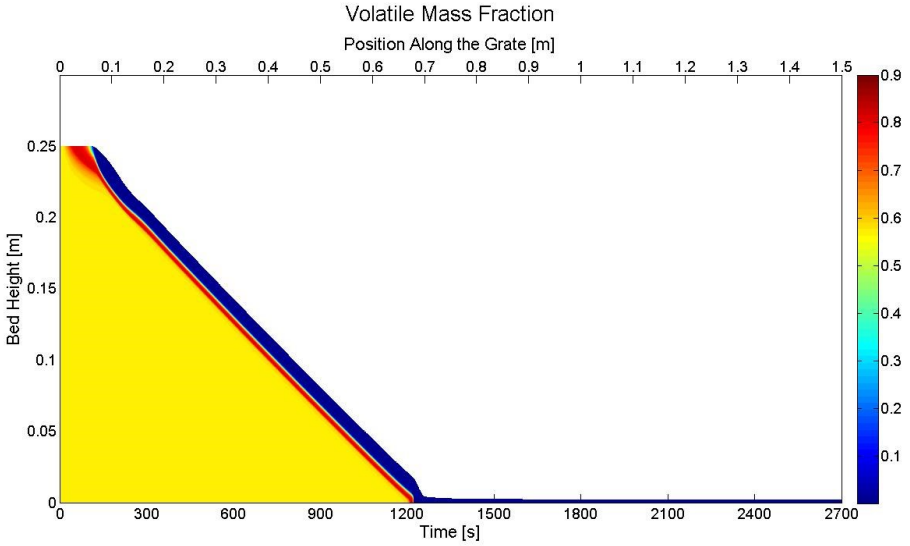

Figure 26 Solid phase volatile mass fraction contour in *Simulation 2.*

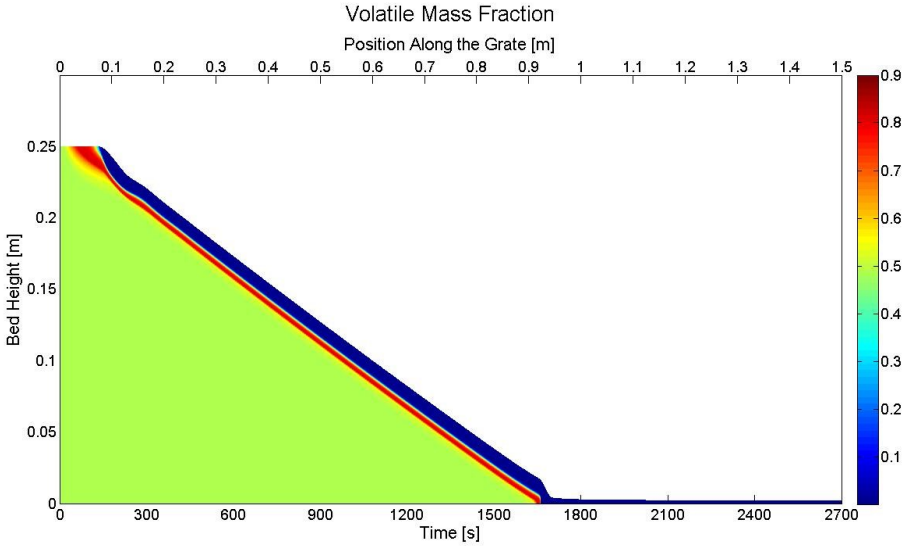

Figure 27 Solid phase volatile mass fraction contour in *Simulation 5.*

where this value passes from 1770 to 1660 s, with a reduction of more than 100 s. This behaviour can be explained by the reduction of the convective cooling operated by the gases flowing through the bed. The reduced cooling allows higher temperatures inside the bed and, as a consequence, permits higher combustion rates since all the phenomena are governed by an Arrhenius law. This mechanism is possible because the combustion process is in the reaction limited field. Indeed, referring to the work of Shin and Choi [23], it is possible to identify three different fields: oxygen limited, reaction limited and the extinction by convection field.

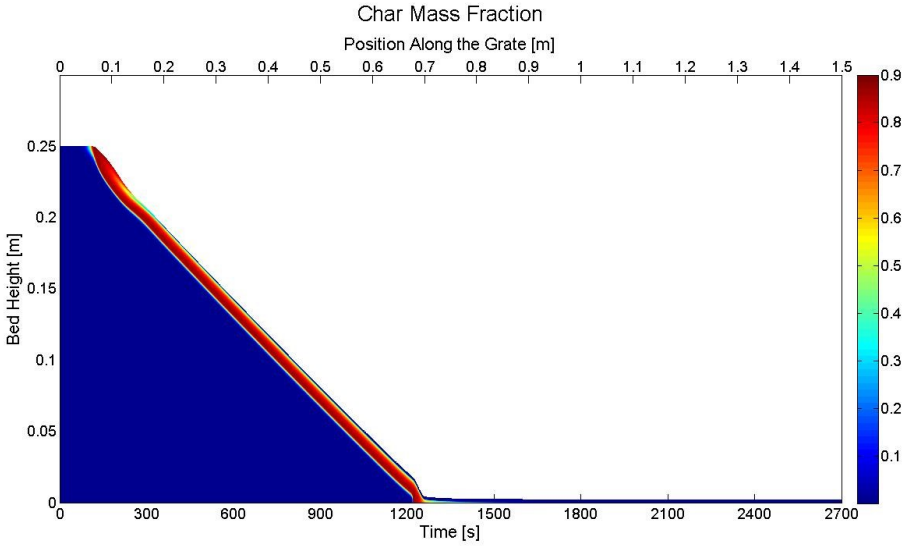

Figure 28 Solid phase char mass fraction contour in *Simulation 2.*

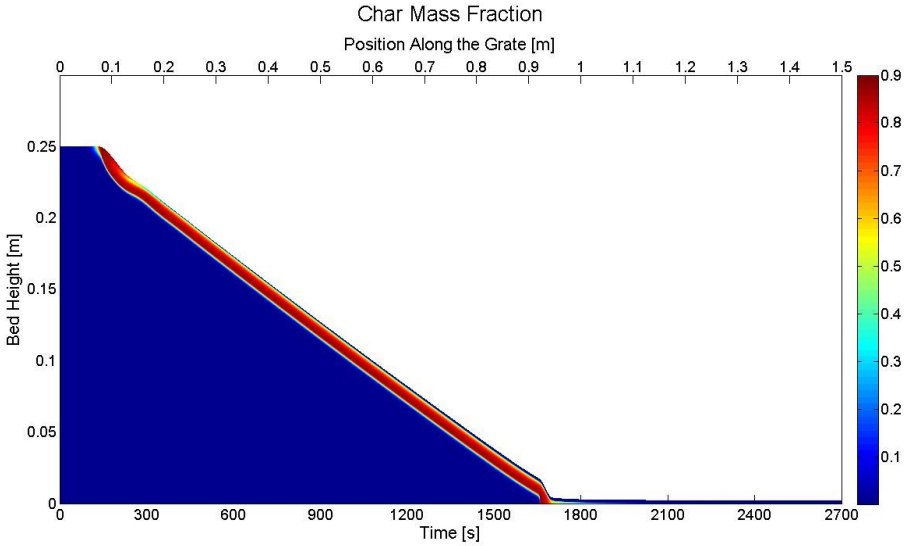

Figure 29 Solid phase char mass fraction contour in *Simulation 5.*

In the oxygen limited field the combustion rate is determined by the oxygen supply rate. If more air is supplied, combustion rate increases till a limit due to the chemical kinetics rates of the involved reactions and the increased convective cooling by the air. In the reaction limited regime the flame can be sustained as long as the heat release rate in the bed exceeds the convective cooling by the air. This means that a reduction of the inlet flow rate, when the process is reaction limited, determines an increase of the combustion rate till the regime

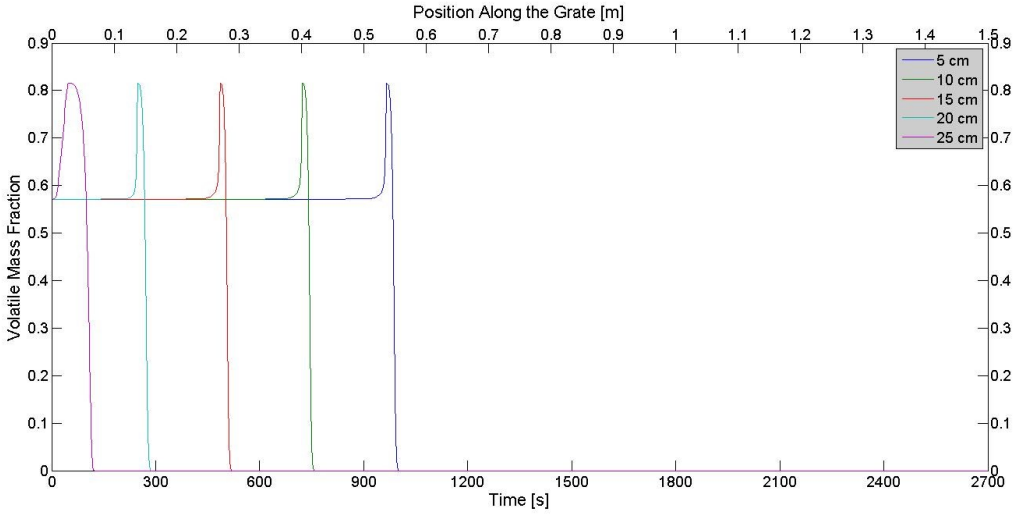

Figure 30 Solid phase volatile mass fraction at different heights from the grate in *Simulation 2.*

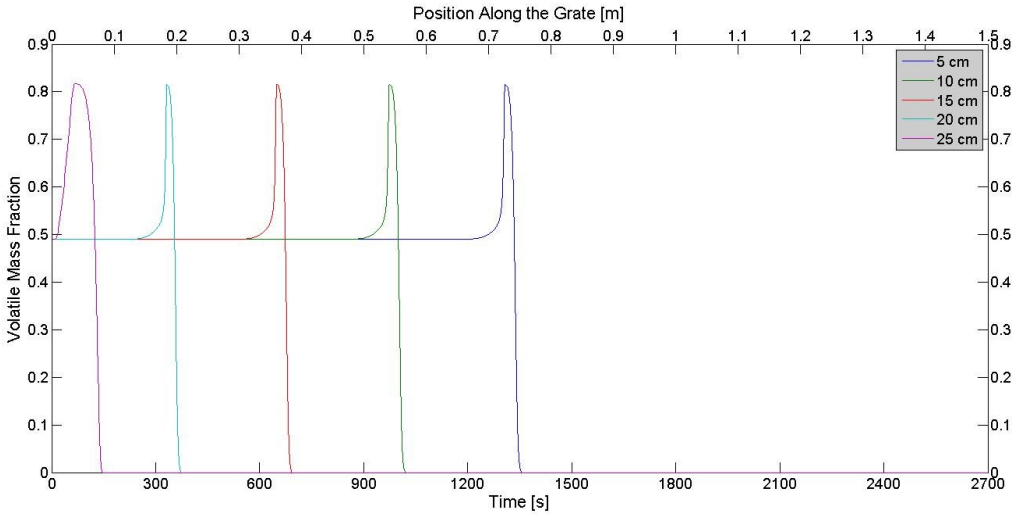

Figure 31 Solid phase volatile mass fraction at different heights from the grate in *Simulation 5.*

passes to oxygen limited. Anyway, high reductions of the inlet air flow rate to achieve faster combustion rates are not recommended since this alternative reduces the amount of oxygen available to complete the gaseous combustion outside the solid bed and reduces turbulence, mixing and combustion rates of the gaseous species.

From Figure 24 to Figure 31, the contours and trends of the different variables, such as moisture, volatile and char mass fraction are presented. Also in this case a reaction front that moves from the top to the bottom of the bed is easily recognisable.

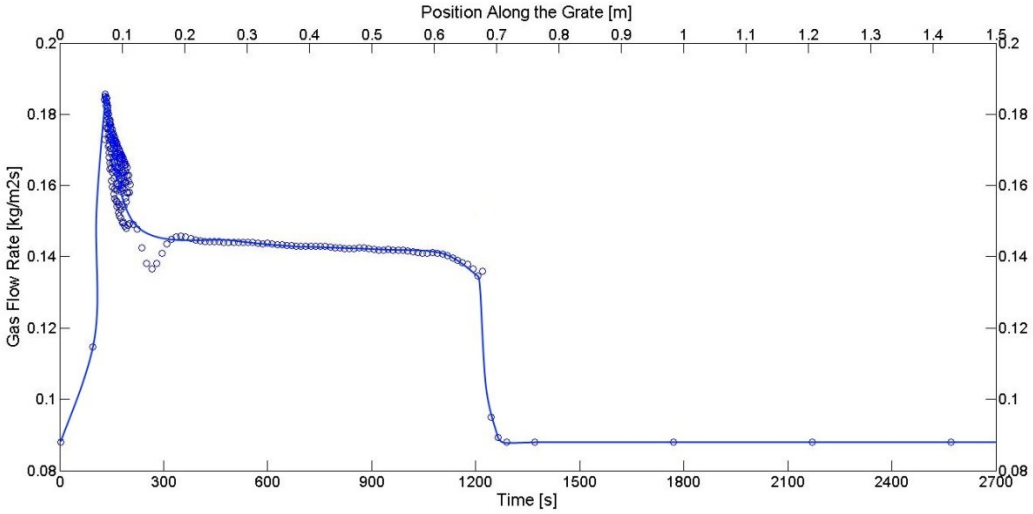

Figure 32 Gas flow rate above the bed surface in *Simulation 2.*

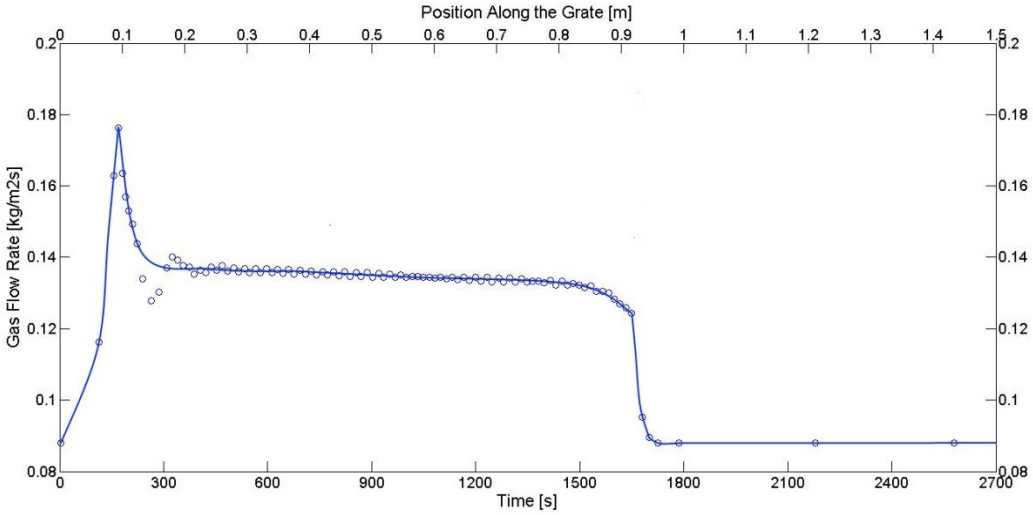

Figure 33 Gas flow rate above the bed surface in *Simulation 5.*

Figure 32 and Figure 33 represent the gas flow rate along the biomass bed surface. As well as in the previous simulations, even in this cases, it is possible to recognise three zones. The first zone characterized by the peak due to the high drying and devolatilization rates, the middle zone where the flow rate is approximately constant and the zone where the gas flow rate goes back to the initial value since the combustion process has ended. Comparing Figure 32 and Figure 33 with Figure 18 and Figure 19, it is immediately evident that the value of the inlet flow rate in *Simulation 2* and *5* is 20 % lower. This results in a lower gas flow rate along the bed surface.

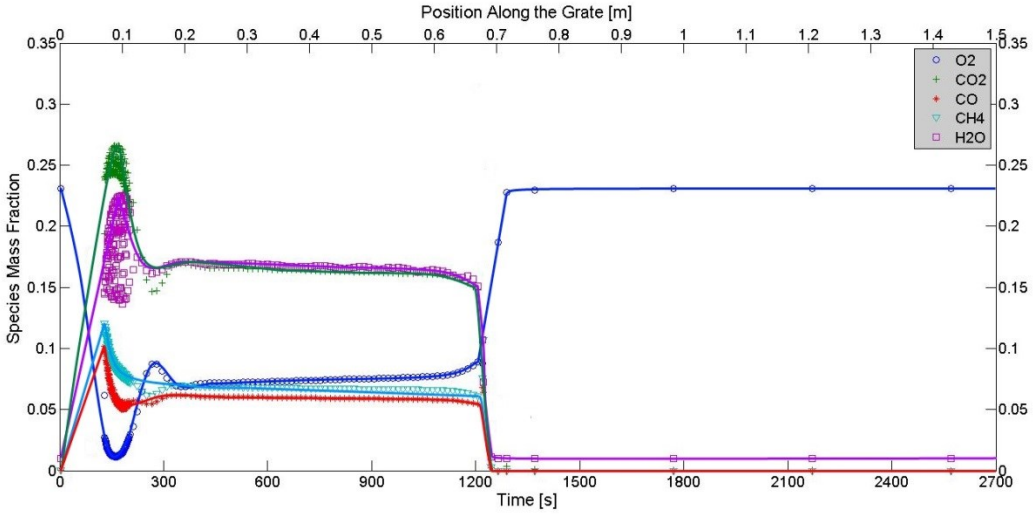

Figure 34 Gaseous species mass fraction above the bed in *Simulation 2.*

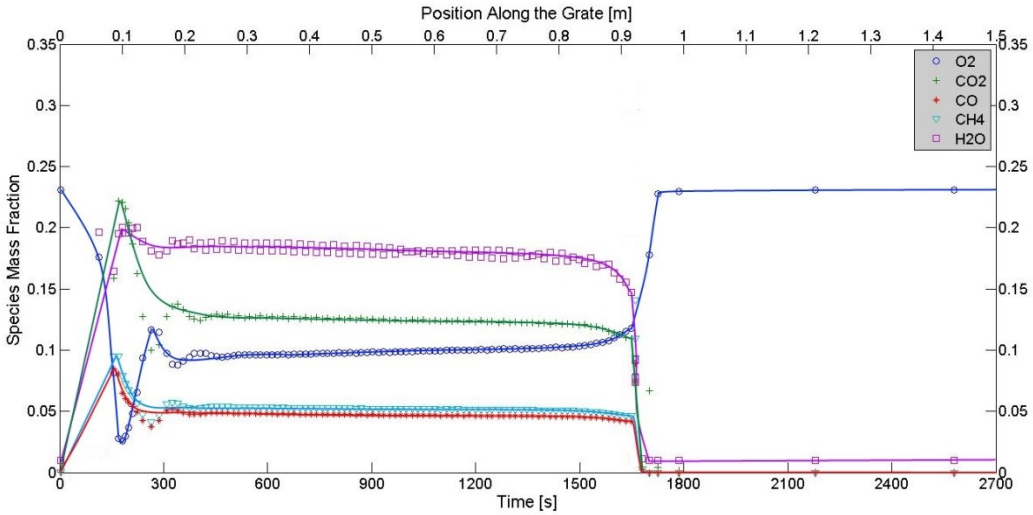

Figure 35 Gaseous species mass fraction above the bed in *Simulation 5.*

Figure 34 and Figure 35 show the species mass fractions on the top of the bed. As can be seen, the oxygen mass fractions in the middle zone are lower than those ones in Figure 20 and Figure 21. This is due to the lower value of the inlet flow rate and higher combustion rate. Moreover, these figures confirm what has been said earlier regarding the combustion field. Indeed, they show that the combustion process is characterized by a reaction limited field, since not all the supplied oxygen is consumed by the oxidation reactions inside the bed.

6.2.3. Simulation 3 Vs. Simulation 6

It is well known that heat recovery from low temperature heat sources is an important method to increase the efficiency of power plants. In the case of biomass power plants, heat recovery can be represented by air pre-heating using the heat power from flue gases or residual water steam. In *Simulation 3* and *Simulation 6* this possibility has been investigated.

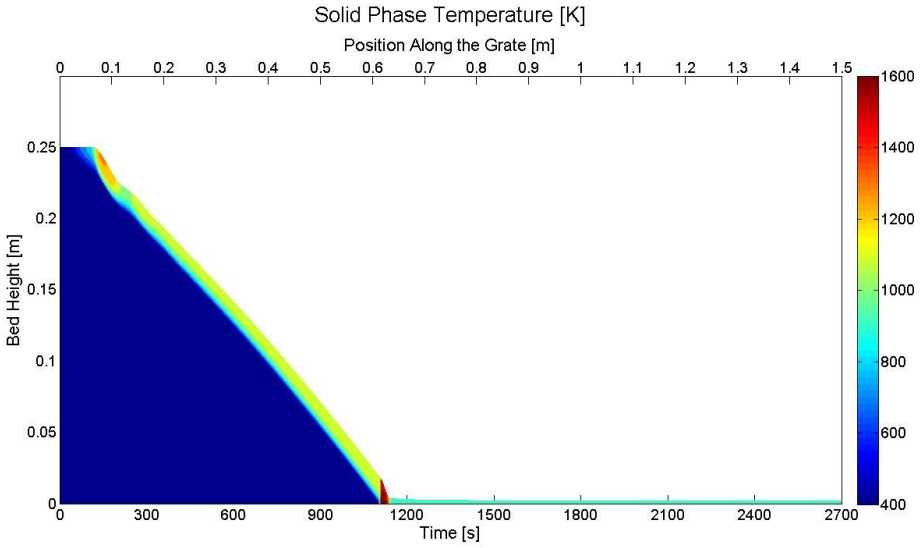

Figure 36 Solid phase temperature contour in *Simulation 3.*

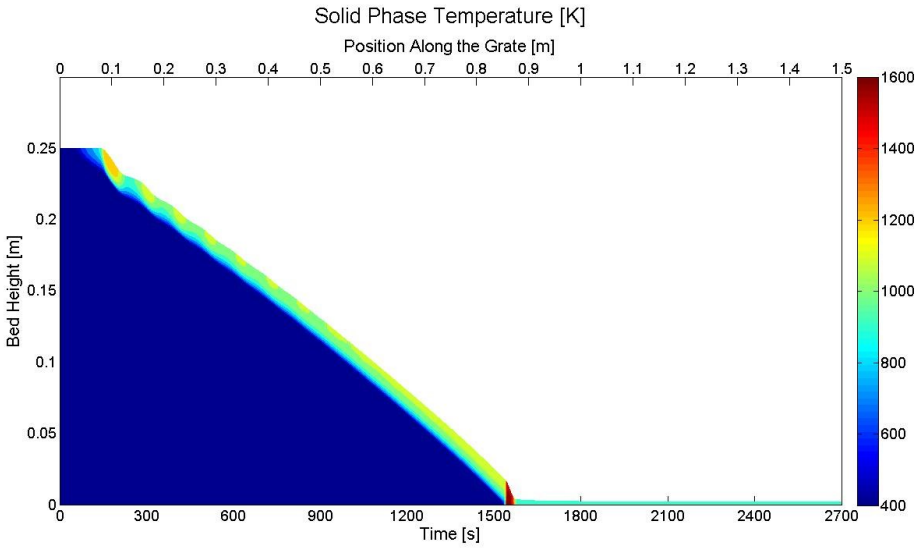

Figure 37 Solid phase temperature contour in *Simulation 6.*

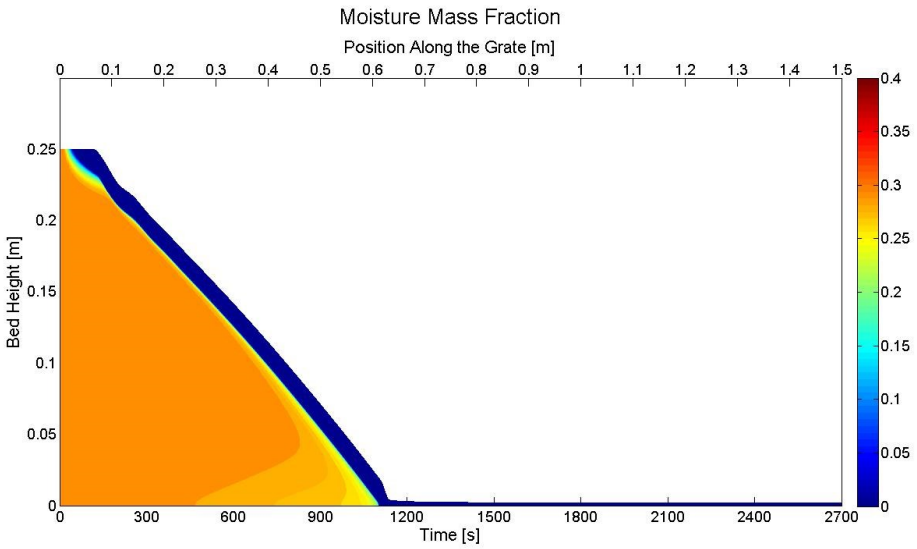

Figure 38 Solid phase moisture mass fraction contour in *Simulation 3.*

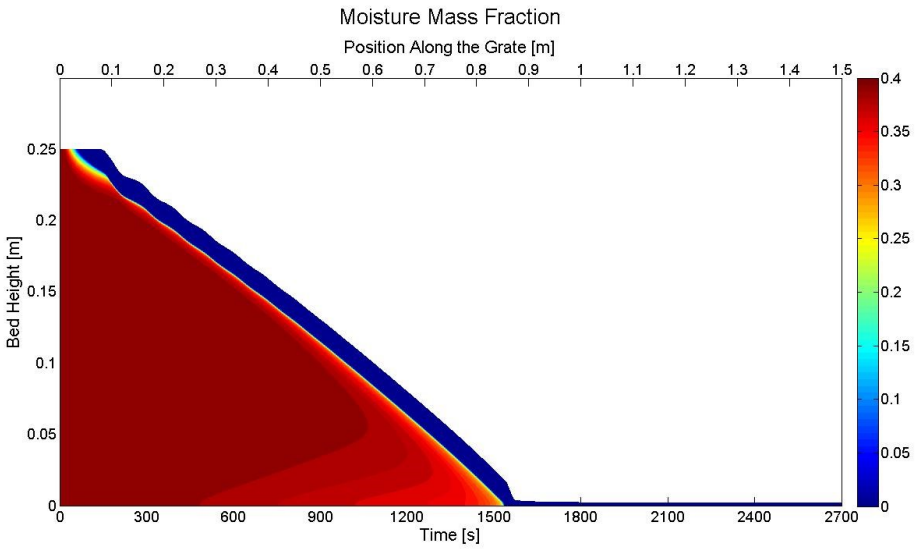

Figure 39 Solid phase moisture mass fraction contour in *Simulation 6.*

The operational conditions of the simulations differ from the reference cases in the value of the inlet air temperature, set to 373 K (100 °C) instead of 298 K (25 °C, ambient temperature). Figure 36 and Figure 37, as well as the other contours figures, show that the combustion time is reduced approximately to 1110 and 1540 s for *Simulation 3* and *Simulation 6*, respectively. The reduction in the combustion time is due to the beneficial effects of the hot air coming from under the grate. Indeed, hot air contributes to the heating up of the biomass fuel in the deeper

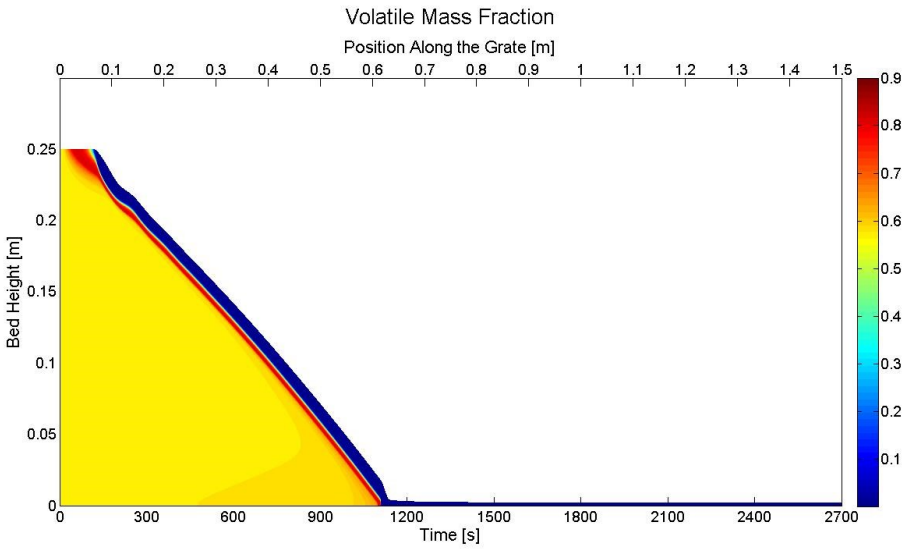

Figure 40 Solid phase volatile mass fraction contour in *Simulation 3.*

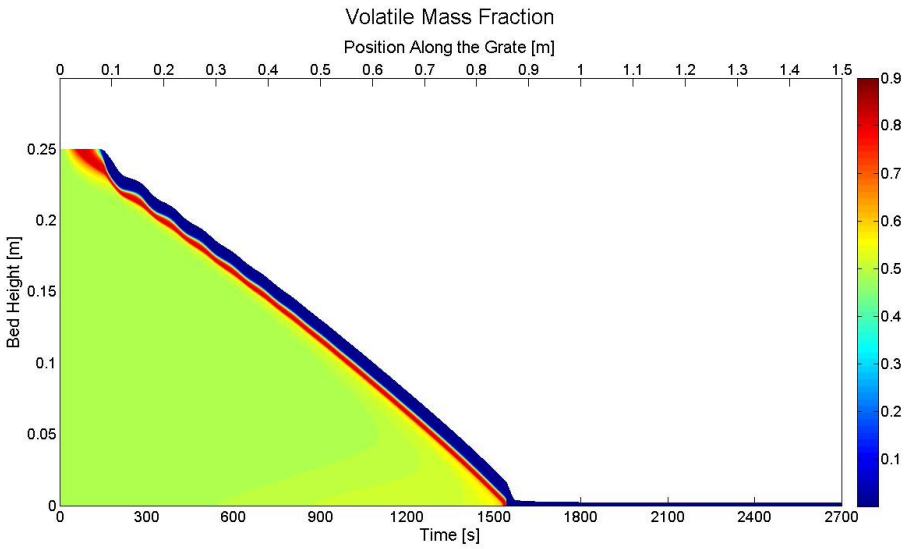

Figure 41 Solid phase volatile mass fraction contour in *Simulation 6.*

layers of the bed, promoting moisture evaporation even in the zones which are not reached from the reaction front, yet. This is evident from Figure 38 and Figure 39 that show a reduction in the moisture mass fraction of the solid bed in the layers close to the grate and in Figure 40 Figure 41 that show an increase in the volatile mass fraction in the same zones.

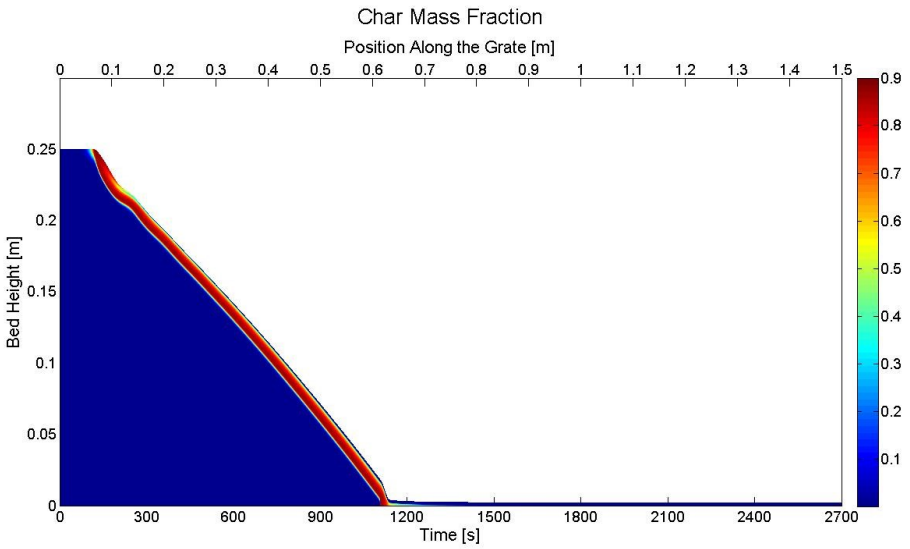

Figure 42 Solid phase char mass fraction contour in *Simulation 3.*

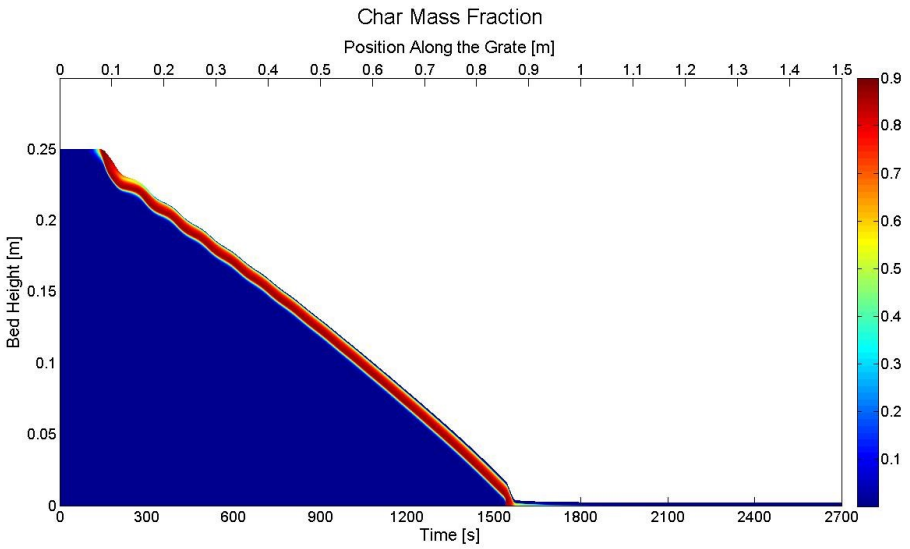

Figure 43 Solid phase char mass fraction contour in *Simulation 6.*

In conclusion, the utilization of pre-heated air brings back to the reaction front a drier and warmer biomass bed which ensures a higher combustion rate. This is also noticeable by the contour of the bed presented from Figure 36 to Figure 43. Indeed, the last part of the bed outline shows, in these figures, a greater slope when compared with outlines of the beds in the equivalent figures of the other simulations.

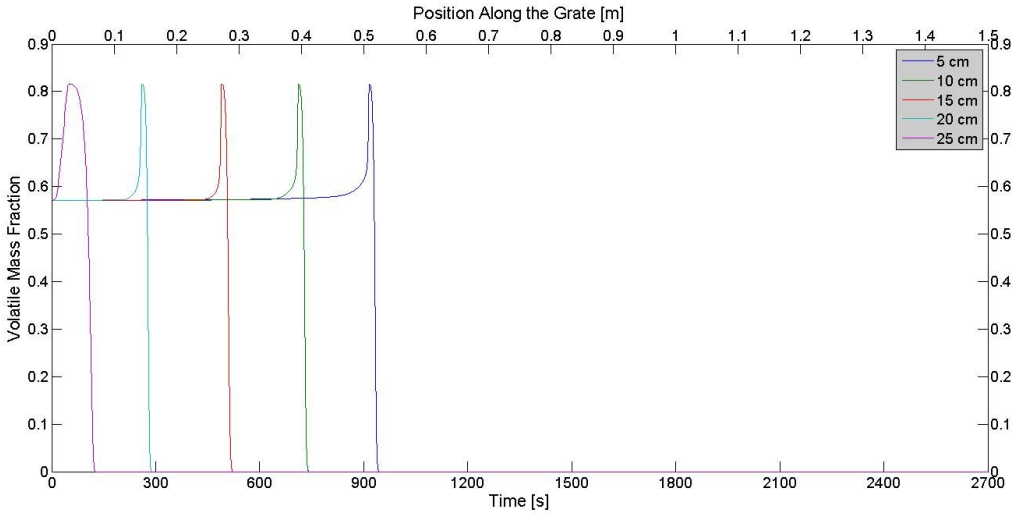

Figure 44 Solid phase volatile mass fraction at different heights from the grate in *Simulation 3.*

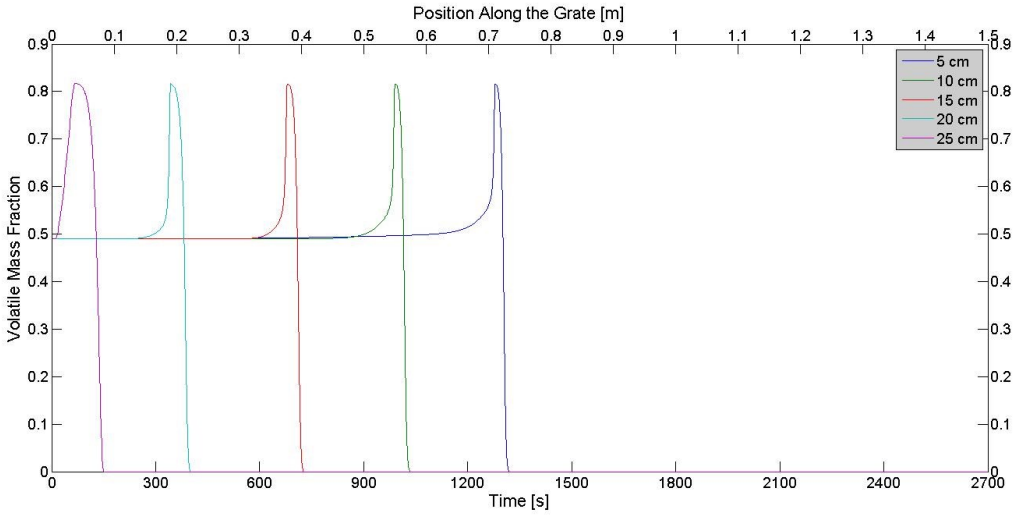

Figure 45 Solid phase volatile mass fraction at different heights from the grate in *Simulation 6.*

Figure 44 and Figure 45 show the volatile mass fraction at different bed depths and confirm that, even if moisture evaporation can occur in the deeper layers because of the hot inlet air, the devolatilization needs higher solid temperatures. The volatile matter contained in the biomass bed is not released till the reaction front does not reach the considered solid layer.

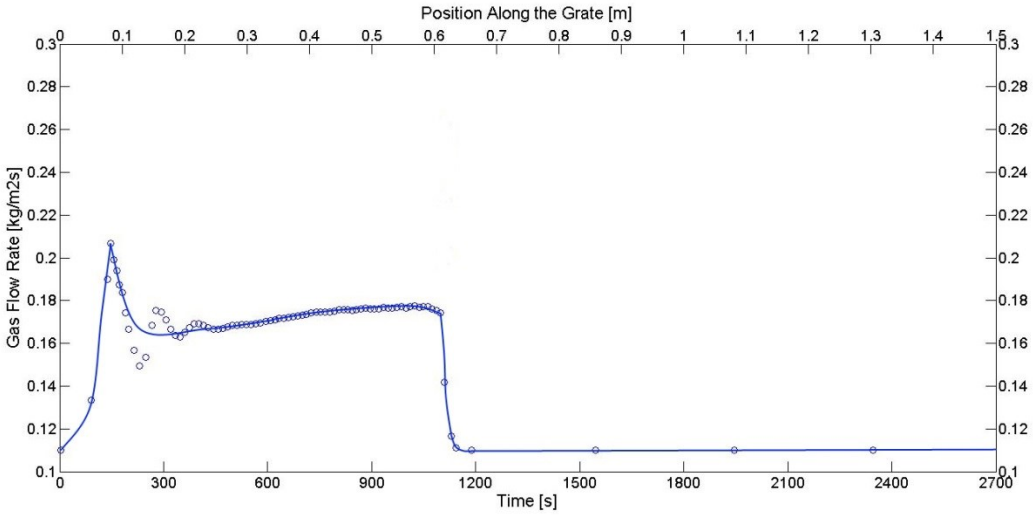

Figure 46 Gas flow rate above the bed surface in *Simulation 3.*

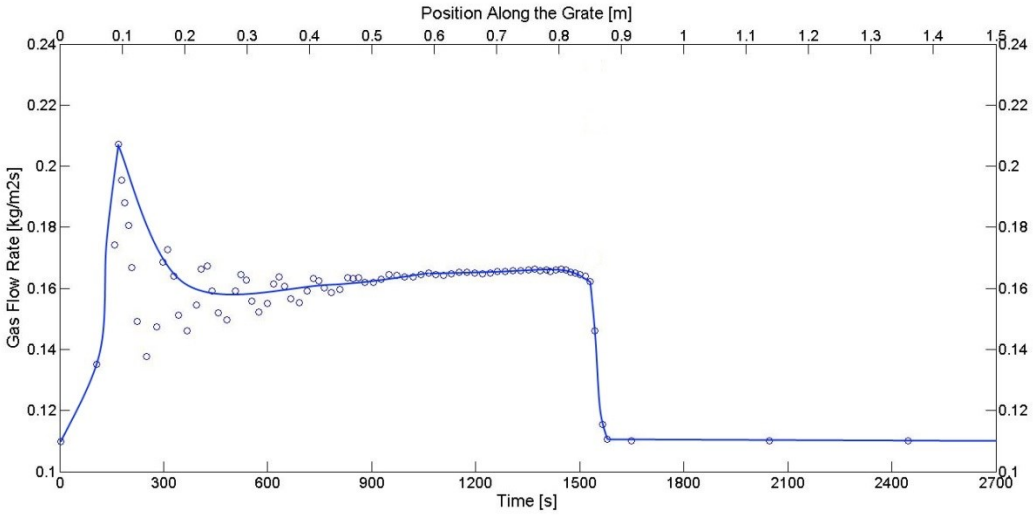

Figure 47 Gas flow rate above the bed surface in *Simulation 6.*

The trends of the gas flow rate and the gaseous species mass fractions above the bed are presented in Figure 46, Figure 47, Figure 48 and Figure 49. These figures give evidence of what has been said earlier about the increase of the combustion rate due to the drier and warmer bed encountered by the reaction front. Indeed, they shown a moderate rise of the gas flow and mass fractions of CO_2 and CO in the last part of the middle zone and, at the same time, a reduction in the oxygen mass fraction.

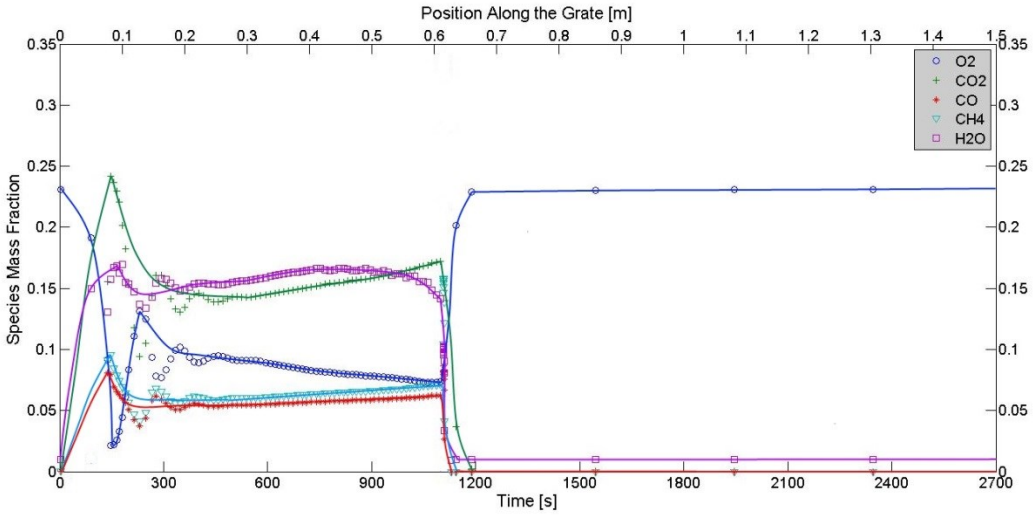

Figure 48 Gaseous species mass fraction above the bed in *Simulation 3.*

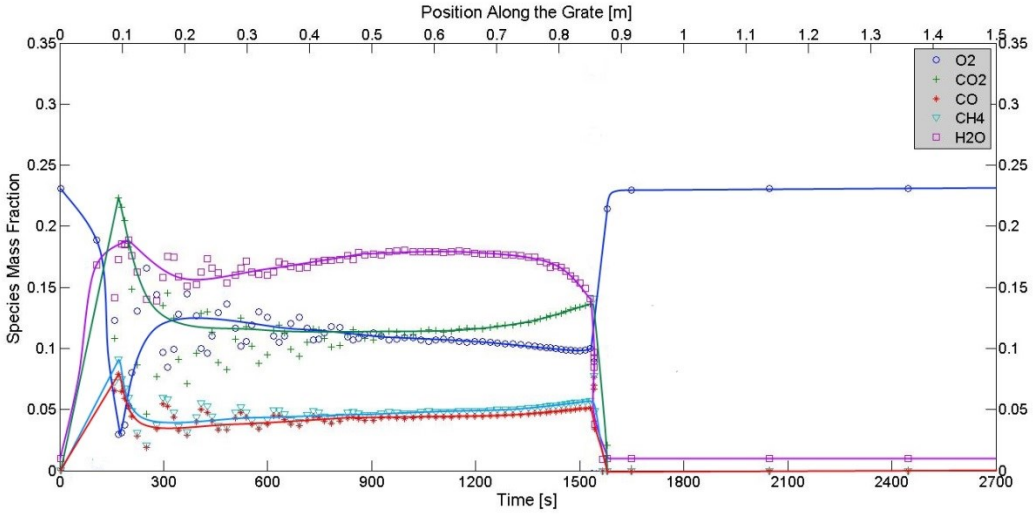

Figure 49 Gaseous species mass fraction above the bed in *Simulation 6.*

7. Conclusion

This thesis reports about the work related with the development of a woody biomass combustion model and its results. In particular, the model is able to simulate biomass combustion in moving grate furnaces with all the physical and chemical phenomena involved: moisture evaporation, volatile matter devolatilization, homogeneous and heterogeneous oxidation reactions, radiative, convective and conductive thermal exchange and bed shrinkage.

To arrive at the formulation of the simulation program an accurate work of literature review on biomass combustion modeling and experiments was done. The outcome of this preliminary activity is reported in Appendix A and B. In particular, in Appendix A an overview on the phenomena involved in biomass combustion and their mathematical models is done, passing through the work of different researchers. In Appendix B the experimental experiences, both on 1-D systems and full scale systems, are introduced and compared. This part represents a complete outline on the state of the art on biomass combustion modeling and experiments.

The experimental validation of the model against experimental results is discussed after reporting an exhaustive examination on the mathematical models chosen to simulate the physical and chemical phenomena that take place in the furnaces. Moreover, the continuity equations, that describe the system's behaviour, and the discretization and solution method applied to solve the PDE's are introduced in Chapter 4. This part is completed by the Appendix C, where a description of the program and its main routines is given.

The comparison between the simulation results and the experimental measurements presented in Chapter 5, shows good prediction capability of the developed program and allows its utilization with the aim to study biomass bed combustion on moving grates furnaces.

With this purpose a series of six simulations were performed and their results are presented and discussed in Chapter 6. The simulations take into account the same kind of woody biomass with two different amounts of moisture and under different operational conditions in terms of inlet air flow rate and temperature. The main conclusions that can be drawn on the basis of the performed calculations are summarized below:

- a higher moisture content increases the combustion time since it reduces the bed temperature and slows down the combustion reaction rate;

- a reduction of the inlet air flow rate reduces the combustion time in case of reaction limited regime because of the reduction of the cooling effect of the gases that pass through the bed;
- the utilization of pre-heated air reduces the duration of the combustion process because the biomass bed at the reaction front is already drier and warmer. This ensures a higher combustion rate.

Therefore, the developed model can be used as an instrument to investigate the combustion process of different types of biomass with different physical and chemical characteristics (particles size, proximate analysis and ultimate analysis) and under different operational conditions (inlet temperature, gas flow rate and grate velocity). This makes it possible to do a parametric investigation of the in bed thermal conversion with the aim of a better furnace design and flexible controlling strategies definition, to reduce pollutant emissions and increase the combustion efficiency.

Furthermore, the output of the model in terms of gas temperature, flow rate and gaseous species concentrations on the top of the bed represent the input for the CFD model of the over bed combustion chamber. Thus, the developed program can be seen as the first stage of a comprehensive biomass combustion model which completes the combustion process taking into account also the homogeneous reactions that occur outside the solid layer, before the gases leave the combustion chamber.

Appendix A - Literature review on packed bed combustion models

In this section all the mathematical models utilized by different authors, taken into account in this work, are presented. First the mathematical relations for physical and chemical phenomena, such as heat exchange, evaporation of moisture, devolatilization and chemical reactions of solid and gaseous phase, are introduced. In the last part, problems related to the nature of solids and fluids, such as shrinkage and changing in specific heat are discussed.

Heat exchange

The mechanisms of heat exchange during biomass combustion are: conduction among the solid particles, convection between the solid and gaseous phase and radiation. The heat due to the radiation comes from the flames and the walls of the furnace which are above the solid bed and from the high temperature particles which are inside the bed. To model the radiative heat exchange two main approaches are possible: the two flux model (Shuster-Schwarzschild approximation) and the Beer's law model. In the last case, the effective thermal conductivity of the bed takes into account also the radiative heat exchange among the particles inside the bed and another term is used to define the heat source that comes from the flames and the hot walls of the combustion chamber. For this reason, conduction and radiation are discussing together, depending on the different way considered to model the radiative heat exchange.

Conductive and radiative heat exchange: two flux model

When the radiative heat exchange is modelled using the two flux model the thermal conductivity of the bed considers the heat exchange among the particles due to the biomass conductivity only. The relations utilized for the two flux model are summarized in Table 11.

Table 11 Radiation intensities for the two flux model [W/m_2].

$$\frac{dI_x^+}{dx} = -(\beta + \omega_s)I_x^+ + \frac{1}{2}\beta E_b + \frac{1}{2}\omega_s(I_x^+ + I_x^-) \quad \text{(A.1)}$$

$$-\frac{dI_x^-}{dx} = -(\beta + \omega_s)I_x^- + \frac{1}{2}\beta E_b + \frac{1}{2}\omega_s(I_x^+ + I_x^-) \quad \text{(A.2)}$$

Where *x* is the direction in the bed height, I_z^+ and I_z^- the two radiation intensities, β and ω_s represent the absorption and scattering coefficients, respectively and E_b is the black-body radiation. By introducing the no-scattering assumption and taking into consideration that the particles in the bed are arranged on a regular grid [23], the previous coefficients can be defined as follows:

Table 12 Two flux model assumption.

$$\omega_s = 0 \quad \text{(A.3)}$$

$$\beta = -\frac{1}{d_p} ln(1 - \epsilon) \quad \text{(A.4)}$$

Where ϵ is the porosity of the bed and d_p the particles diameter.

The conductive heat exchange depends on the gradient of the temperature in the solid phase and the effective thermal conductivity of the bed λ_s. The relations used to define the thermal conductivity by different authors are reported in Table 13.

Table 13 Thermal conductivity [W/m^2K].

$\lambda_{s,eff} = (1 - \epsilon)\lambda_{biomass}$	[23]	(A.5)
$\lambda_{s,eff} = \lambda_{s0} + 0.5PrRe\lambda_g$	[24]	(A.6)
$\lambda_{s,eff} = \lambda_{s0} + \frac{(0.5PrRe\lambda_g)}{\epsilon}$	[34]	(A.7)
$\lambda_{s,eff} = \lambda_{s0} + (0.8\rho_g v_g c_g d_p)$	[37]	(A.8)
$\lambda_{s,eff} = (1 - \epsilon)\lambda_{biomass} + \rho_{s0} c_s D_s$	[30]	(A.9)

Where λ_g, ρ_g, v_g, c_g are the thermal conductivity, density, velocity and specific heat of the gaseous phase, $\lambda_{biomass}$ is the thermal conductivity of the considered biomass, *Pr* and *Re* are the dimensionless number of Prandtl and Reynolds, respectively.

It has to be noted that van der Lans et al [24], Zhou et al [34] and Kuijk et al [37] define the effective thermal conductivity as the value of the thermal conductivity without fluid flow λ_{s0}, corrected with a term which takes into account the contribution of the flow. In a different way, Shin and Choi [23] do not consider this correction but only the adjustment for the bed porosity. Yang et al [30] consider the correction owing to the particles random movements, where ρ_{s0} and c_s are the density and heat capacity of the solid phase and D_s is the particles mixing coefficient for the biomass bed particles, which is the same of the molecular diffusion coefficient for the gaseous phase.

Conduction and radiative heat exchange: Beer's law model

Some authors, such as Asthana et al [39], and Martinez and Nussbaumer [42], prefer to use a Beer's law model for the radiative heat source due to the flames and the walls of the furnace. In this case, the thermal conductivity of the bed considers both, the heat exchange among the particles due to the biomass conductivity and the heat exchange related to the radiation of the high temperature particles. The relations utilized in this scheme are reported in Table 14.

Table 14 Beer's law model for radiative heat exchange.

$\dot{Q}_{rad} = (J_0 - \sigma T_s^4)\beta e^{-\beta x'}$	(A.10)
$\beta = 3(1-\epsilon)/2d_p$	(A.11)
$\lambda_{s,eff} = (1-\epsilon)\lambda_{biomass} + \lambda_{rad}$	(A.12)
$\lambda_{rad} = \frac{16}{3}\sigma d_{e,rad} T_s^3$	(A.13)
$d_{e,rad} = \frac{2\epsilon}{3(1-\epsilon)} d_p = \frac{\epsilon}{\beta}$	(A.14)

Where σ is the Stefan-Boltzmann constant, x' is the distance from the bed surface, J_0 is the incident radiation, T_s is the solid phase temperature, λ_{rad} is the radiant conductivity and $d_{e,rad}$ is the equivalent particle diameter for the radiation. The term J_0depends on the temperature of the walls of the combustion chamber and the temperature of the gases flowing out from the bed.

Johansson et al [29] have demonstrated that the two flux radiation model can be substituted with a less computational-demanding conductivity radiation model without causing more than 10% of change in the estimated ignition rate or bed temperature.

Convection heat exchange

Kuijk et al [37] and van der Lans et al [24] consider the gaseous and solid phase in equilibrium during the combustion phenomena and use a unique temperature for both phases. In these works no convection heat exchange is then considered. Other authors, such as Shin and Choi [23] and Asthana et al [39], use the relations proposed by Wakao and Kaguei [47] to define the convective heat transfer coefficient h_t. The relations proposed by these authors are reported in Table 15.

Table 15 Convective heat transfer coefficient.

$h_t = Nu\lambda_g/d_p$	(A.15)
$Nu = 2 + 1.1Re^{0.6}Pr^{1/3}$	(A.16)
$Re = \frac{\rho_g v_g d_p}{\mu_g}$	(A.17)
$Pr = \frac{c_g \mu_g}{\lambda_g}$	(A.18)

Where *Nu* is the dimensionless number of Nusselt.

Moisture evaporation

Three different models of moisture evaporation can be found in literature. Di Blasi et al [46], Boriouchkine et al [40] and Johansson et al [35] use an Arrhenius law model; Goh et al [25] and Yang et al [29] - [33] use a diffusion model coupled with a radiative model in which: when the biomass temperature is under 273 K the evaporation mechanism is diffusion limited, when the temperature is over 273 K the mechanism is radiative and all the heat power received by biomass fuel is used for to dry the particles. Shin and Choi [23], Zhou et al [34] and Asthana et al [39] prefer to use a diffusion limited model only. The relations used to describe each model are listed in Table 16.

Table 16 Moisture evaporation rates [kg/m^{3}s].

Rates	Reference	
$5.6 \cdot 10^8 e^{(-88000/RT_s)} \rho_s X_{H_2O}$	[40] [46]	(A.19)
$1.6 \cdot 10^{27} e^{(-25000/T_s)} \rho_s X_{H_2O}$	[35]	(A.20)
$\frac{S\left[h_t\left(T_g - T_s\right) + \varepsilon\sigma(T_w^4 - T_s^4)\right]}{H_{evap}}$	[25] [29]	(A.21)
$h_m S\left(C_{ws} - C_{wg}\right)$	[23] [34] [39]	(A.22)

Where R is the universal gas constant, X_{H2O} the mass fraction of moisture in the solid phase, S the specific surface of the particle bed, T_g the gaseous phase temperature, ε the emissivity of the grey body, H_{evap} the latent heat of water evaporation, T_w the temperature of the walls of the combustion chamber, C_{ws} and C_{wg} are the water vapour mass concentrations on the particle surface and in the gaseous phase, respectively.

The mass transfer coefficient h_m is determined using the analogy with convective heat transfer for a packed bed of spherical particles [47]. The relations for the determination of h_m are summarized in Table 17.

Table 17 Convective mass transfer coefficient.

$h_m = ShD_g/d_p$	(A.23)
$Sh = 2 + 1.1Re^{0.6}Sc^{1/3}$	(A.24)
$Sc = \frac{\mu_g}{\rho_g D_g}$	(A.25)

Where Sh and Sc are the dimensionless number of Sherwood and Schmidt, respectively.

Devolatilization of volatile matter

Since the devolatilization is only a part of the more complex biomass combustion process, usually a one-step global model is adopted for simplicity. Some exceptions at the implementation of this scheme are represented by the work of Shin and Choi [23] where a competitive two-reactions model with no tar formation is adopted and the model of Goh et al [25] and Yang et al [30] which use a continuous Gaussian distribution energy model presented

by Smoot and Pratt [53]. In the work of Shin and Choi [23], the model considers two different rates for the devolatilization of volatile matter and char formation as reported in Table 18.

Table 18 Devolatilization rates by Shin and Choi [23].

Product	Frequency factor [1/s]	Activation energy [kJ/mol]	
volatile	$5.16 \cdot 10^{6}$	89	(A.26)
char	$2.66 \cdot 10^{10}$	106	(A.27)

Significant studies on the effect of the devolatilization rate on the combustion of wood chips have been conducted by Yang et al [29]. These studies show that the different values of devolatilization rate utilized have an insignificant effect on the burning rate and reaction zone thickness. Instead, the ignition time is sensitive to the devolatilization rate only if the moisture content increases above 25-30% on wet mass basis. The devolatilization rates analyzed in these studies are reported in Table 19 and are named from *very slow* to *very fast* depending on the magnitude of the frequency factor and the activation energy.

Table 19 Devolatilization rates by Yang et al [29].

Rate velocity	Frequency factor [1/s]	Activation energy [kJ/mol]	
very fast	$5.16 \cdot 10^{6}$	84	(A.28)
fast	$3.4 \cdot 10^{4}$	69	(A.29)
medium	$7.0 \cdot 10^{4}$	83	(A.30)
slow	$3.0 \cdot 10^{3}$	69	(A.31)
very slow	$2.98 \cdot 10^{3}$	73.1	(A.32)

In addition to these rates, in literature it possible to find other different values such as those ones utilized to model the devolatilization of the straw by van der Lans et al [24], Zhou et al [34] and Yang et al [33] and those utilized by Boriouchkine et al [40] which distinguish in the biomass fuel the cellulose and hemicellulose fractions. In the model they use different devolatilization rates for each of these solid species fractions. The values of the frequency factor and activation energy used by these authors are listed in Table 20.

Table 20 Devolatilization rates.

Type of biomass	Frequency factor [1/s]	Activation energy [kJ/mol]	Ref	
straw	$1.56 \cdot 10^{6}$	138	[24]	(A.33)
straw	$1.56 \cdot 10^{10}$	138	[34]	(A.34)
straw	$3.63 \cdot 10^{4}$	77	[33]	(A.35)
wood(cellulose)	$2.0 \cdot 10^{9}$	146	[40]	(A.36)
wood(Hemicellulose)	$7.0 \cdot 10^{4}$	83	[40]	(A.37)

Homogeneous reactions

The number of homogeneous reactions implemented in a biomass combustion model depends on two main factors: the number of chemical species in which the volatile matter, coming from the solid devolatilization, is decomposed and the overall number of chemical species accounted in the model. Some authors, such as Shin and Choi [23] and Yang et al [29] consider the volatile as an unique specie $C_nH_mO_l$, instead, Zhou et al [34] and Asthana et al [39] apply a decomposition of the volatile in different species using constant values. Table 21 resumes the different situation found in literature.

Table 21 Volatile composition (percentage on volatile mass).

γ_{gas}	γ_{tar}	CO	CO_2	H_2	CH_4	H_2O	C_nH_m	Ref
-	-	37	19	-	44	-	-	[33]
71.65	28.35	28.8	63	1.2	3.5	-	3.5	[34]
-	-	20.4	40.7	3.4	27.2	8.3	-	[39]
72	28	15.6	27.1	2.1	3.1	52.1	-	[50]

In the works [34] and [50] the volatile is first divided into tar and gas. Tar is a complex mixture of condensable hydrocarbons and for simplicity is modelled as a unique specie. The chemical formula adopted in these work is reported in Table 22.

Table 22 Tar formula.

Tar formula	g/mol	Ref.
$CH_{1,84}O_{0,96}$	95	[34]
$CH_{1,522}O_{0,028}$	95	[49]

Both the authors consider that the tar is oxidized to produce CO and H_2O. The scheme of reaction and the reaction rates are reported in Table 23.

Table 23 Tar reaction rate [mol/m^{3}s].

Reaction	Reaction rate [mol/m^{3}s]	Ref	
$CH_{1,84}O_{0,96} + 0.48O_2 \rightarrow CO + 0.92H_2O$	$r_{tar} = 2.9 \cdot 10^5 \cdot T_e e^{(-9650/T_e)} C^{0.5}_{CH_{1.84}O_{0.96}} C_{O_2}$	[24]	(A.38)
$CH_{1,522}O_{0,0228} + 0.867O_2 \rightarrow CO + 0.761H_2O$	$r_{tar} = 9.2 \cdot 10^6 \cdot T_g e^{(-80000/RT_g)} C^{0.5}_{CH_{1.522}O_{0.0228}} C_{O_2}$	[34]	(A.39)

Where C_i are the molar concentration of gaseous species and T_e, in the kinetic rate of tar oxidation, is defined as:

$$T_e = \alpha T_g + (1-\alpha) T_s \quad if \;\; T_g \leq T_s \quad with \;\; \alpha = 0{,}5 \tag{A.40}$$

$$T_e = T_g \quad if \;\; T_g > T_s \tag{A.41}$$

Regarding the reactions of the other gaseous species, irrespective of the nature and number of the species considered, in literature it is possible to find two schools of thought: one considers that the gas combustion rate is defined by the chemical reaction rate only and the other one which considers that gaseous species have first to mix with surrounding air before their combustion can take place. This means that also a gas mixing rate is taken into account in the definition of the overall gas combustion rate. In Table 24 the chemical reactions rates utilized by different authors are summarized.

Table 24 Homogeneous reaction rates.

Reaction	Reaction rate	Ref	
$C_nH_m + \left(\frac{1}{2}n + \frac{1}{4}m\right)O_2 \rightarrow nCO + \frac{m}{2}H_2O$	$r_{C_nH_m} = 59.8 \cdot T_g p^{0.3} e^{(-12200/T_g)} C_{O_2} C_{C_nH_m}^{0.5}$	[23]	(A.42)
$CO + \frac{1}{2}O_2 \rightarrow CO_2$	$r_{CO} = 1.3 \cdot 10^{11} e^{(-15105/T_g)} C_{CO} C_{O_2}^{0.5} C_{H_2O}^{0.5}$		(A.43)
$H_2 + \frac{1}{2}O_2 \rightarrow H_2O$	$r_{H_2} = 3.9 \cdot 10^{17} e^{(-20500/T_g)} C_{O_2}^{1.42} C_{H_2}^{0.86} C_{CHO}^{-0.56}$	[29]	(A.44)
$CO + \frac{1}{2}O_2 \rightarrow CO_2$	$r_{CO} = 1.3 \cdot 10^{11} e^{(-62700/T_g)} C_{CO} C_{O_2}^{0.5} C_{H_2O}^{0.5}$		(A.45)
$H_2 + \frac{1}{2}O_2 \rightarrow H_2O$	$r_{H_2} = 51.8 \cdot T_g^{3/2} e^{(-3420/T_g)} C_{O_2} C_{H_2}^{1.5}$		(A.46)
$CH_4 + \frac{3}{2}O_2 \rightarrow CO + 2H_2O$	$r_{CH_4} = 1.6 \cdot 10^{10} e^{(24157/T_g)} C_{CH_4}^{0.7} C_{O_2}^{0.8}$	[34]	(A.47)
$C_nH_m + \left(\frac{1}{2}n + \frac{1}{4}m\right)O_2 \rightarrow nCO + \frac{m}{2}H_2O$	$r_{O_2} = 2{,}7 \cdot 10^{8} {T_g}^{1/2} e^{(-20131/T_g)} C_{C_{2H_6}} C_{O_2}$		(A.48)
$CH_4 + \frac{3}{2}O_2 \rightarrow CO + 2H_2O$	$r_{CH_4} = 1.5 \cdot 10^{8} e^{(24163/T_g)} C_{CH_4}^{0.7} C_{O_2}^{0.8}$		(A.49)
$H_2 + \frac{1}{2}O_2 \rightarrow H_2O$	$r_{H_2} = 1.5 \cdot 10^{13} e^{(-9025/T_g)} C_{O_2} C_{H_2}$	[39]	(A.50)
$CO + \frac{1}{2}O_2 \rightarrow CO_2$	$r_{CO} = 1.3 \cdot 10^{8} e^{(-15102/T_g)} C_{CO} C_{O_2}^{0.5} C_{H_2O}^{0.5}$		(A.51)
$H_2 + \frac{1}{2}O_2 \rightarrow H_2O$	$r_{H_2} = 2.96 \cdot 10^{11} e^{(-6900/T_g)} C_{O_2}^{0.92} C_{H_2}$		(A.52)
$CH_4 + \frac{3}{2}O_2 \rightarrow CO + 2H_2O$	$r_{CH_4} = 5.6 \cdot 10^{12} e^{(12491/T_g)} C_{CH_4}$		(A.53)
$CO + \frac{1}{2}O_2 \rightarrow CO_2$	$r_{CO} = 1.3 \cdot 10^{14} e^{(-15102/T_g)} C_{CO} C_{O_2}^{0.5} C_{H_2O}^{0.5}$	[40]	(A.54)
$C_2H_4 + 3O_2 \rightarrow 2CO + 2H_2O$	$r_{C_2H_4} = 2 \cdot 10^{12} e^{(15162/T_g)} C_{O_2}^{1.65} C_{C_2H_4}^{0.1}$		(A.55)
$C_2H_2 + \frac{5}{2}O_2 \rightarrow 2CO + H_2O$	$r_{C_2H_2} = 605 \cdot 10^{12} e^{(15162/T_g)} C_{O_2}^{1.25} C_{C_2H_2}^{0.5}$		(A.56)

Where C_i are the molar concentrations of gaseous species expressed in [mol/m^3], except for Shin and Choi [23] and Yang et al [29] where they are expressed in [kmol/m^3].

The mixing rate velocity proposed by Yang et al [29] is reported below:

$$r_{mix} = C_{mix}\rho_g \left(150 \frac{D_g(1-\epsilon)^{2/3}}{d_p^2 \epsilon} + 1.75 \frac{v_g(1-\epsilon)^{1/3}}{d_p \epsilon} \right) \cdot min \left\{ \frac{C_{fuel}}{\Omega_{fuel}}, \frac{C_{O_2}}{\Omega_{O_2}} \right\} \quad \text{(A.57)}$$

Where C_{mix} is an empirical constant and Ω the stoichiometric coefficients of the considered species in the chemical reaction.

The actual reaction rate of the gaseous species is taken as the minimum between the chemical and the mixing rate with oxygen.

Heterogeneous reactions

Char combustion is a heterogeneous surface burning that gives as primary products CO and CO_2 [54]. Despite this, some authors, such as Shin and Choi [23] and Kuijk et al [37], prefer to use a simpler model with CO being the only product of char oxidation. In this case the char combustion reaction is defined as follow:

$$Char(C) + \frac{1}{2} O_2 \rightarrow CO \quad \text{(A.58)}$$

If the production of CO_2 is considered in addition to that one of CO, the combustion reaction becomes:

$$C + \frac{1}{\Theta} O_2 \rightarrow 2\left(1 - \frac{1}{\Theta}\right) CO + \left(\frac{2}{\Theta} - 1\right) CO_2 \quad \text{(A.59)}$$

The appropriate stoichiometric coefficient for oxidation of char is not readily apparent and it is necessary to define the term Θ, that depends on the ratio r_c of CO/CO_2 formation rate.

$$\Theta = (1 + 1/r_c)/(1/2 + 1/r_c) \quad \text{(A.60)}$$

The relations used by different authors to define the ratio r_c are listed in Table 25.

Table 25 r_c ratio of CO/CO2 formation rate.

$r_c = CO/CO_2$		Ref	
$1 \quad constant$		[24]	(A.61)
$12e^{(-3300/T_s)}$		[34]	(A.62)
$2500e^{(-6420/T_s)}$		[29] [33]	(A.63)
$1340e^{(-63500/\mathrm{R}T_s)}$	$850 < T_s < 970\ K$		(A.64)
$472 \cdot 10^{-3}e^{(-37700/\mathrm{R}T_s)}$	$970 < T_s < 1220\ K$	[39]	(A.65)
$12.4e^{(-42000/\mathrm{R}T_s)}$	$1220 < T_s < 1650\ K$		(A.66)

Char combustion can occur in two different regimes: chemical regime where the combustion rate depends on the char temperature only, and the diffusional regime where the combustion rate depends on the diffusion rate of the oxygen toward the particles surface. The overall combustion rate is then defined as a combination of the two regimes at the combustion condition. The relations found in literature are reported in Table 26.

Table 26 Char combustion rate.

Char reaction rate		Chemical rate constant		Ref	
$60S_aC_{O_2}\dfrac{1}{1/h_m + 1/k_c\zeta}$	[kmol/s]	$k_c = 2.3T_se^{(-11100/T_s)}$	[m/s]	[23]	(A.67)
$\left(\dfrac{(RT_s/\Theta M_CS)}{h_m} + \dfrac{1}{k_c\rho_s}\right)^{-1} p_{O_2}$	[kg/m^{3}s]	$k_c = 8619e^{(-132259/RT_s)}$	[1/Pas]	[24]	(A.68)
$\left(\dfrac{1}{h_m} + \dfrac{1}{k_c}\right)^{-1} p_{O_2}$	[kg/m^{2}s]	$k_c = 3.0e^{(-10300/T_s)}$	[kg/m^{2}skPa]	[25]	(A.69)
$\left(\dfrac{1}{h_m} + \dfrac{1}{k_c}\right)^{-1} S_{ii}\rho_gY_{O_2}$	[g/cm^{3}s]	$k_c = 6 \cdot 10^4Te^{(-150000/RT)}$	[cm/s]	[37]	(A.70)

Where, referring to these relations, S_a and S_{ii} are the surface area [m^2] and the instantaneous internal surface area [cm^2/cm^3]. ζ is the surface factor for internal burning of char reaction, M_c the molar mass of the carbon, p_{O_2} and Y_{O_2} the oxygen partial pressure and mass fraction in the gaseous phase, respectively.

Regarding the diffusion rate constant, the relations are summarized in Table 27

Table 27 Mass transfer coefficient for char combustion reaction.

Relations available			Ref	
$Sh = 2 + 1.1Re^{0.6}Sc^{1/3}$	$h_m = ShD_g/d_p$	[m/s]	[23]	(A.71)
$h_m = \frac{D_{O_2-N_2}^{2/3} v_g}{v^{2/3}\epsilon}\left(\frac{0.765}{Re^{0.82}} + \frac{0.365}{Re^{0.386}}\right)$		[m/s]	[24]	(A.72)
$Sh = 2 + 0.81\epsilon^{-1/2}Re^{1/2}Sc^{1/3}$	$h_m = ShD_g/d_p$	[cm/s]	[37]	(A.73)

Where v is the kinematic viscosity of the gases flowing through the bed.

The char combustion model presented by Asthana et al [39] has to be discussed separately, since they take into account not only the influence of the oxygen diffusion toward the particles surface, but also the effect of the Stefan flow. Indeed, it represents a perturbation of the external mass transfer caused by the strong outward flow of volatiles due to the devolatilization process. The relations used by these authors are summarized in Table 28.

Table 28 Char combustion rate by Asthana et al [35].

$r_{char} = S\left(\frac{e^{b_{O_2}}}{\Omega_{act} \cdot r_{char,chem}} + \frac{e^{b_{O_2}} - 1}{b_{O_2} \cdot r_{char,diff}}\right)^{-1}$	[kg/m^{3}s]	(A.74)
$r_{char,chem} = 860 \cdot 10^{-3} e^{(-18000/T_s)} p_{O_2}$	[kg/m^{2}s]	(A.75)
$r_{char,diff} = \frac{h_m \theta M_c p_{O_2}}{RT_m}$	[kg/m^{2}s]	(A.76)
$h_m = \frac{D_{O_2-N_2}^{2/3} v_g}{v^{2/3}\epsilon}\left(\frac{0.765}{Re^{0.82}} + \frac{0.365}{Re^{0.386}}\right)$	[m/s]	(A.77)
$b_{O_2} = \frac{N_{vol} d_p}{2D_{O_2-N_2} c_t}$	-	(A.78)

Where, referring to these relations, Ω_{act} is the fractional reduction of reaction surface area, b_{O_2} the Péclet number for Stefan flow, T_m the average temperature between gaseous and solid phase, N_{vol} the molar flux density of the volatile matter [mol/m^{2}s] and c_t the global concentration of the gaseous phase [mol/m^3].

Gaseous phase pressure inside the packed bed

The authors that consider a variation in the gaseous phase pressure during combustion are Goh et al [25], Yang et al [29] - [33], Johansson et al [35] and Asthana et al [39]. The relations used by Yang in his works are the same presented by Goh. They introduce, in the momentum equation for the gaseous phase, a function *F(v_g)* that depends on the different flow regimes defined by the value of Reynolds number. These relations are reported below.

$$\frac{\partial \epsilon v_g \rho_g}{\partial t} + \frac{\partial \epsilon v_g v_g \rho_g}{\partial x} = -\frac{\partial p_g}{\partial x} + F(v_g) \tag{A.79}$$

$$F(v_g) = \frac{\mu_g}{\kappa} v_g \qquad if\ Re < 10 \tag{A.80}$$

$$F(v_g) = \frac{\mu_g}{\kappa} v_g - C\rho_g v_g v_g \qquad if\ Re > 10 \tag{A.81}$$

Where κ is the permeability of the bed [m^2] and *K* and *C* are constants defined as:

$$K = \frac{d_p^2 \epsilon^3}{150(1-\epsilon)^2} \tag{A.82}$$

$$C = \frac{1.75(1-\epsilon)}{d_p \epsilon^3} \tag{A.83}$$

Asthana et al [39], combining the Darcy's law with the continuity equation of the gaseous phase, obtain the following equation in p_g^2.

$$-\frac{\partial}{\partial x}\left(\frac{\kappa M_g}{2RT_g\mu_g}\frac{\partial p_g^2}{\partial x}\right) - \frac{\partial}{\partial y}\left(\frac{\kappa M_g}{2RT_g\mu_g}\frac{\partial p_g^2}{\partial y}\right) = S_g \tag{A.84}$$

Where M_g is the molar weight of the gaseous phase and S_g the gas source. Since they consider a 2-D model also the pressure variation in the direction *y* along the grate is considered. This equation is solved to calculate the pressure field in the bed, which is then used in Darcy's law to derive the gas velocities in both directions.

Johansson et al [35] use the Ergun's equation for rough particles to define the pressure drop inside the bed and specify the pressure value at the bed's surface as 1 bar. The equation is reported below.

$$\frac{\Delta p}{\Delta x} = 180\frac{(1-\epsilon)^2\mu_g v_g}{\epsilon^3 d_p^2} + 4\frac{(1-\epsilon)\rho_g v_g^2}{\epsilon^2 d_p} \quad \text{(A.85)}$$

Other authors, such as Shin and Choi [23], van der Lans [24], Zhou et al [34], van Kuijk et al [37], Boriouchkine et al [40], Miljkovic et al [41] and Martinez and Nussbaumer [42]do not specify a relation for pressure dynamics inside the bed during combustion processes, but they assume a constant value equal to the atmospheric pressure. This assumption can be justified since the release of gaseous species is negligible in comparison with the primary air flow [40].

Volume change of bed during combustion

During combustion process, biomass loses weight due to the evaporation, devolatilization and heterogeneous reactions. The weight lost corresponds to a volume shrinkage of the biomass bed. Some authors, such as van der Lans et al [24] and Zhou et al [34], do not consider the volume shrinkage in their model; some other, such as Goh et al [25], develop elaborate schemes to take this physical phenomenon into account. In Table 29 the relations found in literature are reported.

Table 29 Shrinkage volume model.

Shrinkage model	Ref	
$\Delta x(j,t) = f_s \Delta x(j,0)$		(A.86)
$f_s = \left(u + X_{ash}\frac{\rho_s}{\rho_{ash}}\right) \Big/ \left(1 + X_{ash}\frac{\rho_s}{\rho_{ash}}\right)$		(A.87)
$S = S_{ini}\left(1 + X_{ash}\frac{\rho_s}{\rho_{ash}}\right)u^{3/4}$	[23]	(A.88)
$S_{ini} = \frac{6\epsilon S_{sc}\Delta x(j,0)}{d_p}$		(A.89)
$f_s = \frac{V_p}{V_{p,0}} = 1 - \theta_{drying}\frac{X_{m,0}}{X_{m,\theta}}\left(1 - \frac{X_m}{X_{m,0}}\right) - \theta_{dev}\left(1 - \frac{X_v}{X_{v,0}}\right) - \theta_{comb}\left(1 - \frac{X_c}{X_{c,0}}\right)$		(A.90)
$\theta_{comb} = 1 - \frac{V_{p,ash}}{V_{p,0}} - \theta_{drying}\frac{X_{m,0}}{X_m} - \theta_{dev}$	[35]	(A.91)
$V_{p,ash} = V_{p,0}\left(1 - \theta_{drying}\frac{X_{m,0}}{X_{m,\theta}} - \theta_{dev}\right)\frac{X_{ash,0}}{X_{c,0}}$		(A.92)

$$\Delta x = f_s \Delta x_0$$

$$f_s = \rho_{p,0}\left\{\left(\frac{X_m}{\rho_m}+\frac{X_{cm}}{\rho_{cm}}+\frac{X_c}{\rho_c}\right)\frac{X_{i,0}}{X_i}+\frac{X_{i,0}}{\rho_i} + \left[\left(\frac{X_{m,0}}{\rho_m}+\frac{X_{pyro,0}}{\rho_{pyro}}\right)-\left(\frac{X_m}{\rho_m}+\frac{X_{cm}}{X_{cm,0}}\frac{Y_{pyro,0}}{\rho_{pyro}}\right)\frac{X_{i,0}}{X_i}\right]\left(X_c + X_{c,f}\frac{X_{cm}}{X_{cm,0}}\right)\frac{X_{i,0}}{X_i X_{c,f}}\right\} \quad [39] \quad \text{(A.93)}$$

$$\frac{\Delta x(j,t)}{\Delta x_0} = \frac{X_{cs}(j,t)+X_{ash,0}}{X_{cs,0}} \quad \text{(A.94)}$$

[42]

$$\frac{\partial X_{cs}(j,t)}{\partial t} = -X_{cs}(j,t)\frac{r_{char,comb}}{\rho_c} \quad \text{(A.95)}$$

Referring to the relations reported by Shin an Choi [23], $\Delta x(j,t)$ and $\Delta x(j,0)$ are the volume of the 1-D calculation node at the generic time step *t* and the volume at the initial time step, respectively. f_s is the shrinkage factor, *u* the ratio between the remaining mass and the initial mass in the control volume of the bed, X_{ash} the mass fraction of ash, ρ_{ash} the ash density and S_{sc} the cross sectional area of the bed [m^2].

Since the surface area of the particles bed is an important parameter for the heterogeneous reactions and heat transfer, Shin and Choi [23] introduce a relation to take into account the reduction of this parameter with the progress of the combustion process. They also consider that the ash surface it is not an active surface area and they remove its contribution from the operative surface of the bed.

In the relations reported by Johansson et al [35], θ_{drying} , θ_{dev} and θ_{comb} are the shrinkage factors during drying, devolatilization and char combustion, respectively. With these terms, they define the percentage of volume shrinkage during each phenomenon. For instance, in their studies they vary the devolatilization shrinkage factor θ_{dev} from a minimum of 40% to a maximum of 70%. The other terms X_m, X_v, X_c and X_{ash} represent the mass fractions of moisture, volatile, char and ash in the solid phase. The subscript *0* indicates the initial condition and V_p the volume of the solid particle.

Considering the relations reported by Asthana et al [39], ρ and *X* specify the densities and the mass fractions in the solid phase. Regarding the subscripts, they indicate: *m* moisture, *cm* combustible matter, *i* inert matter, *pyro* pyrolyzable matter, *c* carbon matter, *fix* fixed matter and *0* initial value. The model adopted by these authors is similar to the model developed by Goh et al [25] (which will be discussed later), but in a different way they assume that during drying and devolatilization the mass released is replaced by new internal porosity, with no volume reduction of the bed.

Referring to the relations reported by Martinez and Nussbaumer [42], X_{ash} and X_{cs} are the mass fractions of ash and solid combustible, $r_{char,comb}$ the combustion rate char, ρ_c the char density and the subscript *0* indicates the initial condition. It can be noted that they associate the reduction of the bed volume only with the consumption of the char.

The model of the bed volume change developed by Goh et al [25] and adopted in the works of Yang [29] - [33] needs to be discussed separately. The model considers that when a unit of volume of fuel undergoes a physical or chemical reaction two phenomena can occur: increasing of the interior porosity of the fuel and decreasing of the solid volume. To take in to account these two phenomena a coefficient F_i, for each species considered in the solid, is introduced. The coefficients have a value between 0 and 1. When F_i is equal to 0 there is no increase in the pore space, when it is equal to 1 the increase of the pore space is equal to the volume of species *i* removed during a particular process (drying, devolatilization and char combustion). The solid species taken into account in the model are: gas (void space), moisture, volatile matter, fixed carbon, ash and internal pore space. Thus, while the combustion process of the fuel proceeds, these solid species can be replaced by pores or can cause a bed volume reduction. A detailed description of the model can be found in the work of Goh et al [25], where all the relations are given.

Solid particles mixing

Solid particles mixing by grate movements can influence biomass combustion increasing the burning and the mass loss rate. Studies related to particles mixing have been done by Yang et al [30] - [32], Ryu et al [56] and Menard [57].

Ryu et al [56] propose two simple ways to model the particles mixing: in the first one (layer-overfed case) a new fuel layer is supplied upon the top of the bed at a certain time, in the second one (layer-exchanged case) a selected section of the bed moves from the bottom to the top. The two different cases are shown in Figure 50 together with the no-mixing case.

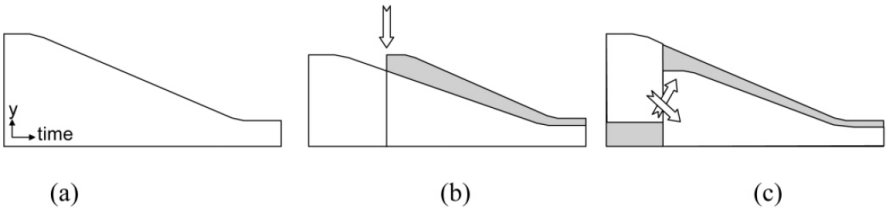

Figure 50 Mixing models: a) no-mixing; b) layer-overfed; c) layer-exchanged.

Using these two models they discovered that the complete burn-out time of the bed is not shortened noticeably when compared to no-mixing case, since the fuel bed is generally in reach combustion conditions. For this reason, they performed other investigations supplying different air flow rates in different sections of the grate, in order to provide sufficient air during

the active combustion period (gaseous species combustion and char combustion). In these simulations they assumed a sinusoidal mixing pattern for 11 different sections of the bed (see Figure 51).

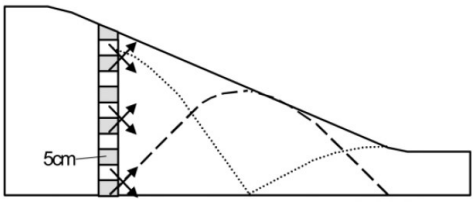

Figure 51 Sinusoidal mixing pattern.

Whit this configuration, for a bed of 55 cm, the overall time of combustion was reduced with approximately 10 min when compared to an undisturbed bed.

Yang et al [32], differently from the previous authors, introduce a diffusion model to simulate the random movements of the particles in a local scale. This means that the Fick's law can be used to simulate the molecular diffusion in the gaseous phase as well as the particle movements in the solid bed. To apply this model they defined the value of the solid diffusion coefficient experimentally whit both scale model measurements and full scale plant tests [32]. Using this model the solid species continuity equation for a 1-D scheme becomes:

$$Solidspeciescontinuity\colon \frac{\partial\left((1-\epsilon)\rho_s X_i\right)}{\partial t} = \frac{\partial}{\partial x}\left(D_s \frac{\partial \rho_s X_i}{\partial x}\right) - S_i \qquad \text{(A.96)}$$

Where D_s is the solid species diffusion coefficient.

From the simulation performed using different values of the diffusion coefficient they concluded that lower mixing results in a slower mass loss rate of the bed, while high mixing produces a shorter but intensive combustion stage. Excessive value of the mixing results in a significant delay in ignition.

Menard [57] uses the sinusoidal mixing pattern in his model that has already been utilized by Ryu et al [56] and shown in **Errore. L'origine riferimento non è stata trovata.**. The intention of the author was not to simulate with precision the mixing process inside the furnace, but to evaluate the influence of the mixing on the combustion process by comparing the results obtained in the case of mixing and in the case of no-mixing.

Physical properties of gaseous and solid phase

During combustion, physical properties of gaseous and solid phase change due to the variation of their temperature and composition. Indeed, the solid phase releases moisture, volatile and

gases of combustion that enrich the gaseous phase. The main physical property that changes during the combustion process is the specific heat of the two phases. Also in this case, in literature it is possible to find different approaches to the problem. Shin and Choi [23] consider the specific heat of solid species (wood, ash and water) to be independent of temperature and the specific heat of the main gases (N_2, O_2, H_2O, CO_2) linearly dependent on temperature. For the other gaseous species they assume a constant value of 1100 J/kgK (specific heat of the air at 800 K). Zhou et al [34] use temperature dependent equations for both solid and gaseous phase. In Table 30, the relations utilized by different authors are listed.

Table 30 Specific heat of gaseous and solid species.

Specie	Relation		Ref	
N_2	$980 + 0.2 \cdot T_g$	[J/kgK]		(A.97)
O_2	$854.7 + 0.1782 \cdot T_g$	[J/kgK]		(A.98)
H_2O	$1666 + 0.622 \cdot T_g$	[J/kgK]		(A.99)
CO_2	$708 + 0.478 \cdot T_g$	[J/kgK]	[23]	(A.100)
Wood	2400	[J/kgK]		(A.101)
Ash	800	[J/kgK]		(A.102)
Moisture	4200	[J/kgK]		(A.103)
Gas	$\left(0.99 + 1.22 \cdot 10^{-4} T_g - 5.68 \cdot 10^{3} T_g^{-2}\right) \cdot 10^{3}$	[J/molK]	[34]	(A.104)
Straw	$977.75 \ln(T_s) - 4144.4$	[J/molK]		(A.105)
Moisture	4180	[J/kgK]		(A.106)
Dry Wood	$103.1 + 3.87 \cdot T_s$	[J/kgK]	[42]	(A.107)
Char	$1390 + 0.36 \cdot T_s$	[J/kgK]		(A.108)
Ash	800	[J/kgK]		(A.109)

An interesting workpiece on biomass properties has been made by Ragland et al [13]. They resume physical and chemical properties of wood for combustion analysis such as: dry bulk density of typical woody fuels, specific heat and thermal conductivity of solid species, average

value of ultimate analysis of different types of wood, distribution of pyrolysis products of dry wood under combustion conditions and ash fusion temperatures. Some of these data are reported in Table 31.

Table 31 Properties of wood [55].

Species	Specific heat		
Dry Wood	$103.1 + 3.867 \cdot T_s$	[J/kgK]	(A.110)
Wet Wood	$\left(23.55 \cdot T_s - 1320 \cdot Y_{H_2O} - 6191\right) Y_{H_2O}$	[J/kgK]	(A.111)
Char	$1390 + 0.36 \cdot T_s$	[J/kgK]	(A.112)
Species	Thermal conductivity		
Wood	$S_g\left(0.1941 + 0.4064 X_{H_2O}\right) + 0.01864$	[W/mK]	(A.113)
Char	$0.67 S_g - 0.071$	[W/mK]	(A.114)

Where, referring to these relations, S_g is the specific gravity based on the volume at the current moisture content.

Appendix B – Literature review on packed bed combustion experiments

Together with the simulation results, some authors present experimental results used to validate the combustion model. The experiments are usually performed in cylindrical reactors equipped with thermocouples and gas probes with the aim to record the temperature profile inside the bed and the evolution of the gaseous species in the flue gas. This type of reactor represents the behaviour of a 1-D system very well. Experiments on multi-dimensional systems present a high level of compliance, for this reason only few examples can be found in literature. In this section the experimental works found in literature will be presented.

Experiments on cylindrical reactors

The experimental facility combined with the cylindrical reactor is similar among the different authors, for this reason the configuration utilized by Zhou et al [34] is chosen as example (see Figure 52) of a typical experimental setup.

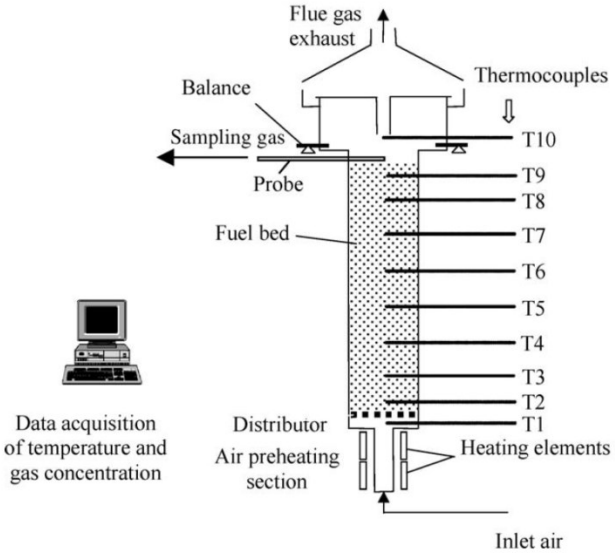

Figure 52 Schematic representation of the experimental facility by Zhou et al [34].

Table 32 Experimental setups for different authors.

Author	Tube height [mm]	Internal tube diameter [mm]	n. of thermometers	Species of gases analyzed	Fuel type	LHV [MJ/kg]	Bed Height [mm]	Air Flow rate [kg/m^{2}s]
Shin and Choi [23]	-	150	8	O_2	Lauan wood cubes plus inert matter	4.2 – 9.2	450	0.012 – 0.96
van der Lans et al [24]	1370	150	8	O_2 CO CO_2 NO_x NH_3 C_xH_y SO_3	Cut straw Straw pellet	16.7 -	-	0.07 – 0.18
Goh et al [25]	1500	200	7	O_2 CO CO_2 NO VOC	Simulated MSW	22.7	600	40 [l/min]
Yang et al [29]	1500	200	7	O_2 CO CO_2 NO VOC	Simulated MSW	6.9	580	0.052 (100 °C)
Yang et al [30][29]	1500	200	7	O_2 CO CO_2 NO VOC	Potatoes and cardboard	11.7	580	0.13 (15 °C)
Zhou et al [34]	1275	154	10	O_2 CO CO_2	Whole straw and cut straw	16.7	1000	0.07 – 0.5 (20 °C)
Asthana et al [39]	300	250	13	O_2 CO CO_2H_2O C_xH_y	Wood chips plus inert matter	9.2	250	0.11 (25 °C)

Table 32 resumes the setups of the experimental facilities used by different authors. A comparison among the results obtained in the cited experiments is not readily organisable due to the different choices of the experimental parameters, such as: type and LHV of the fuel, inlet air flow rate, bed height and particle dimension. Apart from the above, through a qualitative analysis of the reported results, some typical behaviours of biomass combustion and some important differences can be underlined.

When first looking at the bed temperature behaviour, it is evident that a reaction front moves downward through the fuel bed. The reaction front can be thought of as formed by the drying, heating up, devolatilization and combustion fronts. As a first step, the moisture evaporation occurs and the temperature remains around 373 K, once the biomass is dried the temperature starts to rise and biomass particles undergo devolatilization. In this phase the local temperature rises quickly, due to the chemical reactions, to values between 900 – 1200 K. When the reaction front reaches the bottom of the bed a new increase in temperature can be observed. This is due to the char burnout front that is moving in the opposite direction in respect to the reaction front. However, the presence of the char burnout front is not detected by Shin and Choi [23] and Goh et al [25]. The explanation to this is the fact that they perform experiments with fuel-lean combustion, whereas the other authors perform experiments with fuel-rich combustion. Obviously, in the case of biomass combustion the terms lean and rich are referring to the active combustion period, i.e. when the chemical reactions of the volatiles and char occur. In the case of fuel-rich combustion, during the active period, all the oxygen supplied by the flowing air is mainly consumed by the homogeneous reactions. For this reason the char burnout can occur only when the devolatilization front has reached the grate.

Also the trends of the gaseous species concentration depends on the particular experimental conditions, but through a qualitative analysis, it is possible to identify three different phases. In the first one, since the occurring phenomenon is the evaporation, the concentrations of CO and CO_2 remain close to zero and the concentration of O_2 is reduced only due to the dilution with H_2O. When the devolatilization and the chemical reactions take place, the second phase starts. This phase is characterized by a quick rise of CO and CO_2 concentration. Typical values of CO_2 concentrations are between 15 and 20 %vol. The concentration of CO is usually higher in the experiments with straw (10-15 %vol [24] and [34]) than in the experiments with wood or simulated MSW (5-10 %vol [29] and [39]). The concentration of the oxygen drops to zero if the combustion is fuel-rich [24], [29] and [39] or to values around 5 %vol if the combustion is fuel-lean [23] and [25]. When the reaction front reaches the grate, the third phase is experienced by the bed with fuel-rich combustion. During this phase the char burnout occurs and the temperature of the bed rises to values around 1400 K and, in some cases, an increase in the concentration of CO can be detected [39]. After this phase, the bed combustion is completed and the concentrations of CO and CO_2 drop to zero while the O_2 concentration rises to the ambient value.

Another important variable of biomass combustion processes is the combustion rate of the bed. Different authors show how this rate is affected by various combustion parameters such as: inlet air flow rate, preheating temperature of the air, particles size, LHV and moisture content of the fuel. Typical values of the combustion rate are between 0.06 and 0.09 kg/m^{2}s for straw [24] and [34] and 0.02 – 0.11 kg/m^{2}s for wood chips and simulated MSW [29]. The mayor parameter affecting the combustion rate is the air flow rate. At low air flow rate, oxygen is completely consumed by the chemical reactions (homogeneous gas reactions and heterogeneous char reaction). This regime is named oxygen limited since the combustion rate is determined by the oxygen supply rate. If more air is supplied, the combustion rate increases till a limit due to the chemical kinetics rate of the reactions involved and the increased convective cooling by the air. This regime is reaction limited, and the flame can be sustained as long as the heat release rate in the bed exceeds the convective cooling by the air [23].

Combustion characterization in moving grate furnaces

Experiments for the characterization of the combustion process in pilot and full scale moving grate furnaces are not so diffuse. Lundgren et al [59] have conducted experiments on small scale grate furnaces with the main aim of performance evaluation of the furnaces during steady-state operation in the complete thermal output range. Fleckl at al [60] used an in-situ Fourier transform infrared (FT-IR) absorption spectroscopy with the aim of obtaining information about the volatilisation of gaseous compounds from the fuel bed as well as the further reactions of these compounds during the combustion process. Both the works give information about the gaseous phase temperature and the gaseous species concentration only in some section of the furnace and for this reason it is impossible to characterize the fuel bed combustion process along the grate.

More interesting experiments have been performed by Razmjoo et al [58] and Frey et al [61]. Indeed, in order to investigate the performance of the combustion chamber, the concentrations of different gaseous species have been determined in various sections along the grate.

Razmjoo et al [58] performed experiments on a moving grate boiler of 4 MW, using residues produced after debarking and sawing of logs as fuel. The flue gas was sampled through 4 measuring ports above the fuel layer in order to determine the concentration profile of various gaseous components. The results show that in the first section of the grate only evaporation and devolatilization occur without significant combustion reactions since the oxygen concentration is about 14 %vol while the concentration of CO and NO is very low. In the following sections the concentration of oxygen drops while the concentration of CO and NO increase around 3-4 %vol and 40 -50 ppm, respectively. This means that the combustion processes are taking place. In conclusion the trend of the species concentration confirm the presence of different combustion zones along the grate, but no distinct separation of these zones is possible.

An interesting work has been carried out by Frey et al [61], who monitored the concentration of O_2, CO, CO_2, H_2, TOC, C and CH_4 during the combustion process. During the experiments also the temperature of the grate, of the fuel bed (5 cm above the grate) and of the flue gas (10 cm above the bed) have been measured. The measurements have been done in 5 different sections of the grate as shown in Figure 53.

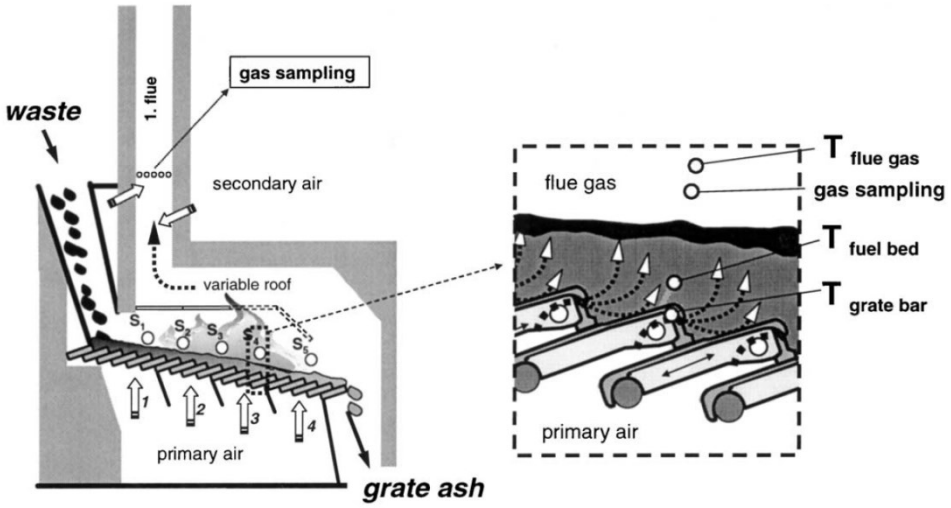

Figure 53 Probes position in the experiments of Frey et al [61].

The temperature profile of the grate bars, of the fuel bed and of the flue gas above the bed show significant temperature gradients along the bed height, confirming what has been said earlier in paragraph 5.3 and that the combustion starts from the surface and extends to the bottom of the fuel bed. Moreover, as observed by Razmjoo et al [58], there is no distinct axial separation of the individual regions of drying, devolatilization and char burnout, but the concentration profiles of O_2, CO and CO_2 demonstrate that maximum rate conversion of carbon in the bed takes place in the middle section of the grate.

Appendix C – The biomass combustion program

The solution method implemented in the computer program developed to simulate the biomass combustion process in moving grate furnaces, together with the discretization method applied to the PDE's system and the boundary conditions, has been described in paragraph 4.2. The simulation program has been developed in Matlab and can be divided into three main parts: a first part where the solver and simulation parameters as well as the initial and the boundary conditions are defined, a part where the mathematical calculation of the solution vector is performed and the last part where a post processing of the calculated data is executed. When the mathematical calculation is performed two important sub-routines are called by the program. They can be considered the *Brain* and the *Heart* of the program since they chose the actual time step and define the solution vector of the simulation. In this appendix a brief description of the simulation program and its main routines is given.

The main menu

From the main menu it is possible to browse to the different sections of the program as shown in Figure 54.

In the sections 2, 3, and 4 the solver parameters as well as the process phenomena and constants can be set. These values are usually changed depending on the simulation which needs to be made. For instance in the section *Solver Parameters* the simulation time, the initial time step, the initial node dimension and the number of nodes are set (see Figure 55).

In the section *Process Switches and Booleans* the physical and chemical phenomena that occur during biomass combustion can be switched ON or OFF as shown in Figure 56.

The section *Process Constants* is made by different subsections where it is possible to change the different constant parameters of the combustion process. For instance, in the sub-section *Process Parameters* it is possible to set the inlet temperature of the gaseous and solid phase, the inlet flow rate of air supplied, the temperature of the internal wall of the furnace and the physical and chemical characteristic of the biomass such as the low heating value and the proximate and ultimate analysis (see Figure 57).

BCM Version 1.0

```
%%%%%%%%%%%%%%%%%%%%%%%%%%%%%%%%%%%%%%%%%%%%
%%%%BIOMASS COMBUSTION IN MOVING GRATE%%%%
%%%%%%%%%%%%A 1D TRANSIENT MODEL%%%%%%%%%%%%
```

0) Program Initialization

```
Initialize
```

1) Global Variables and Codification

```
Global
```

2) Solver Parameters

```
Solver_Parameter
```

3) Process Switches & Booleans

```
Switches
```

4) Process Costants

```
Process_Constant
```

5) Initial Conditions

```
Initial_Condition
```

6) System Dimension and Solution Vector Initialization

```
Sys_Dim
```

7) Time Loop

```
Time_Loop
```

8) Display

```
Display
```

9) Post Processing

```
Post_Procesing
```

10) Workspace Cleaning

```
Cleaning
```

Figure 54 Main menu of the program.

2) Set Solver Parameters

```
%simulation type
bSimType=bTimeDependent;
%simulation time [s]
simtime=3600;
%initial time step [s]
tstep=1;
%max time step [s]
tstepmax=1;
%initial node dimension [m]
lx0=0.001;
%number of nodes
g=250;
%initial time definition
if start_again==0
    simtime=simtime;
else
    simtime=t+simtime;
end
%max number of iterations
nmaxiter=100;
%convergence criteria
epsilon=1e-6;
%disturbance (numerical derivate)
delta=1e-4;
deltax=1e-7;
%max number of converged iteration before double tstep
nTimeStepmax=10;
```

Figure 55 Solver Parameters.

3) Process Switches & Booleans

```
%Switches
%jacob pattern calculation
% 0 for Jpat calculation
% 1 for Jpat read
JacobPattern=0;

if start_again==1
    JacobPattern=1;
end

%evaporation model
% 0 No evaporation
% 1 Arrhenius model
evaporation_model=1;

%devolatilization model
% 0 no dev
% 1 chose dev_speed
%devolatilization speed
% 1 very slow
% 2 slow
% 3 medium
% 4 fast
% 5 very fast
dev_model=1;
dev_speed=1;

%char combustion model
% 0 no char comb
% 1 char comb
%char comb model
% 1 Menard - Asthana model
% 2 Menard - Asthana with Stefan flow effect
char_comb=1;
char_comb_model=1;
```

Figure 56 Process Switches and Booleans (a partial representation).

Process parameters

```
%inlet solid temperature [K]
Ts0=25+273;
%inlet gas temperature [K]
Tg0=20+273;
%inlet flow rate [kg/m2s]
mg0=0.11;
%wall temperature [K]
Tw=850+273;

%proximate analysis - wet mass basis
%moisture
Xm0=0.238;
%volatile
Xv0=0.45;
%fixed carbon
Xc0=0.107;
%ash
Xa0=0.205;

%ultimate analisys
C=0.4845;
H=0.0585;
O=0.4369;
Su=0.0001;
N=0.0047;

%LHV of biomass [J/kg]
LHVw=9.2e6;
```

Figure 57 Process Parameter (sub-section of Process Constant).

The Brain and the Heart of the program

In the section *Time Loop* (see Figure 54) the mathematical calculation of the solution vector for each time step is executed. This calculation is performed calling two important sub-routines which can be referred to as the *Brain* and the *Heart* of the program.

The sub-routine *Brain* defines the time step that the program has to use at each simulation time. The time step is dynamically changed depending on the outcome of the last iteration. Figure 58 shows the flow chart of this sub-routine.

The inputs of the subroutine are: the time step *tstep* used in the last iteration, the boolean *bSolverError* which can be false or true depending on whether the last iteration converged or not, the boolean *bJCalculation* which can be false or true depending on whether new Jacob matrix calculation is needed, the number of steps *nStep* done to achieve the actual simulation

time and the number of iterations done in the last step *nSubStep*. If the last iteration did not converge *bSolverError* is

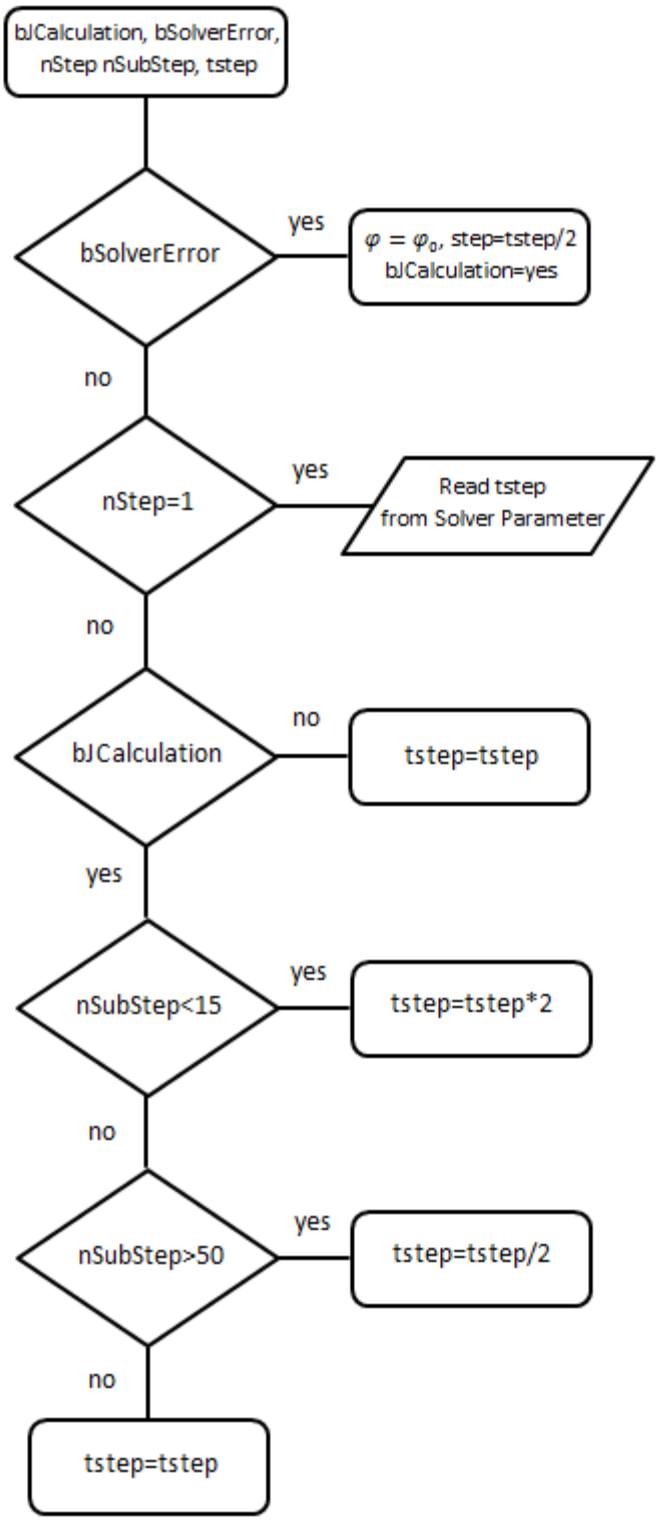

Figure 58 Flow chart of the Brain sub-routine.

true, the solution vector is reset to the previous value ($\varphi = \varphi_0$), the time step is halved and a new Jacobian matrix calculation is performed. If the simulation is at the first time step (*nStep*=1 and *bSolverError*=false) the value of the time step is read from the *Solver Parameters* section. If the last iteration converged (*bSolverError*=false), the simulation is not at the first time step (*nStep*>1) and a new Jacobian matrix calculation is not needed (*bJCalculation*=false), then the actual time step remains the same. If the previous conditions are respected but a new Jacob matrix calculation is needed (*bJCalculation*=true), three cases are possible: if *nSubStep<15* the time step is double, if *nSubStep>50* the time step is halved and if *nSubStep* is between these two values the time step remains the same.

In conclusion the way of thinking of the *Brain* can be resumed as follows: if the calculation did not converge or is converging but takes too long then the program has to use a smaller time step, if the calculation is converging using few iterations the program can use a bigger time step. In all other cases the time step remains the same.

The sub-routine *Heart* computes the solution vector at each iteration. The solution vector is calculated using the modified Newton method as defined in the paragraph 4.2. The method is an iterative method and is applied till the convergence is reached. Figure 59 shows the flow chart of this sub-routines.

The input values of the subroutines are: the solution vector of the previous time step φ^t, the last Jacobian matrix calculated J^t, the age of the Jacobian matrix *nJAge* and the boolean *bJCalculation.* If the boolean *bJCalculation* is true a new Jacobian matrix calculation is performed and the Jacobian age is set equal to zero; in the other case the old Jacobian matrix is used in the following steps. Once the correction vector $\Delta\varphi^{t+\Delta t}$ has been calculated, is used in the updating of the solution vector. The updating is done using a relaxing term ω^n, already encountered and named *iteration steplenght* in the paragraph 4.2. If the relation $\|r(\varphi^{t+\Delta t})\|_2 \leq \|\bar{r}(\varphi^t)\|_2$ is not satisfied for *n=0* (this means $\omega^n = 1$) the value of the exponent *n* is increased. This loop continues until the condition is satisfied or when *n* reaches the maximum value (typically equal to 10). When the condition on the norm of the residues vector is satisfied, then the condition on the maximum absolute value of the residue vector has to be checked. If this value is higher than the convergence parameter ε (typically equal to 10^{-6}) another iteration has to be performed with the aim to reduce the error; if it is smaller than ε the iteration converged and the new solution vector has been defined.

In a few words, when a new solution vector has to be calculated, the correction vector is defined using a new Jacob matrix or an old one depending on the age of the matrix (typically the Jacob matrix is updated every the successful calculation of ten time steps). The correction vector is used coupled with a relaxing term which increases the reliability of the calculation. If no solution vector that satisfies the condition on the norm is found, then an error message is returned and the calculation comes back to the *Brain* of the program. In the other cases the calculation is iterated till convergence is reached.

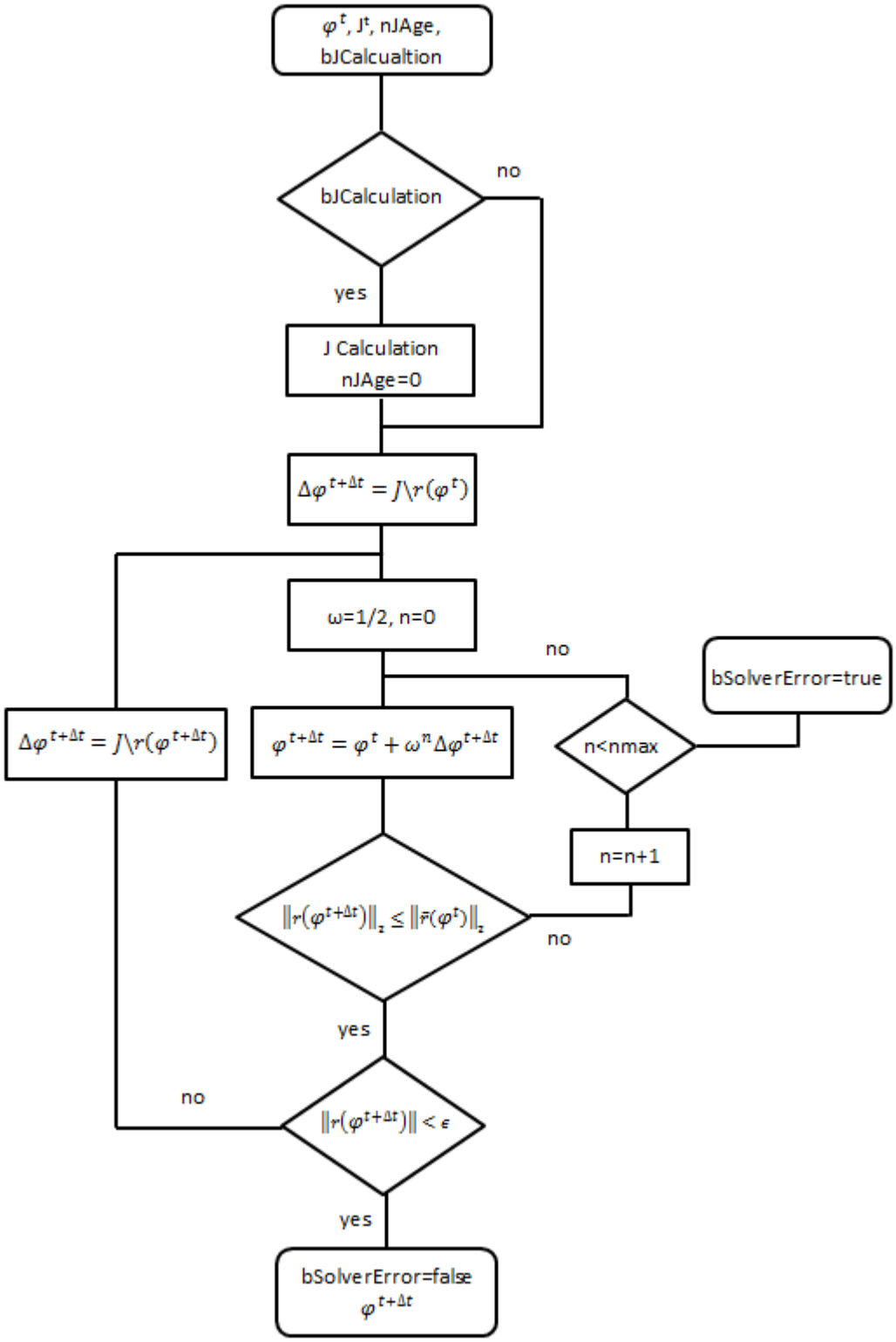

Figure 59 Flow chart of the Heart sub-routine.

Nomenclature

A	Frequency factor of Arrhenius law
C	Species concentration [mol/m^3]
C_{wg}	water vapor concentration in the gas phase [kg/m^3]
C_{ws}	water vapor concentration on particle surface [kg/m^3]
c	specific heat [J/kg K]
D	molecular diffusion coefficient [m^2/s]
$D_{a,eff}$	effective axial dispersion coefficient [m^2/s]
d_p	particle diameter [m]
$d_{e,rad}$	equivalent particle diameter for radiation [m]
E	Activation energy [J/mol]
E_b	black body radiation [W/m^2]
f_s	shrinking factor
G	number of calculation nodes
H_{evap}	latent heat of water evaporation [J/kg]
h_m	mass transfer coefficient [m/s]
h_t	convective heat transfer coefficient [W/m^{2}K]
I_x^+ I_x^-	radiation intensities in positive and negative direction, respectively [W/m^2]
i	variables index
J	Jacobian matrix
j	grid point index
J_0	incident radiation [W/m^2]
k	reaction rate coefficient [m/s]
M	molar mass [g/mol]
n	iteration index

Nu	Nusselt number
p	pressure [Pa]
Pr	Prandtl number
$\dot{Q}$	heat source per unit of volume [W/m^3]
R	ideal gas constant [J/mol K]
$\bar{r}$	vector of the residuals
r_c	ratio of CO/CO_2 formation rate
Re	Reynolds number
S	specific surface area per unit of volume of solid matter [m^2/m^3]
Sc	Schmidt number
Sh	Sherwood number
S_g	Gaseous phase source [kg/m^3s]
T	temperature [K]
t	time [s]
V	number of variables
v	velocity [m/s]
X_i	mass fraction of specie *i* in the solid phase
x	direction in the bed length [m]
Y	mass fraction of species *i* in the gaseous phase
x'	distance from the bed surface [m]

Greek letters

β	absorption coefficient [1/m]
Γ	generic diffusion coefficient
Δt	discrete time step [s]
Δx	discrete spatial step [m]
ϵ	void fraction of bed
ζ	surface factor for internal burning of char reaction
ν	kinematic viscosity [m^2s]
ρ	density [kg/m^3]
Θ	stoichiometric ratio for the char combustion
σ	Stefan-Boltzmann constant [W/m^2K^4]
λ	thermal conductivity [W/mK]

μ	dynamic viscosity [Pas]
φ	generic variable
χ	active surface reduction coefficient
ω	radiation scattering coefficient [1/m]

Subscripts

cond	conductive
conv	convective
evap	evaporation
eff	effective
g	gaseous phase
rad	radiation
s	solid phase
w	internal walls of the furnaces

References

[1] AEBIOM, European Biomass Association, European Bioenergy Outlook 2012.

[2] N. Troccia, F. Palmieri, F. Gallucci. Combustion modeling of a biomass packed bed in moving grate furnaces. 20th European Biomass Conference & Exhibition -Milan, June 2012.

[3] N. Troccia, F. Palmieri, F. Gallucci, M Amalfi. Combustion model of woody biomass in moving grate furnaces. 21st European Biomass Conference & Exhibition -Copenhagen, June 2013.

[4] F. Gallucci, L. Pari, R. Bellacima, M. Barontini. Storage of poplar chips: comparison between two different methods of conservation and between different chips size. 20th European Biomass Conference & Exhibition -Milan, June 2012.

[5] M. Barontini, A. Scarfone, E. Santangelo, F. Gallucci, R. Spinelli, L. Pari. The Cra-Ing Experience on Storage of Poplar Wood Chips. 21st European Biomass Conference & Exhibition -Copenhagen, June 2013.

[6] L. Pari, G. Gallucci, G. Chiatti, F. Palmieri, M. Amalfi. Influence of woody biomass type on pollutant emission in moving grate furnaces – experimental study. 22nd European Biomass Conference & Exhibition -Hamburg, June 2014.

[7] L. Pari, G. Gallucci, G. Chiatti, F. Palmieri, M. Amalfi. Biomass combustion in moving grate furnaces – A case experimental study from wood to ashes. American Society of Agricultural and Biological Engineers, submitted.

[8] L. Pari, G. Gallucci, G. Chiatti, F. Palmieri, M. Amalfi. Influence of woody biomass type on pollutant emission in moving grate furnaces. 5th International Conference on Engineering for Waste and Biomass Valorisation - Rio de Janeiro, August 2014.

[9] http://ec.europa.eu/clima/policies/package/

[10] A. Acampora, S. Croce, A. Assirelli, A. Del Giudice, A. Suardi, R. Spinelli, L. Pari. Product contamination and harvesting losses from mechanized recovery of olive tree pruning residues for energy use. Renewable Energy 53 (2013) 350-353.

[11] A. Assirelli, V. Civitarese, R. Fanigliulo, L. Pari, D. Pochi, E. Santangelo, R. Spinelli. Effect of piece size and tree part on chipper performance. Biomass and Bioenergy 54 (2013) 77-82.

[12] A. Assirelli, S. Croce, A. Acampora, V. Civitarese, A. Suardi, E. Santangelo, L. Pari. An innovative system for conditioning biomass sorghum [Sorghum Bicolor (L.) Moench]. Transactions of the ASABE 56 (2013) 829-837

[13] A. Asikainen, J. Routa, R. Björheden, J. Laitila, D. Röser. Large Scale Supply of Forest Fuels in the EU - Transfer of Nordic Technology and Experience to other Countries. 21st European Biomass Conference & Exhibition -Copenhagen, June 2013.

[14] J. Windisch, P. Anttila, A. Asikainen, K. Väätäinen, J. Laitila. Precision Supply of Forest Biomass to Combined Heat and Power and Bio Oil Plants. 21st European Biomass Windisch, J., Anttila, P., Asikainen, A., Väätäinen, K., Laitila, J.

[15] M. Amalfi. Sviluppo di un impianto sperimentale per l'utilizzazione energetica delle biomasse legnose. Roma Tre University. Master Thesis, 2012.

[16] S. van Loop and J. Koppejan. The Handbook of Biomass Combustion and Co-firing. Earthscan – London, 2008.

[17] W. C. Park, A. Atrena, H. R. Baum. Experimental and theoretical investigation of heat and mas transfer processes during wood pyrolysis. Combustion and Flame 157 (2010) 481-494.

[18] R. Bilbao, J.F. Mastral, M.E. Aldea, J, Ceamanos.Modelling of the pyrolysis of wet wood. Journal of Analytical and Applied Pyrolysis 36 (1) (1996) 81–97.

[19] C. Di Blasi, C. Branca, A. Santoro, E. G. Hernandez.Pyrolytic behavior and products of some wood varieties. Combustion and Flame 124 (1-2) (2001) 165–177.

[20] M.G. Gronli, M.C. Melaaen. Mathematical model for wood pyrolysis –comparison of experimental measurements with model predictions. Energy & Fuels 14 (4) (2000) 791–800.

[21] C. Di Blasi. Modeling and simulation of combustion processes of charring and non-charring solid fuels. Prog. Energy Combust. Sci. 19 (1993) 71-104.

[22] Y.B. Yang, C.N. Lim, J. Goodfellow, V.N. Sharifi, J. Swithenbank. A diffusion model for particle mixing in a packed bed of burning solids. Fuel 84 (2–3) (2005) 213–225.

[23] D. Shin and S. Choi. The combustion of simulated waste particles in a fixed bed. Combustion and Flame 121 (2000) 167-180.

[24] R. P. van del Lans, L. T. Pdersen, A. Jensen , P. Glarborg, K. Dam-Johansen. Modelling and experiments of straw combustion in a grate furnace. Biomass and Bioenergy 19 (2000) 199-208.

[25] Y. R. Goh, Y. B. Yang, R. Zakaria, R. G. Siddal, V. Nasserzadeh, J. Swithenbank.Development of an incinerator bed model for municipal solid waste incineration. Combustion Science and Technology 162 (2001) 37-58.

[26] Y. B. Yang, V. Nasserzadeh, J. Goodfellow J, Y. R. Goh, J. Swithenbank. Parameter study on the incineration of municipal solid waste fuels in packed beds. J Inst. Energ. (2002) 66-80-

[27] Y. B. Yang,J. Goodfellow, Y. R. Goh, V. Nasserzadeh J, J. Swithenbank. Investigation of channel formation due to random packing in a burning waste bed. Trans IChemE 79 Part B (2001) 267-277.

[28] Y. B. Yang, H. Yamauchi, V. Nasserzadeh, J. Swithenbank. Effect of moisture content in fuel on the combustion behavior of biomass and municipal solid waste in a packed bed. J Inst. Energ. (2003) 104-114.

[29] Y. B. Yang, H. Yamauchi, V. Nasserzadeh, J. Swithenbank. Effects of fuel devolatilization on the combustion of wood chips and incineration of simulated municipal solid wastes in a packed bed. Fuel 82 (2003) 2205-2221.

[30] Y. B. Yang, Y. R. Goh, R. Zakaria, V. Nasserzadeh, J. Swithenbank. Mathematical modelling of MSW incinerator on travelling bed. Waste Management 22 (2002) 369-380.

[31] Y. B. Yang, C. Ryu, A. Khor, N. Yates, V. N. Sharifi, J. Swithenbank. Effect of fuel properties on biomass combustion. Part II. Modelling approach-identification of the controlling factors. Fuel 84 (2005) 2116-2130.

[32] Y. B. Yang, C. N. Lim,J. Goodfellow, V. N. SharifiJ, J. Swithenbank. A diffusion model for particles mixing in a packed bed of burning solids. Fuel 84 (2005) 213-225.

[33] Y. B. Yang, R. Newman, V. Sharifi, J. Swithenbank, J. Ariss. Mathematical Modelling of Straw Combustion in a 38 MWe power plant furnace and effect of operating condition. Fuel 86 (2007) 129-142.

[34] H. Zhou, A. D. Jensen, P. Glaborg, P. A. Jensen, A. Kavaliauskas. Numerical modeling of straw combustion in a fixed bed. Fuel 84 (2005) 389-403.

[35] R. Johansson, H. Thunman, B. Leckner. Sensitivity analysis of a fixed bed combustion model. Energy & Fuels (2007) 21 1493-1503.

[36] B. A. Albrecht, S. Zahirovic, R. J. M. Bastiaans, J. A. van Oijen, L. P. H. de Goey. A Premixed Flamelet – PDF Model for Biomass Combustion in a Grate furnace. Energy & Fuels 22 (2008) 1570-1580.

[37] H. van Kuijk, J. A. van Oijen, R. J. M. Bastiaans, L. P. H. de Goey. Reverse combustion: Kinetically controlled and mass transfer controlled conversion front structures. Combustion and Flame 153 (2008) 417–433.

[38] H. van Kuijk, J. A. van Oijen, R. J. M. Bastiaans, L. P. H. de Goey. Grate Furnaces Combustion: A Submadel for the Solid Fuel Layer. International Journal of Multiscale Engineering.

[39] A. Astana, M. Yannick, P. Sessiecq, F. Patisson. Modeling on-grate MSW incinerator with experimental validation in a batch incinerator. Ind. Eng. Chem. Res 49 (2010) 7597-7604.

[40] A. Boriouchkine, A. Zakharov, S. L. Jämsä-Jounela. Dynamic modeling of combustion in a BioGrate furnace: The effect of operation parameters on biomass firing. Chemical Engineering Science 69 (2012) 669-678.

[41] B. Miljkovic, I Pesenjanski, M. Vicevic. Mathematical Modelling of Straw Combustion in a Moving bed Combustor: A Two Dimensional Approach. Fuel 104 (2013) 351-364.

[42] J. Martinez, T. Nussbaumer. A One-Dimensional Transient Solid Fuel Conversion Model for Grate Combustion Optimisation. 21st European Biomass Conference & Exhibition - Copenhagen, June 2013.

[43] S. J. Kowalski. Thermomechanics of drying processes. Book, Springer, Verlag Berlin Heidelberg, 2003.

[44] R. Younsi, D. Kocaefe, S. Poncsak, Y. Kocaefe. Computational modeling of heat and mass transfer during high temperature treatment of wood. Applied thermal engineering 27 (2007) 1424-1431.

[45] C. Di Blasi. Multi-phase moisture transfer in the high-temperature drying of wood chips. Chemical engineering and science 53 (1998) 353-366.

[46] C. Di Blasi, C. Branca, S. Sparano, B. La Mantia. Drying characteristic of wood cylinders for condition pertinent to fixed bed counter-current gasification. Biomass and Bioenergy 25 (2003) 45-58.

[47] N. Wakao and S. Kaguei. Heat and mass transfer in packed beds. New york: Gordon and Breach, 1982.

[48] E. Grieco, G. Baldi. Analysis and modelling of wood pyrolysis. Chemical Engineering Science 66 (2011) 650-660.

[49] F. Shafizadeh and P. P. S. Chin. Thermal deterioration of wood. ACS Symp. Ser. (1977) 43-57.

[50] C. Di Blasi. Dynamic behavior of stratified downdraft gasifiers. Chemical Engineering Science 55 (2000) 2931-2944.

[51] S. V. Patankar. Numerical heat transfer and fluid flow. Taylor and Francis, 1980.

[52] L. M. T. Somers. The simulation of flat flames with detailed and reduced chemical models. Eindhoven Technology University. PhDThesis, 1994.

[53] L. D. Smoot and D. T. Pratt. Pulverized-coal Combustion and Gasification. Plenum Press, 1979.

[54] I. Glassman and R. A. Yetter. Combustion. Elsevier - Fourth Edition, 2008.

[55] K. W. Ragland, D. J. Aerts, A. J. Baker. Properties of wood for combustion analysis. Bioresource Technology 37 (1991) 161-168.

[56] C. Ryu, D. Shin, S. Choi. Effect of fuel layer mixing in waste bed combustion. Advances in Environmental Research 5 (2001) 259-267.

[57] Y. Menard. Modelisation de l'incineration sur grille d'ordures menageres et approche themodynamique du comportement des metaux lourds. Institut National Polytechnique de Lorraine. PhD Thesis, 2003.

[58] N. Razmjoo, H. Sefidari, M. Strand, J. Yang. Gas measurements and characterization of wood combustion in a traveling grate boiler. 21st European Biomass Conference & Exhibition - Copenhagen, June 2013.

[59] J. Lundgren, R. Hermansson, J. Dahl. Experimental studies of a biomass boiler suitable for small district heating systems. Biomass and Bioenergy 26 (2004) 443-453.

[60] T. Fleckl, H. Jager, I. Obernberger. Combustion diagnostic at a biomass-fired grate furnace using FT-IR absorption spectroscopy for hot gas measurements. Proceedings of the 5th European Conference on Industrial Furnaces and Boilers – Porto, April 2000.

[61] H. H. Frey, B. Peters, H. Hunsinger, J. Vehlow. Characterization of municipal solid waste combustion in a grate furnaces. Waste Management 23 (2003) 689-701.